#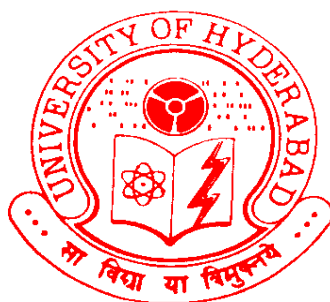 Structural elucidation and proteomic characterization of PSI-LHCI complexes under iron deficiency in Chlamydomonas and Rice

A Thesis submitted to the University of Hyderabad for the award
of a Ph. D. degree in Department of Biochemistry,
School of Life Sciences

By

VENKATESWARLU YADAVALLI

(06LBPH08)

Department of Biochemistry
School of Life Sciences
University of Hyderabad

Hyderabad - 500 046

Andhra Pradesh (India)

May, 2011

University of Hyderabad
School of Life Sciences
Department of Biochemistry

DECLARATION

I, Venkateswarlu Yadavalli, hereby declare that this thesis entitled **"Structural Elucidation and Proteomic Characterization of PSI-LHCI Complexes Under Iron Deficiency in Chlamydomonas and Rice"** submitted by me under the guidance and supervision of Dr. S. Rajagopal, is an original and independent research work. I also declare that it has not been submitted previously in part or in full to this University or any other University or Institution for the award of any degree or diploma.

Place: Hyderabad

Date: 09-05-2011

Venkateswarlu Yadavalli

Regd. No. 06LBPH08

University of Hyderabad
School of Life Sciences
Department of Biochemistry

CERTIFICATE

This is to certify that this thesis entitled **"Structural elucidation and proteomic characterization of PSI-LHCI complexes under iron deficiency in Chlamydomonas and Rice"** is a record of bonafide work done by **Venkateswarlu Yadavalli**, a research scholar for Ph.D. programme in Department of Biochemistry, School of Life Sciences, University of Hyderabad under my guidance and supervision.

The thesis has not been submitted previously in part or in full to this or any other University or Institution for the award of any degree or diploma.

Signature of the Supervisor

Head of the Department   Dean of the School

Dedicated to

My beloved son, Khajith

University of Hyderabad
School of Life Sciences
Department of Biochemistry

ACKNOWLEDGEMENTS

*It's a great privilege to express my deep sense of gratitude to my supervisor **Dr. S. Rajagopal** for giving me the opportunity to work in his laboratory. He was always accessible and willing to help his students. As a result, research life became smooth and rewarding for me.*

*I thank **Prof. K.V. A. Ramaiah,** Head, Department of Biochemistry, and former Head, **Prof. M. Ramanadham,** for making my research feasible with excellent infrastructure and lab facilities.*

*I thank **Prof. M. Ramanadham,** Dean, School of Life Sciences, and former Dean, **Prof. A. S. Raghavendra,** for providing the general facilities of the school.*

*I am indebted to **Prof. Prasanna Mohanty,** former professor from J.N.U, New Delhi for his kind suggestions.*

*I would like to thank my Doctoral Committee members **Prof. O.H setty and Prof. N Siva kumar** for assessing my research work in between and for the useful discussions.*

*I thank Prof. **Győző Garab, Drs.** László Kovács**, Zsuzsanna Várkonyi, **and** Ottó Zsiros**, for giving useful suggestions when I was at Biological Research Centre, Szeged, Hungary.*

*I thank **Prof. Petra Fromme** and **Dr. Craig Jolley**, Department of Chemistry and Biochemistry, Arizona State University, U.S.A for providing the peptides and useful discussions on iron deficiency studies.*

Y. venkateswarlu

Contents

<u>CONTENTS</u>

LIST OF FIGURES

LIST OF TABLES

Abbreviations

LIST OF ABBREVIATIONS

2DE	Two-dimensional electrophoresis.
β-DM	β-dodecyl-$â$-D-maltoside
ABS	Absorption flux
CD	Circular dichroism
Chl	Chlorophyll
CS	Leaf cross-section
Cyt	Cytochrome
DI	Dissipation flux
DOPE	Discrete Optimized Protein Energy
DTT	Dithiothreitol
EDTA	Ethylenediaminetetraacetic acid
ET	Electron transport flux
F_0	Fluorescence of dark-adapted leaves in time 0
Fd	Ferredoxin
FDAS	Fluorescence decay-associated spectra
Fm	Maximum fluorescence in dark-adapted leaves
Fv	Fluorescence change between F0 and Fm (Fv = Fm $-F_0$)
Fv/Fm	Quantum efficiency of energy trapping in PS2 reaction centres
HCl	Hydrochloric acid
HEPES	4-(2-hydroxyethyl)-1-piperazineethanesulfonic acid
HRP	Horseradish peroxidase
IAA-NHS	Indole 3-acetic acid N-Hydroxy succinamide ester
IPG	**Immobilized pH gradient**
KLH	Keyhole limpet hemocyanin
KOH	Potassium hydroxide
LHCI	Light-harvesting complex I
LHCII	Light-harvesting complex II
MALDI-TOF	Matrix assisted laser desorption ionization time-of-fight mass spectrometry
NaCl	Sodium chloride

NADPH	Nicotinamide adenine dinucleotide phosphate
NPQ	Non-photochemical quenching
PDB	Protein data bank
PIabs	Performance index based on the equal absorption
PPFD	Photosynthetic photon flux density
PSI	Photosystem I
PSII	Photosystem II
PVDF	Polyvinylidene Fluoride
QA	Primary quinine electron acceptor of PS2
QB	Secondary quinone electron acceptor of PS2
RC	Reaction centre
RMSD	Root mean square difference.
SDS	Sodium dodecyl sulphate
SDS-PAGE	Sodium dodecyl sulfate polyacrylamide gel electrophoresis.
SOD	Superoxide dismutase
TR	Energy flux for trapping
Tris	Tris(hydroxymethyl)-aminomethane
WT	Wild type

Introduction

Chapter 1

1.   Introduction

General Introduction

1.1   Photosynthesis

Photosynthesis requires two processes which can be distinguished functionally, although they work as a unit within the chloroplast. The first process is known as the light reactions, while the second is known by analogy as the light independent reactions. The light reactions are rapid changes in the subatomic arrangements of molecules that ultimately split water in the presence of light (photo oxidation). Hydrogen ions (H^+) from the water are used to reduce nicotinamide adenine dinucleotide phosphate (NADP) to $NADPH_2$, and are then used to reduce CO_2 to $(CH_2O)n$. The photooxidation of water in the presence of chloroplast fragments is known as the Hill Reaction. It results from the physical capture of light quanta (energy) into the electron orbit of chlorophyll molecules and the subsequent transfer of an "excited" electron to the orbit of an adjacent molecule. The end products of this reaction are free hydrogen, oxygen and electrons. The electrons are utilized for further chemical reduction reactions, the hydrogen becomes the ultimate hydrogen acceptor in the reactions; and oxygen is a by-product.

In oxygen-evolving photosynthetic organisms two photosystems (PSI and PSII) operate in series to transfer electrons from water to NADP. Each photosystem is a multiprotein component containing chlorophylls and carotenoid molecules. Each holocomplex can be divided into two components: (a) the core complex (PSI or PSII) containing the photochemical reaction center and a relatively small internal antenna and (b) the light-harvesting complex (LHCI or LHCII) which serves as an antenna that collects the light energy and transfers it to the core complex (Albertsson, 2001). The

conversion of usable sunlight energy into chemical energy is associated with the action of the green pigment chlorophyll. Several modifications of chlorophyll occur among plants and other photosynthetic organisms. All photosynthetic organisms have chlorophyll *a*. Accessory pigments include chlorophyll b (also c, d, and e in algae and protists), xanthophylls, and carotenoids (such as β-carotene). Chlorophyll absorbs energy at 665 nm and 465 nm.

The thylakoid is the structural and functional unit of photosynthesis. Both photosynthetic prokaryotes and eukaryotes have these flattened sacs/vesicles containing photosynthetic units. Only eukaryotes have chloroplasts with a surrounding membrane. A thylakoid is a membrane-bound compartment inside chloroplasts, cyanobacteria, and red algae. They are the site of the light-dependent reactions of photosynthesis. Chloroplast thylakoids frequently form stacks of disks referred to as grana (singular: granum). Grana are connected by intergrana or stroma thylakoids, which join granum stacks together as a single functional compartment. The absorbed light energy by chlorophyll will be excited and electron is transferred to another molecule (called a primary electron acceptor). The chlorophyll molecule is oxidized (loss of electron) and has a positive charge. Photoactivation of chlorophyll *a* results in the splitting of water molecules and the transfer of energy to ATP and reduced nicotinamide adenine NADP.

The chemical reactions involved include:

- Condensation reactions - responsible for water molecules splitting out, including phosphorylation (the addition of a phosphate group to an organic compound)

- Oxidation/reduction (redox) reactions involving electron transfer

Photosynthesis is a two stage process

1.1.1 Light dependent reactions

In a light-dependent series of reactions which occur in the grana, and require the direct energy of light to make energy-carrier molecules that are used in the second process. A schematic model detailing the main photosynthetic complexes involved in oxygenic photosynthesis is shown in Figure 1.1.

In higher plants (eukaryotes), photosynthetic and carbon fixation reactions are housed in the chloroplasts. Light reactions of photosynthesis take place in the chloroplast's thylakoid membranes and are driven by light, as captured by the LHCI and LHCII antenna that are bound to PSI and PSII, respectively. Linear electron transport involves electrons (e^-) being derived from the splitting of water, by PSII, and sequentially passed along the photosynthetic e^- transport chain by plastoquinone (PQ), cytochrome b_6f (Cyt b_6f), plastocyanin (PC), Photosystem I (PSI) and PSI-bound ferredoxin (Fd), before being used for producing NADPH by ferredoxin–$NADP^+$ oxido-reductase in the stromal matrix (stroma). From this splitting of water (water oxidation), and from the Q-cycle operating about Cyt b_6f, protons (H^+) accumulate in the thylakoid's lumenal space (lumen), thereby generating a gradient which provides for ATP production by proton motive force (chemiosmosis) via chloroplastic ATP synthase (CF_oF_1 ATP synthase). Under conditions causing the phenomenon of 'cyclic e^- transport' that operates about Photosystem One (PSI), protons (H^+) are reduced to molecular hydrogen (H_2) *via* hydrogenases. The products of the above, ATP and NADPH, are consumed during carbon dioxide (CO_2) fixation, where a separate enzyme, ribulose-1,5-bisphosphate carboxylase oxygenase (RuBisCO), is responsible for

incorporating CO_2 into RuBP, ultimately forming sugar phosphates in the light independent reactions (Hoober, 1989).
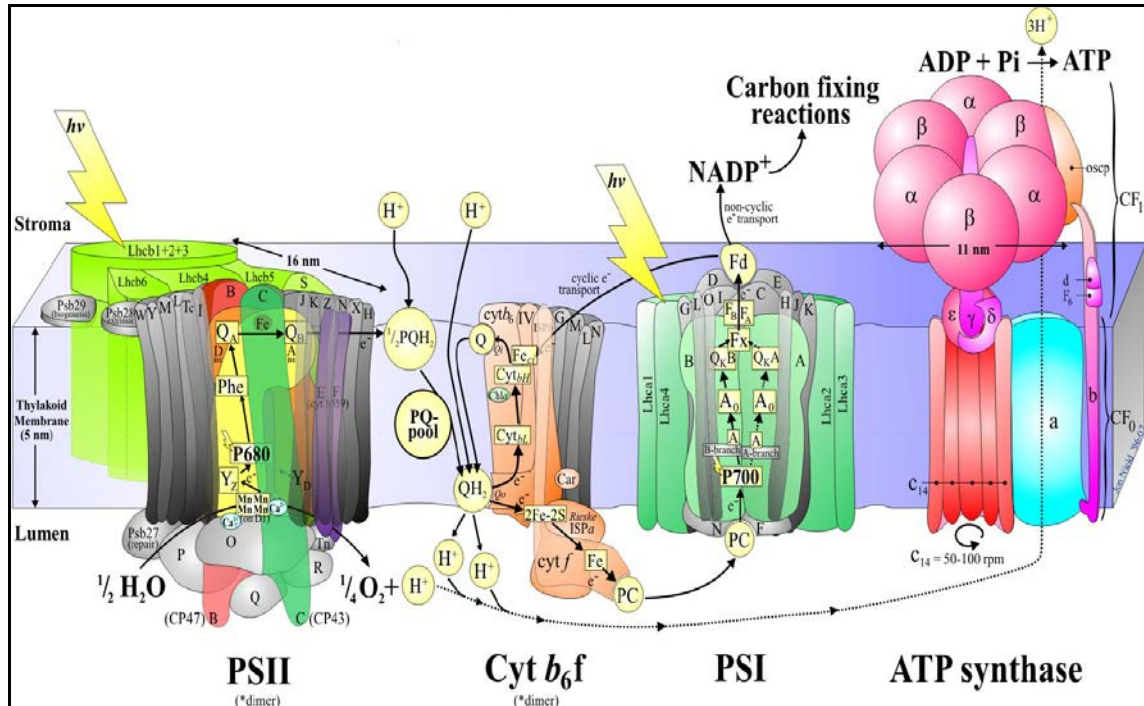
Figure 1.1 Schematic representation of the four complexes *viz.,* PS II, Cyt b$_6$f, PS I and ATP synthase of the thylakoid membrane (adapted from Hoober (1989)).

1.1.2   Light-independent reactions

In a light-independent series of reactions which occur in the stroma of the chloroplasts, when the products of the light reaction, ATP and NADPH, are used to make carbohydrates from carbon dioxide (reduction); initially glyceraldehyde 3-phosphate (a 3-carbon atom molecule) is formed.

1.2. Membrane complexes of the thylakoid membrane

1.2. 1. Photosystem II-Light harvesting complex II (PSII-LHCII)

The core of the PSII reaction center (RC) consists of a heterodimer of the proteins D1 and D2, encoded by the chloroplast *psbA* and *psbD* genes respectively, surrounded by two chlorophyll *a*-binding proteins CP43 (*psbC* gene) and CP47 (*psbB*), and several proteins of lower molecular weight, including cytochrome *b* 559 (*psbE* and *psbF*). Peripheral to this core are a monomeric antenna comprising the chlorophyll *a/b*-binding CP29 and CP26 proteins and a major trimeric antenna of LHCII proteins. Excitation energy is transferred from CP43 and CP47 to the core reaction center, where charge separation occurs in chlorophyll P680 (Hoober, 1989).

LHCI and LHCII designate the light-harvesting antennae of PSI and PSII, respectively. Within each of these groups, the proteins are identified as Lhca (LHCI complex) or Lhcab (LHCII complex). These include proteins formerly known as Cab, for chlorophyll *a/b* binding. Sequences are similar enough among the various LHC proteins to suggest a common origin. The LHCI and LHCII complexes collect light energy for photosynthesis and can also regulate the amount of light energy that is transferred to the photosystems.

1.2.2. Cytb$_6$/f complex

The cyt *b$_6$/f* complex is functionally a plastoquinol‑plastocyanin reductase, and is the intermediate between PSII and PSI. It is evolutionarily related to the respiratory *bc1* complex, and comprises four large and four small subunits. The major proteins are cytochrome *f*, cytochrome *b6*, the rieske iron sulphur protein, and a protein known as

subunit IV. The cyt*b6/f* complex can also participate in cyclic electron transport with plastoquinone and Photosystem I (Hoober, 1989).

1.2.3. PSI-LHCI supercomplexes

Structurally, plant PSI consists of two membrane complexes: the core complex, also referred to as the RC complex, where the bulk of the light capturing and the charge separation reaction take place. The light-harvesting complex I (LHCI), which serves as an additional antenna system that maximizes light harvesting by collecting solar radiation and transmitting the energy to the core complex (Chitnis, 2001). The supercomplex is composed of 17 currently known protein subunits (PsaA to L, N and P are known as PSI core subunits and Lhca1 to 4 are known as LHCI subunits) and approximately 193 non-covalently bound cofactors spread between the core complex and the LHCI in higher plants (Amunts et al., 2010) where as *C.reinhardtii* PSI-LHCI is much larger than higher plant, which contain 23 subunits (PsaA to L, N and O and Lhca1 to 9 LHCI subunits) and 260 noncovalently bound cofactors spread between the core complex and the LHCI. Till now 9 LHCI identified in *C.reinhardtii* (Takahashi et al., 2004) but it reported to consists of 14 LHCI subunits which are identified by electron microscopy (Germano et al., 2002). Thus, unicellular green algae, whose lineage diverged from land plants over 1 billion years ago, LHCI is about three times larger than that of higher plants. The important functions of the core subunits were shown with their function in Table 1.1.

Table 1.1. Photosystem I subunits and their function

Protein	Molecular mass (kDa)*	Cofactors	Function
PsaA	83.2	$\approx$ 79 Chl a, β-carotene, P700, A_0, A_1, F_X	Both PsaA and PsaB bind P700, the primary electron donor of PSI, as well as the electron acceptors A_0, A_1 and F_X. PSI is a plastocyanin-ferredoxin oxidoreductase, converting photonic excitation into a charge separation, which transfers an electron from the donor P700 chlorophyll pair to the spectroscopically characterized acceptors A_0, A_1, F_X, F_A and F_B in turn. Oxidized P700 is reduced on the lumenal side of the thylakoid membrane by plastocyanin
PsaB	82.5		
PsaC	8.9	F_A, F_B	Apoprotein for the two 4Fe-4S centers F_A and F_B of PSI; essential for photochemical activity. F_B is the terminal electron acceptor of PSI, donating electrons to ferredoxin. The C-terminus interacts with psaA/B/D and helps assemble the protein into the PSI complex. Required for binding of psaD and psaE to PSI. PSI is a plastocyanin-ferredoxin oxidoreductase, converting photonic excitation into a charge separation, which transfers an electron from the donor P700 chlorophyll pair to the spectroscopically characterized acceptors A_0, A_1, F_X, F_A and F_B in turn
PsaD	17.9/17.7		PsaD can form complexes with ferredoxin and ferredoxin-oxidoreductase in PSI reaction center. PsaD may encode the ferredoxin-docking protein
PsaE	10.4/10.5		Stabilizes the interaction between psaC and the PSI core, assists the docking of the ferredoxin to PSI and interacts with ferredoxin-NADP oxidoreductase
PsaF	17.3		Participates in efficiency of electron transfer from plastocyanin to P700 (or cytochrome c553 in algae and cyanobacteria). This plastocyanin-docking protein contributes to the specific association of plastocyanin to PSI.
PsaG	11	1 Chl a 1–2 β-carotene	Binding of Lhca1/4 and regulation of PSI
PsaH	10.4/10.4	1 Chl a	Binding of LHCII (state transitions) and

			stabilization of PsaD
PsaI	4.1		Stabilization of PsaL
PsaJ	5	2 Chl a	Stabilization of PsaF
PsaK	8.5	2 Chl a	Binding of Lhca2/3
PsaL	18	3 Chl a	Stabilization of PsaH and PsaO
PsaN	9.7		Docking of plastocyanin
PsaO	10.1		Binding of LHCII (state transitions)
PsaP			Not known

* The predicted molecular mass of the mature *Arabidopsis* protein is indicated. The predicted masses are for the apoproteins without cofactors. Cleavage sites for signal and transit peptides were predicted by alignment with homologous sequences with known cleavage sites from other species.

Among the PSI core proteins only PsaA, B, and C are directly involved in binding the electron transport cofactors P700 (a chlorophyll dimer), A_0 (a chlorophyll a molecule), A_1 (a phylloquinone), Fx (a [4Fe–4S] iron–sulfur cluster), F_A and F_B (both [4Fe–4S] iron–sulphur clusters). The remainder of the protein subunits fulfil other functions: PsaF and PsaN are important for interaction with the lumenal electron donor plastocyanin; PsaD and PsaE provide the docking site for soluble ferredoxin on the stromal side of the thylakoid membrane (Fromme et al., 2001; Jordan et al., 2001; Jensen et al., 2007). The existence of a Chl *a/b* antenna specifically associated to higher plants PSI containing four polypeptides with molecular mass between 20 and 24 kDa as belonging to LHCI of PSI (Mullet et al., 1980). LHCI was later isolated in two different pigment–protein fractions: one, monomeric, was enriched in Lhca2 and Lhca3 while another, dimeric, contained Lhca1 and Lhca4 (Lam et al., 1984). According to their emission peaks at low temperature, the two fractions were named LHCI-680 and LHCI-730 respectively (Knoetzel et al., 1992; Tjus et al., 1995).

1.3   Importance of iron deficiency and its relation to the PSI-LHCI supercomplexes

Among the abiotic stresses, iron deficiency constitutes a major factor leading to reductions in crop yield. Although iron (Fe) is the fourth most abundant element in the earth's crust, its low bioavailability makes it a limiting nutrient for life. Most living organisms require iron for growth and reproduction, and the iron absorbed by plants constitutes a major iron source for animals and humans. Although iron is abundant in soils, however, it is sparingly soluble under aerobic conditions at high pH. Consequently, in calcareous soils, which constitute ~30% of the world's cultivated soils, plants often exhibit iron deficiency symptoms manifested as chlorosis (yellowing caused by chlorophyll deficiency), reducing crop yield and quality. Chlorosis is the earliest symptom to occur in the course of iron deficiency (Price, 1968). In photosynthetic organisms, the major symptom is chlorosis (chlorophyll deficiency), mainly on young leaves, which is concomitant with decreased abundance of the photosynthetic machinery (Spiller and Terry, 1980). Iron deficiency stress is correlated with changes in chloroplast ultrastructure, decreased expression of the small and large subunits of rubisco, and of chlorophyll a/b-binding proteins, as well as decreased chlorophyll synthesis (Spiller et al., 1987; Winder and Nishio, 1995; Belkhodja et al., 1998). Chlorosis has been usually attributed to inhibition of chlorophyll synthesis, which requires the function of iron containing enzymes. In nature, iron is mostly found as stable Fe^{3+} oxides, which are insoluble in aerobic environments at biological pH (Guerinot and Yi, 1994). Iron deficiency is a common disorder affecting crop plants world-wide. This problem has a great economic significance for plant production (Fernandez and Ebert, 2003).

Engineering crops to release more iron-solubilizing chelators may increase their yield in alkaline soils. Iron is one of three nutrients (nitrogen and phosphorus are the others) that most commonly limit plant growth (Guerinot, 2001).
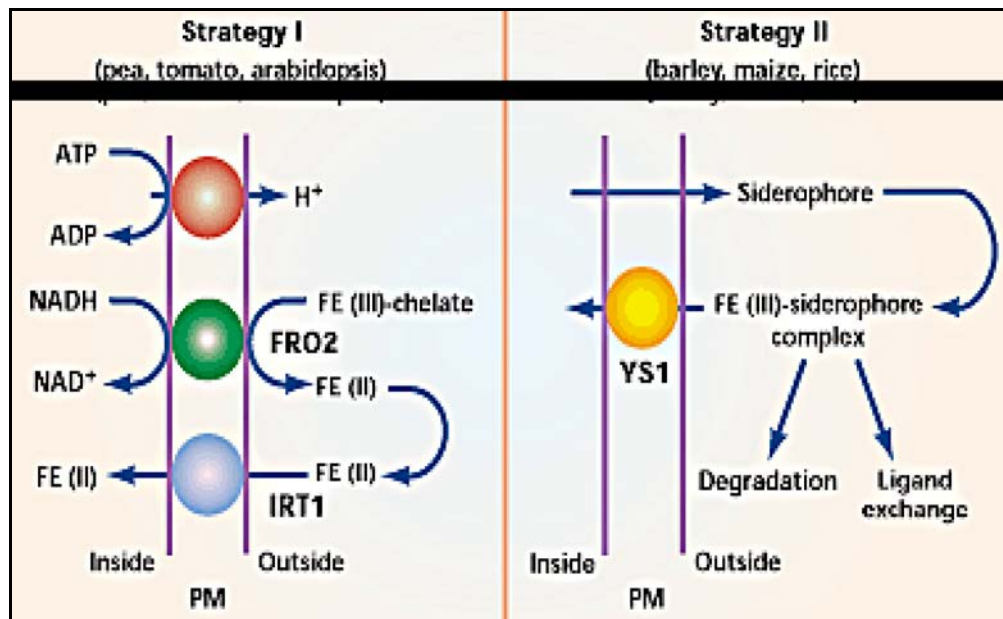
Figure 1.2 Uptake of iron by plants. Strategy I plants reduce Fe (III) to Fe (II), which is then transported across the plasma membrane. Strategy II plants release Fe(III) chelating siderophores and then transport Fe (III)–siderophore complexes across the plasma membrane. Ligand exchange and degradation are alternative fates for the Fe (III) complex. FRO2, ferric reductase-oxidase 2; IRT1, iron-regulated transporter 1; YS1, yellow stripe 1 (adapted from (Guerinot, 2001)).

Plants respond to iron deprivation by inducing a series of physiological and morphological responses to counteract the nutrient deficiency. These responses include: (i) the acidification of the extracellular medium, (ii) the reduction of ferric ion and (iii)

the increased transport of ferrous ion inside of root cells. Plants have developed two strategies for high-affinity iron uptake (Curie and Briat, 2003; Grotz and Guerinot, 2006). Dicots and non-graminaceous monocots use strategy I (or reduction strategy) where the soil is acidified by H^+ ATPases to solubilize iron, Fe(III) is reduced by ferric chelate reductases, and Fe(II) uptake is mediated by IRT1, a protein of the ZIP family. On the other hand, grasses use strategy II (or chelation strategy) where phytosiderophores (*i.e.*, high-affi nity Fe(III) chelators) are released, and Fe(III) chelates are subsequently taken up by the YS1 transporter, a member of the OPT family (Curie et al., 2001; Guerinot, 2001) (Figure 1.2). The Strategy II mechanism is specific to graminaceous plants and is mediated by natural iron chelators, the mugineic acid family phytosiderophores (MAs) (Itai et al., 2000).

Iron's control on photosynthetic systems has been well documented by the stimulation of algal blooms following the addition of nanomolar concentrations of iron to several open ocean locations that receive very low natural iron inputs. Besides oceanic plankton communities, iron-deficiency has been well documented in plants and in heterotrophs. Organisms have developed complex systems for iron acquisition and for adjusting their biochemistries to survive in low iron environments (Philpott, 2006; Walker and Connolly, 2008). The majority of iron in algae and plants is believed to be associated with the chloroplast (Briat et al., 2007). In oxygenic photosynthesis, iron is a cofactor in PSII, PSI, the cyt b_6/f complex, and in algae, cyt *c6* as well. PSI seems to be a focus during iron limitation, due to its high iron content (12 Fe per PSI) (Sandmann and Malkin, 1983). A reduction in the number of reaction centres decreases the ability of the photosynthetic apparatus to use light energy, and iron-limited algae and cyanobacteria show decreased PSII function, inter-photosystem electron transport,

carbon fixation rates, and ultimately decreased growth (Vassiliev et al., 1995; Ivanov et al., 2000). The effect of iron deficiency on PSI was not studied well and it is one of the prime target for iron deficiency (Naumann et al., 2005). To compensate for the change in the abundance of photosystems, cyanobacteria modify their remaining PSI to maximize light harvesting while minimizing photooxidative damage (Kouril et al., 2005). The global impact of iron deficiency on photosynthetic productivity has been shown in vast ocean regions that are severely limited in iron (Behrenfeld and Kolber 1999).

1.4 *Chlamydomonas reinhardtii*

C.reinhardtii belongs to Kingdom: **Protistae**, Division: **Chlorophyta**, Class: **Chlorophyceae**, Order: **Volvocales**, Family: **Chlamydomonadaceae**, Genus: **Chlamydomonas**, Species: *C. reinhardtii.* It is a motile single celled green alga about 10 µm in diameter that swims with two flagella (Figure 1.3)*.* These algae are commonly found in soil and fresh water. They have a cell wall made of hydroxyproline-rich glycoproteins, a large cup-shaped chloroplast, a large pyrenoid, and an "eyespot" that senses light. Normal chlamydomonas can grow on a simple medium of inorganic salts in the light, using photosynthesis to provide energy. They can also grow in total darkness if acetate is provided as a carbon source. *C. reinhardtii* in the green plant lineage, is a reference organism for the study of chloroplast metabolism and photosynthesis (Harris, 2001; Rochaix, 2002). This unicellular alga can grow photo-trophically in the light, hetero-trophically with acetate in the dark, or mixo-trophically on acetate in the light. *C.reinhardtii* has emerged as the predominant laboratory species of *Chlamydomonas*, primarily owing to its ability to grow non-photosynthetically with acetate as its sole carbon source (Harris, 2001). A single cup-shaped chloroplast occupies the basal two

thirds of the cell and partially surrounds the nucleus. Thylakoid membranes are arranged in well-defined appressed and non-appressed domains whose composition and functional organization have been extensively investigated in wild-type and mutant strains of Chlamydomonas. A distinctive body within the chloroplast, the pyrenoid, is the site of CO_2 fixation and the dark reactions of photosynthesis (Harris, 2001).
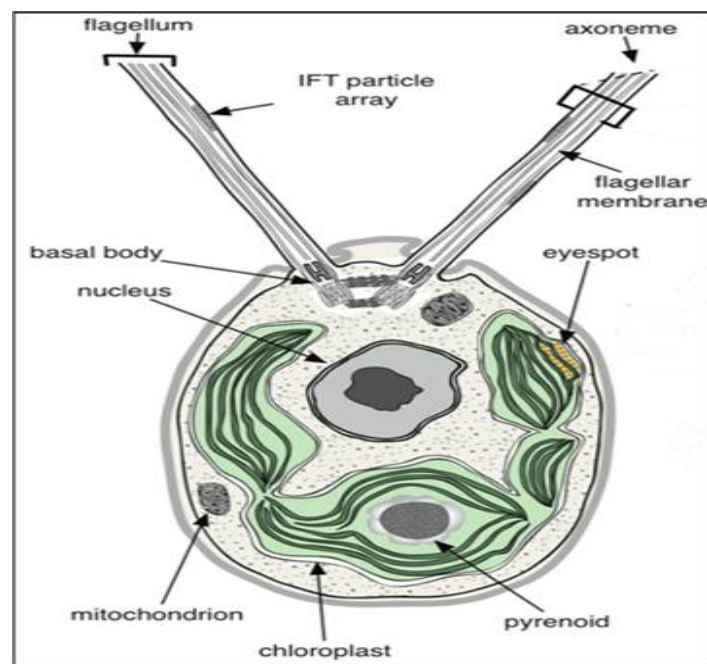
Figure 1.3 Chlamydomonas cell from transmission electron micrographs. Adopted from Merchant et al (2007).

In the present study *C. reinhardtii* strain WTCC125 used as a model organism for studying strategy I mechanism of iron uptake (Hoober, 1989) to study the effect of iron deficiency on PSI-LHCI supercomplexes by biochemical and proteomic aspects. Iron-limited cultures are visibly chlorotic owing to the programmed destruction of reaction centers and LHCIs (Moseley et al., 2002; Naumann et al., 2005). The structure

of PSI-LHCI supercomplexes were different than that of higher plants especially in LHCI subunit content. Unlike higher plants, *C.reinhardtii* have an additional five LHCI subunits also exist which are identified by proteomic approach as well as electron microscopy observations showing the complexity of light harvesting proteins at the protein level (Stauber and Hippler, 2004; Dekker and Boekema, 2005). The arrangement of LHCI subunits in higher plants is Lhca1, Lhca4, Lhca2 and Lhca3 flanking the core subunits (Amunts et al., 2007), in case of *C.reinhardtii* the sequential arrangement of nine LHCI subunits are not known (Figure 1.4).
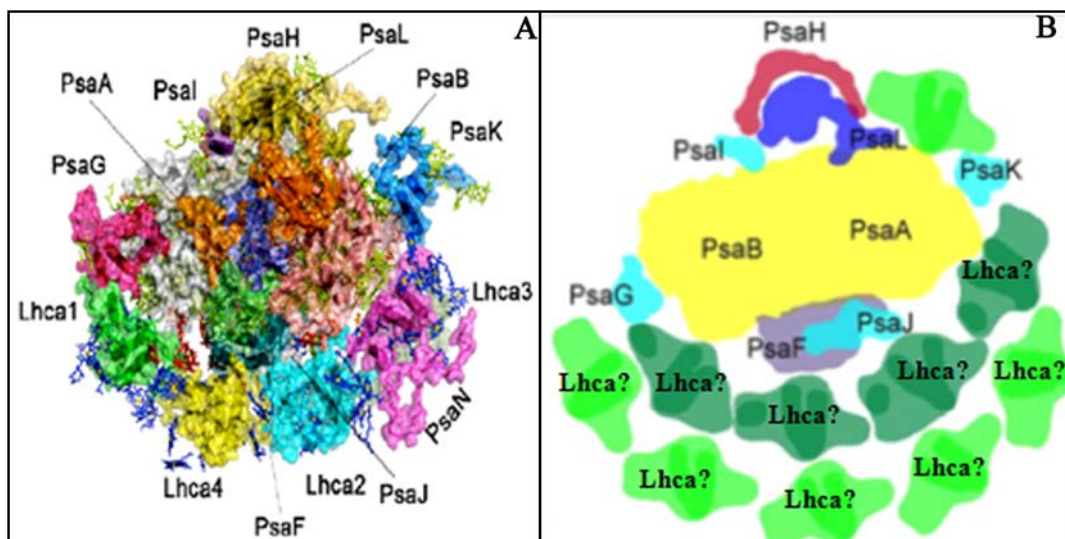
Figure 1.4 Comparison of PSI-LHC1 supercomplexes present in (A) higher plants and (B) Chlamydomonas. Adopted from (Dekker and Boekema, 2005; Amunts et al., 2010).

In order to understand the function and structure of PSI-LHCI supercomplexes in *C.reinhardtii*, it is necessary to obtain the structural information. However, obtaining the crystallographic structures of *C.reinhardtii* PSI-LHCI supercomplexes is highly difficult as its complexity nature (Stauber et al., 2009). Apart from the PSI-LHCI

structure, there are no antibodies are available for studying the affect of iron deficiency on PSI-LHCI supercomplexes. Therefore, peptide tag antibodies were developed against LHCI subunits of *C.reinhardtii* for understanding protein expression levels under iron deficiency conditions.

1.5   Rice (*Oryza sativa* L.)

Rice (*Oryza sativa* L.), is a cereal food crop that belongs to the grass family (Family: Poaceae) of the plant kingdom. It is the most important staple food for a large part of the world's human population. Although it can grow in diverse environments, it grows faster and more vigorously in wet and warm conditions. It is the grain with the second-highest worldwide production, after maize. Iron deficiency is widespread problem in developing countries. In particular, children appear to be much more deficient in iron. Under aerobic conditions and neutral or alkaline pH, iron often forms highly insoluble ferric-hydroxide precipitates that limit its availability for plants (Guerinot and Yi, 1994). Unlike other nutrient limitations, however, iron deficiency cannot be remedied through the use of fertilizers because the problem is not one of abundance, but rather one of solubility (Guerinot, 2001). Graminaceous plants secrete MAs from their roots to solubilize rhizospheric Fe(III). Subsequently Fe(III)–MAs complexes are taken up through the Fe(III)–MAs transporter, YS1(Curie et al., 2001). Rice varieties are low in iron and are highly susceptible to iron deficiency (Datta et al., 2003). Fe is an essential micronutrient for plant growth, which promotes the absorption of other nutrient elements by phytoplankton (Tsuda et al., 2003) and is crucial to electron transport, photosynthesis, and respiration in the process of phytoplankton growth. Under nutrient deprivation, plant cells undergo extensive metabolic changes for

their continued survival (Sperotto et al., 2007). The iron in chloroplasts is mainly constituted of plant iron protein, cytochrome, Fe-S protein, and hemoglobin. Fe deficiency caused injury to chloroplast ultramicrostructure, the decrease of granum and the lamellae of granum thylakoids, and a confused arrangement of granum and stroma thylakoids. Serious iron deficiency result in the dissociation and vacuolation of chloroplasts, and in the formation of chlorophyll (Curie et al., 2001).

The rice structure of PSI is similar to the published crystal structure of higher plants (Amunts et al., 2010). Antibodies for the PSI and LHCI subunits were commercially available (Agrisera, Sweden). Therefore, I directly proceeded to biochemical and proteomic studies to understand the PSI-LHCI complexes under iron deficiency conditions.

1.6   Objectives of the study

❖   **3D modeling of *C.reinhardtii* photosystem I (PSI)- light harvesting complex (LHCI) supercomplexes**

❖   **Development of peptide tag antibodies against *C. reinhardtii* LHC I subunits**

❖   **Proteomic and biochemical characterization of PS I-LHC I supercomplexes under iron deficiency *in C. reinhardtii***

❖   **Protein level changes of photosystem I under iron deficiency in *Oryza sativa***

3D modelling of PSI-LHCI supercomplexes of *C. reinhardtii*

Chapter 2

2.1 Introduction

Photosynthesis is the process where energy from sunlight used to produce energy in the plants, algae and some bacteria by means of two large protein complexes located in the thylakoids membranes: PSI and PSII (Scheller et al., 2001; Nelson and Ben-Shem, 2004; Jensen et al., 2007). Photosynthesis occur in thylakoid membranes catabolised by several multimeric membrane supercomplexes that include PSI, PSII, their associated light harvesting complexes, Cyt b_6f complex and ATP synthase (Loll et al., 2005; Nelson and Yocum, 2006). They harvest the sunlight through extended antenna systems and use the energy to excite the primary electron donors (P700 at PSI and P680 at PSII), each releasing one electron per reaction cycle. These electrons are translocated across the thylakoid membrane along organic and inorganic cofactors, known as the electron transfer chains (ETCs) (Saenger et al., 2002).

The structure of PS II reaction centres from purple photosynthetic bacteria, *Rhodopseudomonas* viridis at 3.0 Å (Deisenhofer et al., 1985), *Rhodobacter sphaeroides* at 2.5 Å (Camara-Artigas et al., 2002) and at 2.8 Å (Allen et al., 1987; Allen et al., 1988) provided a blueprint that has guided for the subsequent crystallographic models (Heathcote et al., 2003). Crystal structure of PS II has been reported at resolutions from 3.8 to 2.9Å from *Thermosynechococcus vulcanus* (Kamiya and Shen, 2003; Muh et al., 2008). Recently PS II from another species of Thermococcus *i.e. Thermococcus elongates* at 3.6 Å gave much information. The monomer of its PS II have, 19 protein subunits, 35 chlorophylls, two pheophytins, the non-heme iron, the primary plastoquinone Q(A), two heme groups, eleven beta-carotenes, 22 lipids, seven detergent molecules and the Mn(4)Ca cluster of the water oxidizing complexes (Broser et al., 2010). However, very recent PSII structure at 1.9 Å

reveals in detail structure includes the site of photosynthetic water oxidation and contains 20 subunits with a total molecular mass of 350 kDa. Also, they have provided much information on the arrangement of protein subunits and cofactors but are insufficient to reveal the detailed structure of the catalytic centre of water splitting (Umena et al., 2011).

PSI is the most efficient photoelectric apparatus exhibiting a quantum efficiency of almost 100% in its utilization of light for electron transport (Fromme et al., 2001; Nelson and Yocum, 2006; Amunts et al., 2010). The structure of plant PSI supercomplex comprises of core subunits and light harvesting complexes, chlorophylls, phylloquinones and Fe_4S_4 clusters (Ben-Shem et al., 2003; Jensen et al., 2007). PSI catalyzes the light-driven electron transfer from the soluble electron carrier plastocyanin, located at the lumenal side (inside) of the thylakoid membrane, to ferredoxin at the stromal side (outside) of the natural photosynthetic membrane. The crystal structure of photosystem I resolved at 2.5 Å from the thermophilic cyanobacterium *Synechococcus elongatus* have 12 protein subunits and 127 cofactors comprising 96 chlorophylls, 2 phylloquinones, 3 Fe_4S_4 clusters, 22 carotenoids, 4 lipids, a putative Ca^{2+} ion and 201 water molecules (Jordan et al., 2001). Cyanobacterial Photosystem I is a trimer consisting of 36 proteins to which 381 cofactors are non-covalently attached. Later crystal structure of PSI from Pea at 4.4 Å resolution comprises of 12 core subunits, 4 different light-harvesting membrane proteins (LHCI) assembled in a half-moon shape on one side of the core, 45 transmembrane helices, 167 chlorophylls, 3 Fe-S clusters and 2 phylloquinones (Benshem et al., 2004). Further an improved crystallographic model at 3.3 Å resolution yielded identification and tracing

of subunit PsaK, an additional 10 ß-carotenes as well as 5 chlorophylls and several loop regions, are now modelled (Amunts et al., 2010).

The structure of PSI supercomplexes is highly conserved between cyanobacteria and higher plants, which acts as a light driven plastocyanin-ferridoxin-oxidoreductase contained several nucleate and chloroplast encoded subunits (Fyfe et al., 2002; Rochaix, 2002). *C.reinhardtii* is used as model organism for studying the photosynthesis because it doubles its cell number in 5-7 h, when grown on acetate and completes its sexual cycle in less than two weeks, genetic analysis is rapid and efficient transformation methods has been established for nuclear and chloroplast compartments (Grossman, 2000; Harris, 2001; Rochaix, 2002). Unlike angiosperms, it grows in the dark on an organic carbon source while maintaining a functional photosynthetic apparatus (Merchant et al., 2007).

The structure of *C.reinhardtii* PSI-LHCI supercomplexes were not well understood because of its complexity. Unlike higher plants, *C.reinhardtii* have an additional five LHCI subunits exist which are identified by proteomic approach as well as electron microscopy observations showing the complexity of light harvesting proteins at the protein level (Hippler et al., 2001; Stauber et al., 2003; Stauber and Hippler, 2004; Dekker and Boekema, 2005; Mozzo et al., 2010). The arrangement of LHCI subunits in higher plants is Lhca1, Lhca4, Lhca2 and Lhca3 flanking the core subunits, in case of *C.reinhardtii* the sequential arrangement of nine LHCI subunits is not known. In addition, the association and structural integrity of LHCI subunits with PSI core is not understood very well in *C.reinhardtii*. In order to understand the function and structure of PSI-LHCI supercomplexes in *C.reinhardtii*, it is necessary to obtain the structural information. However, obtaining the crystallographic structures of *C.reinhardtii* PSI-

LHCI supercomplexes is highly difficult due to its complexity nature (Stauber et al., 2009). Thus, based on the crystallographic model of improved plant PSI model, a 3D model was built. Computational protein structure modeling techniques have the potential to bridge this sequence-structure gap. When a template structure with more than 40% sequence identity to the target protein is available, the model is likely to have about 90% of the main chain atoms modelled with an rms deviation from the X-ray structure of approximately 1 Å (Eswar et al., 2007). MODELLER is a program for comparative protein modelling by satisfaction of spatial restraints. The models have good stereochemistry and are at least as similar to the crystallographic structures as the closest template structures (Sali et al., 1995).

In this objective based on the crystallographic model of plant PS I at 3.4Å (Amunts et al., 2010) which contain PsaA to L and N core subunits and four LHCI subunits, 173 chlorophylls, 2 phylloquinones and 3 Fe_4S_4 clusters, a 3D model was bult by using Modeller 9v8. Protein-protein interactions were elucidated by both computational and experimental methods.

2.2 Materials and Methods

2.2.1 Protein sequences collection from expasy database

Protein sequences for *C.reinhardtii* PSI-LHCI were collected from expasy sequence database (Gasteiger et al., 2003). The sequences consists of core PSI subunits containing different chains *viz.,* PsaA to L, N and O and nine light harvesting complex polypeptides (LHCI) *viz.,* Lhca1 to 9 (Appendix I). All these sequences were used for

building the 3D model. Here after *C.reinhardtii* PSI-LHCI sequences were referred to as 'Target sequence'.

2.2.2 Template search by using BLAST

Target sequences were used for getting the template that have detectable similarity to the target sequence by using BLAST (Altschul et al., 1990). All the sequences were taken as a single FASTA format file where in each chain has been separated and scanned against a library of sequences extracted from known protein structures in the Protein Data Bank (PDB) to find the templates. Structural information of proteins are available in the PDB structure database (Deshpande et al., 2005), an international repository for crystal structure proteins.

2.2.3 Target : Template pair wise sequence alignment by using CLUSTALW

The most significant step of a 3D model process is to obtain the correct sequence alignment of the target sequence with the homologues. All chains of both target and templates with their highest percentage of identity were individually aligned in CLUSTALW (Thompson et al., 1994). The output file was in the PIR format of target and template sequence alignment. The target sequences were aligned with template (2WSC) sequence. Here after, 2WSC was referred to as 'template sequence'. All the target sequences were put together manually to make a single long chain of 5325 residues separated by "/" symbol at the end of each chain in order from Lhca1-9, and then PsaA to N (except PsaM which doesn't exist in algae). All the template sequences which were aligned in CLUSTALW were manually set with appropriate gaps to model them using multi chain and multi template combo modeling wherein each chain of target sequence would be derived from its corresponding template sequence. The output

alignment of multiple sequences was exported to .ali and .pap of the previous PIR and PAP formats, respectively. The individual alignments generated were merged both in a way that all the target sequences were combined to form a single complex of multiple subunits with more than 5000 residues and sequences of individual subunits of templates were kept as the whole alignment made for multi template modeling.

2.2.4   Loop modelling

PsaO core subunit of *C.reinhardtii* was unique for which similarity was not found with any of the template sequence. Threading method is the better choice to build a model for such subunit, wherein threading uses not only the alignment of the sequence but it carries out the fold recognition of query sequence with respect to the fold of several templates available in threading server. This mechanism was carried out by calculating the force fields of the individual residues available in sequence with the force fields of all available structures in the server threading database and co-ordinates. Best model out of all possible outputs on forcefield calculations were selected based on cumulative results of statistically accepted highest value that is z-score and scores generated by both global and local alignment methods. Threading model was carried out by submitting the sequences to WURST threading server situated at Hamburg University (Torda et al., 2004). Gaps in the alignment may also be due to deletions or insertions with no structural information derived from template structure, such gaps were filled by WURST threading server.

2.2.5   3D modelling

Best aligned target sequences to the template sequences were used for building the 3D model. 3D models containing all nonhydrogen atoms were automatically

obtained using the method implemented in MODELLER 9v8. 3D modelling of aligned file, which contains 5289 amino acid residues, was run on Modeller 9v8 version (Sali et al., 1995). Homology modelling procedure relies on rules of spacing between atoms, bond lengths, bond angles, dihedral angles, etc. This information was extracted from the template by using spatial restraints by MODELLER 9v8.

2.2.6 Model evaluation

The details of each model which are generated by Modeller were present in the log file that contain a summary of each calculation at the bottom of the file with, the DOPE (Discrete Optimized Protein Energy) pseudo-energy value and the value of the GA341 score. These scores can be used to identify the most accurate model. The geometrical parameters of the created models were evaluated and compared with those obtained for the native structure of the templates using the PROCHECK (Laskowski et al., 1993). PDBsum structural tool was used for studying the protein-protein interactions among PSI-LHCI supercomplexes (Laskowski et al., 1997; Laskowski et al., 2005). Hydrogen bonds interaction of LHCI subunits with other subunits were determined using 'chimera' tool (Kostek et al., 2006).

2.2.7 Separation of LHCI from PSI core of PSI-LHCI supercomplexes

C.reinhardtii cells were grown under continuous light at 50µmol m^{-1}s^{-1}. PSI-LHCI supercomplexes were isolated as previously described (Subramanyam et al., 2006; Subramanyam et al., 2010). From the sucrose density gradient centrifugation three bands were separated after 16 h spin at 1,80,000 xg in which lowest band was considered as PSI-LHCI supercomplexes as described previously (Subramanyam et al., 2006). Thus, the lowest band was collected and diluted with three volumes of 5 mM

Tris–HCl pH 8.0, 0.05% β –Dodecyl Maltoside (β-DM), 5 mM $CaCl_2$. The diluted samples were then concentrated using a Centricon 100 ultra filtration device (Amicon, Beverly, MA, USA) at 4,000 xg in a Sorvall SS-34 rotor at 4°C. These PSI-LHCI supercomplexes were subjected to harsh detergent (0.5% β-DM) treatment to disrupt the protein-protein interaction among the supercomplexes and again centrifuged at 1,80,000 xg for 10 h.

2.3   Results

2.3.1   Percentage of similarity in PSI-LHCI supercomplexes between *C.reinhardtii* and higher plants (2WSC)

The sequence identity between target sequences and template sequences were from 36 to 85%. PSI core subunits of *C.reinhardtii* have 38 to 85% similarity with the template of 2WSC. Similarly, LHCI polypeptides of *C.reinhardtii* have 36 to 56% (Table 2.1) homology. 2WSC considered as the template for the PSI core subunits and Lhca1, Lhca2, Lhca3 and Lhca7 sequences. Among the all subunits, PsaA, PsaB, and PsaC were most identical and shown 100% sequence coverage with template. These three subunits were highly conserved among several species.

2.3.2   Arrangement of LHCI subunits of *C.reinhardtii*

The individual LHCI polypeptides models of *C.reinhardtii* were built by using the LHCI subunits of template (Figure 2.1). The arrangement of Lhca1 to Lhca9 subunits in a sequential manner based on spatial restraints shown in Figure 2.2 suggests the unique arrangement which was entirely different from that of higher plants, where Lhca1 and 4 form one dimer and Lhca2 and Lhca3 form another dimer in a half moon

Table 2.1 Subunit identity of *C.reinhardtii* PSI-LHCI supercomplexes with template sequences and other important parameters.

Subunit	Template	% Identity	Query coverage	E-value	Total Score	Number of residues 2WSC*	*C.reinhardtii*
PsaA	2WSC A	84	100	0.0	1319	730	751
PsaB	2WSC B	80	100	0.0	1221	733	735
PsaC	2WSC C	85	100	5e-37	148	81	81
PsaD	2WSC D	60	94	1e-59	224	138	196
PsaE	2WSC E	71	56	2e-16	80.1	65	97
PsaF	2WSC F	51	93	7e-53	202	154	227
PsaG	2WSC G	38	74	2e-14	73.9	95	126
PsaH	2WSC H	40	76	3e-15	76.3	69	130
PsaI	2WSC I	63	25	4e-05	42.7	30	106
PsaJ	2WSC J	68	100	1e-10	61.2	42	41
PsaK	2WSC K	53	99	3e-23	102	84	113
PsaL	2WSC L	59	85	1e-40	162	161	196
PsaN	2WSC N	56	56	1e-21	97.4	85	139
Lhca1	2WSC 1	52	87	4e-50	193	165	228
Lhca2	2WSC 2	36	78	1e-32	135	176	246
Lhca3	2WSC 3	56	97	4e-83	303	162	267
Lhca4	2WSC 4	52	69	4e-47	184	166	264
Sequence Identity with threading models							
Lhc5	2o01A	98.2					
Lhc6	1gs5A	73.2					
Lhc7	1rwtA	87.5					
Lhc8	1epxA	85.2					
Lhc9	1bvuA	80.2					
PsaO	1dt3A	83.3					

*Higher plant photosystem I crystal structure (Amunts et al., 2010)

shape surrounding PSI core (Nelson and Yocum, 2006). The predicted arrangement of *C.reinhardtii* LHCI polypeptides in sequence as Lhca5, Lhca1, Lhca6, Lhca4, Lhca7, Lhca8, Lhca2, Lhca9, and Lhca3 based on spatial restraints by taking coordinates of the template. All these LHCI subunits shares significant homology with the higher plants
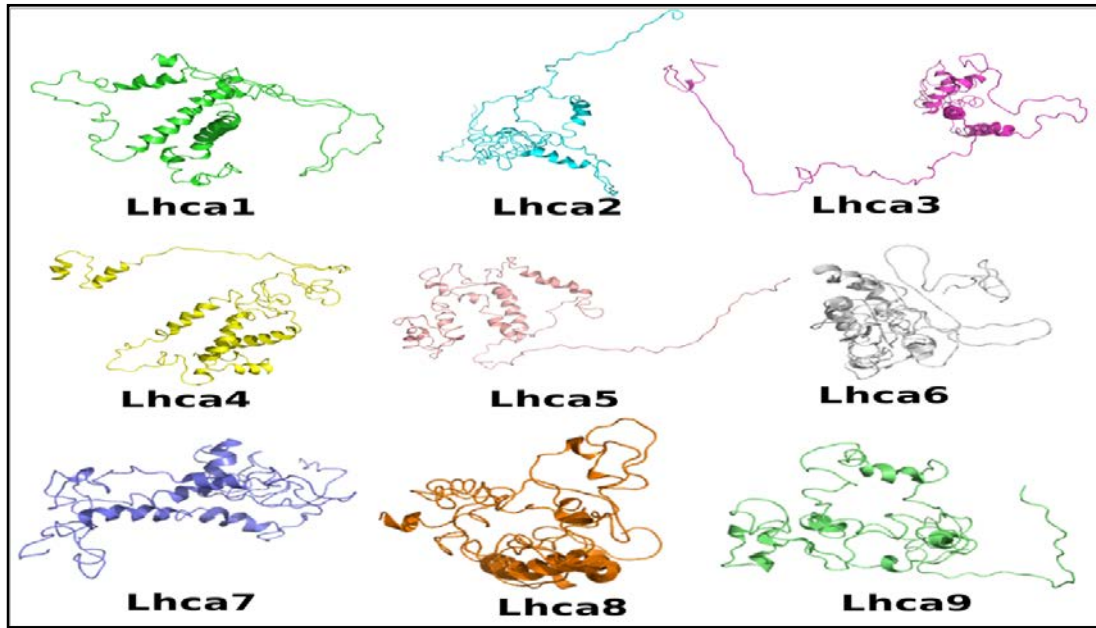
Figure 2.1 *C.reinhardtii* **LHCI individual subunits of 3D models Lhca1 to 9 were shown. Lhca1 to 4 were built based on the 2WSC template and Lhca 5 to 9 were built by threading model.**
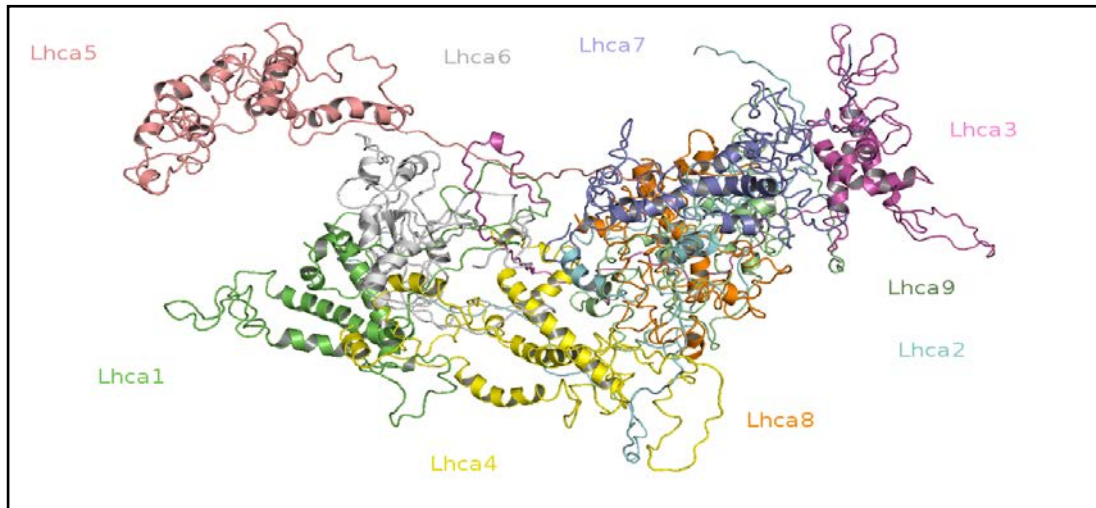
Figure 2.2 The arrangement of Lhca1 to Lhca9 of *C.reinhardtii* **based on spatial restraints of the Modeller9v8. The arrangement of LHCI subunits follows as: Lhca 5, Lhca 1, Lhca 6, Lhca 4, Lhca 7, Lhca 8, Lhca 2 Lhca 9 and Lhca 3.**

LHCI subunits. Among all LHCI subunits, Lhca6 and Lhca7 were exists inner side thus these have more interaction with PSI core subunits. The presence of extra LHCI may help in efficient light energy trapping mechanism and thus helps in maximum utilization of solar energy.

2.3.3 PSI core subunits of *C.reinhardtii*

There are 14 PSI core subunits existing in PSI core of *C.reinhardtii* among which 13 were identical to that of template and the extra subunit *i.e.,* PsaO subunit is unique in *C.reinhardtii*. Figure 2.3 shows the relative arrangement of all PSI core subunits. PsaA subunit of *C.reinhardtii* has two extra helical turns than the template and the location of this subunit is same as that of higher plants and cyanobacteria. PsaB subunit of *C.reinhardtii* have two helical turns less than that of template and having the same location as that of the template. PsaA and PsaB are the major subunits, which has the highest similarity to that of template positioned in the same location. PsaC subunit has same number of residues in both template and target sequence but PsaC has two extra helical turns than the template without any disulphide bridges, where as template has only one helical turn and one disulphide bridge. PsaE subunit exposed to stroma region in both cases and it has N-terminal extended region and two beta hairpins in case of *C.reinhardtii*. PsaF is one of the integral membrane protein located in the same region in both template and target. In addition, PsaF subunit of *C.reinhardtii* has two additional small helical regions. PsaH is located on stromal side like in higher plants and cyanobacteria.
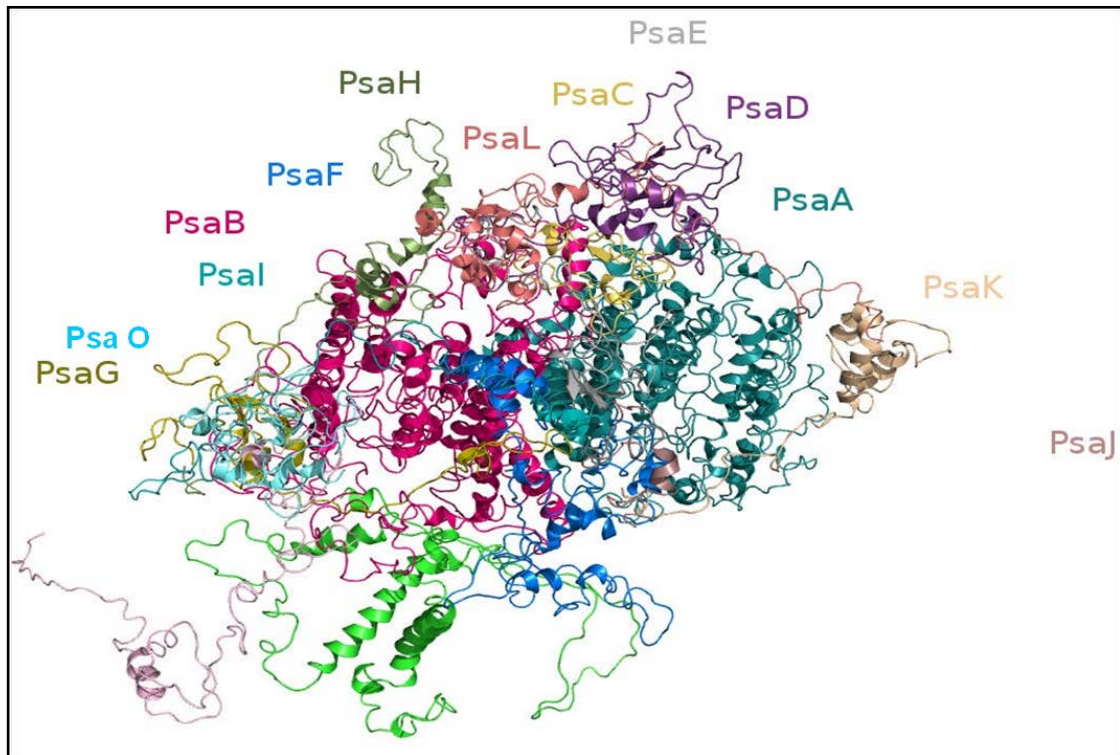
Figure 2.3 Homology model of PSI core subunits of *C reinhardtii* arranged based on higher plant model. PsaO subunit was located at PsaH, PsaI and PsaL subunits.
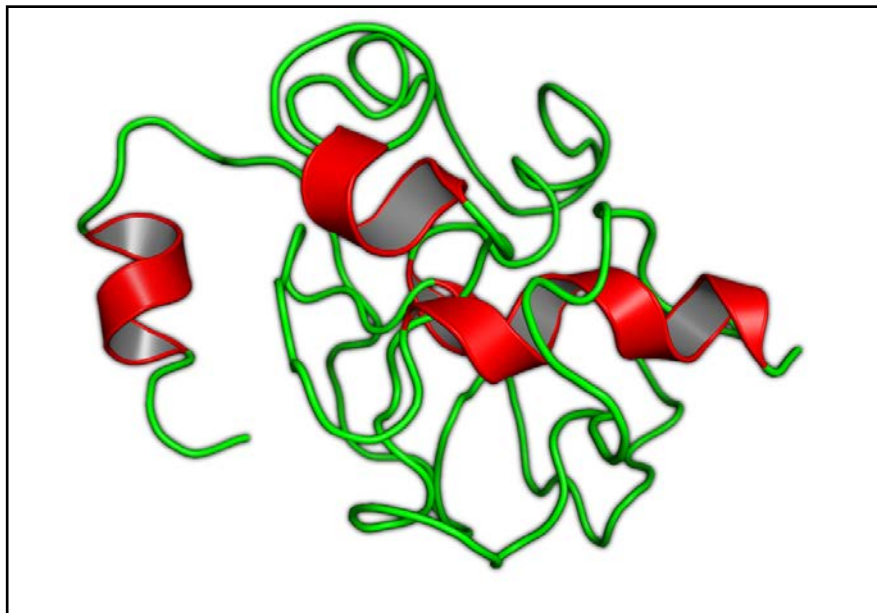
Figure 2.4 Threading model of PsaO subunit of *C.reinhardtii*. It contains three transmembrane helices.

PsaO subunit of *C.reinhardtii* built by threading model has three transmembrane helices and its position is located at PsaH, PsaI and PsaL core subunits (Figure 2.4). PsaO subunit has 126 amino acid residues, containing three helical regions and several β turns with three transmembrane helices. The location of PsaO subunit among the core subunits suggests that it may play a major role in state transition mechanism in *C.reinhardtii* and stabilization of PSI core.

2.3.4 Overall 3D structure of PSI-LHCI of *C.reinhardtii*

The overall arrangement of all PSI core subunits and LHCI subunits in *C.reinhardtii* and higher plants appears same especially with PSI core subunits. PSI core subunits such as PsaE, PsaF, PsaG, PsaI, PsaJ, PsaK, PsaN, and PsaO are closely associated with the LHCI subunits of *C.reinhardtii* (Figure 2.5).
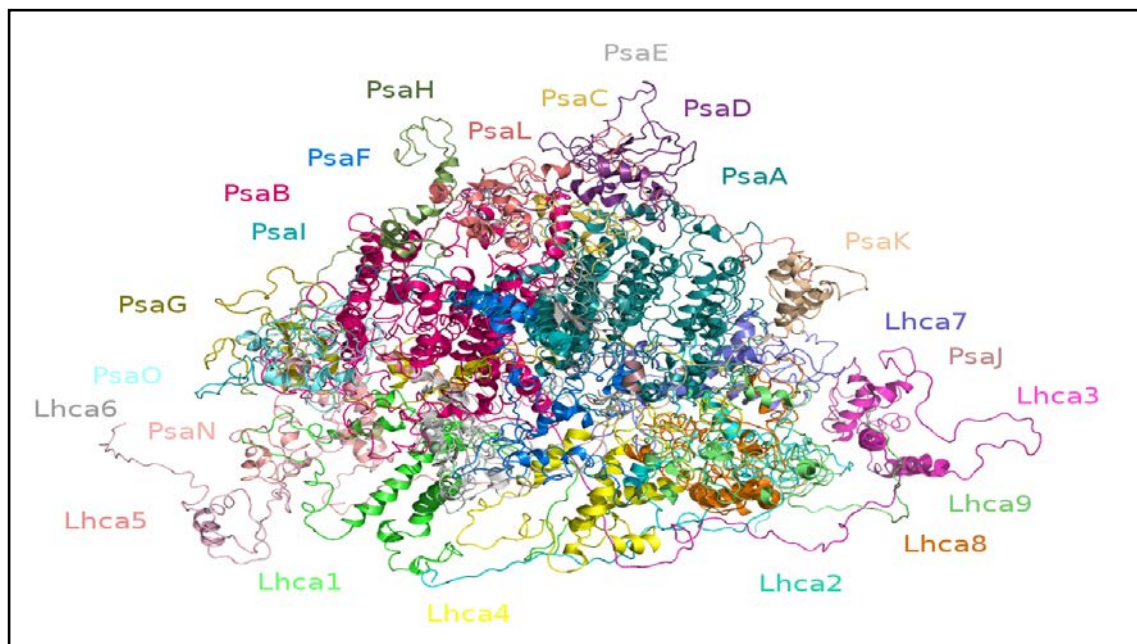
Figure 2.5 3D model of PSI-LHCI supercomplex of *C.reinhardtii*. The arrangement of LHCI subunits along the core in half-moon shape as that of higher plants. Lhca6 is localized towards the core.

2.3.5 Distribution of amino acid residues in the ramachandran plot and the quality of the 3D model

The results of PROCHECK analysis showed that most of the amino acid residues lie in the allowed regions (Figure 2.6 and Table 2.2). The total number of amino acid residues fall in to four major regions. Residues which are present in most favourable regions (A,B,L) constitutes 72.2% compare to the template of PDB 2WSC which accounts only 43.7% (Amunts et al., 2010). Residues in disallowed regions are very less about 3.7% of the 3D model PSI-LHCI supercomplex of *C.reinhardtii* compare to the 8.4% in the template of PDB 2WSC.
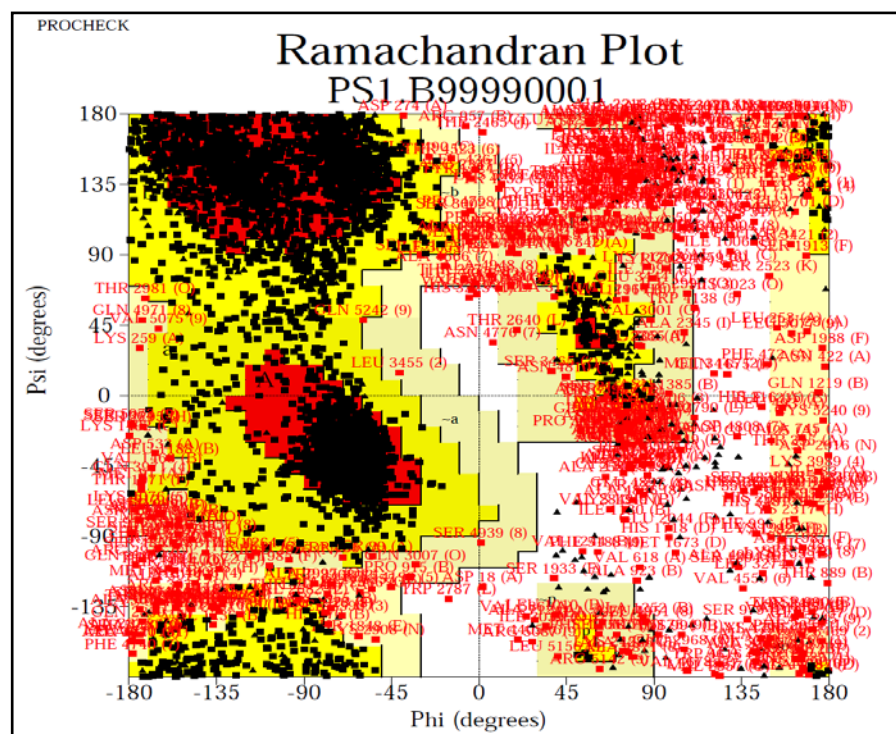
Figure 2.6 Distribution of amino acid residues in different regions by Procheck analysis using Ramachandran plot.

The R-factor most unusual value is -1.0, where the PSI-LHCI model built stands at -0.87 Å deviation indicates that the present model is better than the template structure (PDB:2WSC) which possess -0.9 Å deviation. Superimposed model with the template shared major part of co-ordinates and it was found that RMSD equals to 2.7, which was in a better state of existence and not deviating much from the main template. Thus, the model generated by Modeller 9v8 of PSI-LHCI supercomplexes of *C.reinhardtii* was the most reliable method for understanding the various structural domains.

Table 2.2 Ramachandran plot statistics of PSI-LHCI of *C.reinhardtii* and PSI-LHCI of Higher plants (PDB: 2WSC)

Important parameters	PSI-LHCI of *C. reinhardtii*		PSI-LHCI of higher plants (PDB: 2WSC)	
	Number of amino acid residues	Percentage (%)	Number of amino acid residues	Percentage (%)
Residues in most favoured regions [A,B,L]	3119	70.2	1170	43.7
Residues in additional allowed regions [a,b,l,p]	878	19.8	931	34.8
Residues in generously allowed regions [~a,~b,~l,~p]	258	5.8	353	13.2
Residues in disallowed regions	190	4.3	225	8.4
Number of non-glycine and non-proline residues	4445	100.0	2679	100.0
Number of end-residues (excl. Gly and Pro)	42		38	
Number of glycine residues (shown as triangles)	498		302	
Number of proline residues	304		170	
Total number of residues	5289		3189	

2.3.6 Protein-protein interactions among PSI-LHCI supercomplexes

Results obtained by PDBsum structural tool showed several protein-protein interactions among the PSI-LHCI subunits and the size of the protein (Figure 2.7A) compare to higher plant (Figure 2.7B). The reason may be due to the existence of more number of LHCI subunits in *C.reinhardtii.* The non-covalent interaction in between LHCI subunits and PSI core are stronger. It is surprising that these interactions were stronger with PSI core to LHCI. However, in higher plants these interactions are very less (Figure 2.4B). Thus, existence of much stronger interactions is one of the reasons making difficulties in purifying individual LHCI subunits in *C. reinhardtii.*
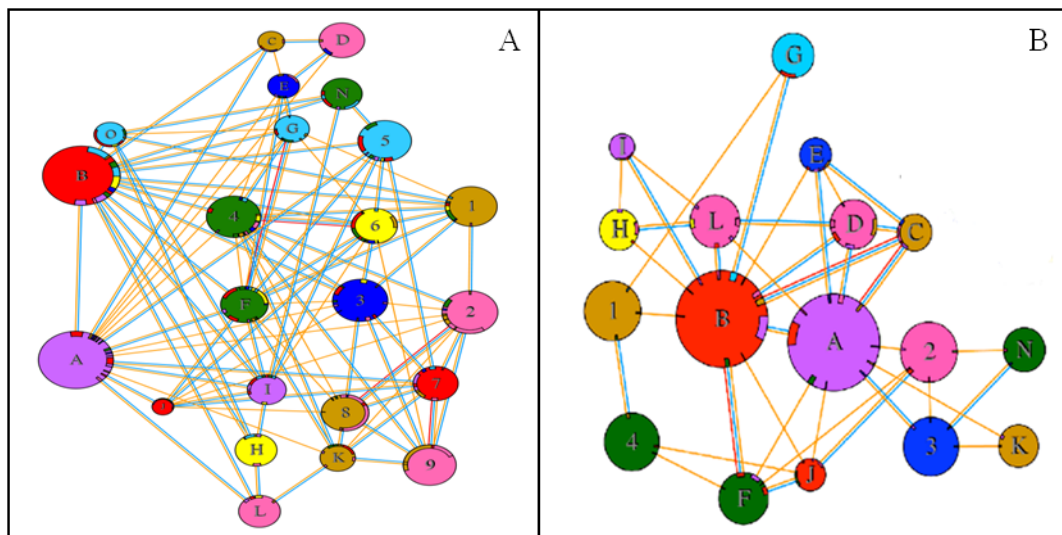
Figure 2.7 A) Protein-Protein interactions of *C.reinhardtii* PSI-LHCI supercomplexes, and B) in higher plants (adapted from Amunts et al (2010)). The area of each sphere is proportional to the surface area of corresponding protein chain. The extent of the interface region on each chain is represented by a coloured wedge whose colour corresponds to the colour of the other chain and whose size signifies the interface surface area. A to L and N corresponds to the photosystem I subunits and 1-9 attributes to light harvesting complex I.

2.3.7 H-bonding pattern of LHCI subunits with other PSI-LHCI supercomplex subunits

The results of chimera tool, which used to find the H-bonding pattern of LHCI subunits with other subunits of PSI-LHCI supercomplex were shown in Table 2.3. There are minimum of 11 hydrogen bonds (11) with Lhca2 and the maximum of the H-bonds (65) were observed with Lhca2 subunit. Except Lhca2 subunit, rest of the LHCI subunits were at least one H-bonded with the PSI core subunits. PsaB core subunit has many H-bonding interactions with the LHCI subunits. The nature of the H-bonding pattern among the LHCI subunits and with the core signifies that strong interaction between the PSI core subunits and LHCI subunits. This data also indicates that the hydrogen bonds among the LHCI subunits are more prominent than that with PSI core subunits.

2.3.8 Experimental evidence of LHCI subunits associated with PSI core in PSI-LHCI supercomplexes

The protein-protein interactions generated from the model shows that there are more noncovalent interactions between LHCI and LHCI to PSI core. In order to evaluate the model purification of the PSI core complexes from *C.reinhardtii* was carriedout. Figure 2.8 shows the sucrose density purification of PSI-LHCI supercomplexes obtained in which there are four major bands and the lower two bands attributed to the PSI-LHCI supercomplexes. These supercomplexes were again solubilised with β-DM (0.5% /mg Chl) and loaded on SDS gel to see the protein pattern of PSI and LHCI. The lanes 1, 2, 3, indicates thylakoids, PSI-LHCI supercomplexes from sucrose density gradient and detergent treatment to the PSI-LHCI supercomplexes. LHCI subunits comprise of molecular weights from 25 to 30 kDa. In this experiment

Table 2.3 H-bonding pattern of LHCI subunits with other PSI-LHCI subunits

Subunit	Total number of H-bonds	H-donor of H-bond		H-acceptor of H-bond		Important interacting subunit(s) by H-bond
		Number H-bonds	Interacting subunits (Number of H-bonds)	Number H-bonds	Interacting subunits (Number of H-bonds)	
Lhca1	29	16	PsaO (1), PsaF (6), Lhca6 (8), Lhca3(1)	13	PsaF (5) Lhca2 (2), Lhca 6 (6),	Lhca6
Lhca2	65	32	Lhca1 (2), Lhca4 (3), Lhca9 (13), Lhca8 (14)	33	Lhca4 (4), Lhca7 (2), Lhca8 (17), Lhca9 (10)	Lhca8
Lhca3	11	6	PsaB (4), lhca6 (1), Lhca4 (1)	5	lhca4 (2), lhca6 (1), PsaB (1), Lhca1 (1)	PsaB
Lhca4	20	11	PsaB (1), lhca6 (4), Lhca2 (4), Lhca3 (2)	9	PsaB (3), PsaK (2) Lhca2 (3), Lhca3 (1)	Lhca2
Lhca5	22	12	PsaB (6), PsaF (2), PsaA (1), lhca6 (1), Lhca7 (2)	10	PsaB (5), PsaN (4), PsaI (1)	PsaB
Lhca6	55	28	PsaB (11), PsaF (9), Lhca1 (6), PsaJ (1), lhca3 (1)	27	PsaB (4), PsaF (9), Lhca1 (8), Lhca4 (4), Lhca3 (1), Lhca5 (1)	PsaF, Lhca1 and PsaB
Lhca7	22	12	PsaA (6), PsaK (3), Lhca9 (1), Lhca2 (2)	10	Lhca8 (4), PsaA (1), PsaK (3), Lhca5 (2)	PsaA
Lhca8	57	31	Lhca7 (4), Lhca9 (9), Lhca2(17), PsaK (1)	26	Lhca9 (12), Lhca2 (14)	Lhca9
Lhca9	48	22	Lhca2 (10), Lhca8 (12)	26	PsaK (3), Lhca2 (13), Lhca7 (1), Lhca8 (9)	Lhca2 and Lhca8
PsaO	39	21	PsaN (2), PsaB (18), PsaH (1)	18	PsaB (11), PsaH (4), PsaI (3)	PsaB

with harsh treatment of detergent to PSI-LHCI supercomplexes, there was no disturbance observed in the integrity of PSI-LHCI supercomplexes. These results exhibits that it is highly difficult to separate individual complexes of PSI and LHCI from PSI-LHCI supercomplexes even with harsh detergent treatment. However, it is very easy to separate PSI-LHCI supercomplexes from higher plants that's why crystal structure of pea at 3.3Å has been resolved by Amunts et al. (2010).
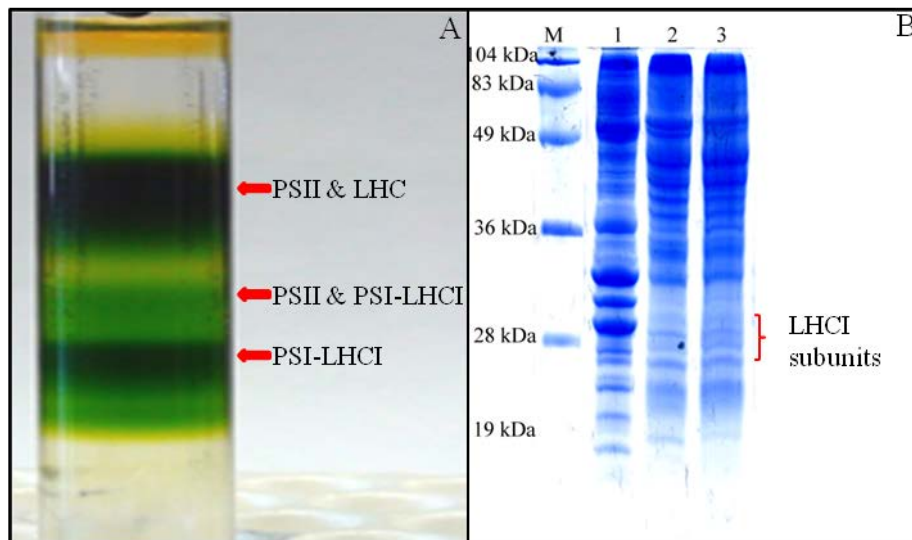
Figure 2.8 Separation of LHCI subunits from PSI core. A) Sucrose density gradient centrifugation of solubilized thylakoids and B) Protein profile of thylakoids (lane 1), PSI-LHCI (lane 2) and PSI-LHCI after harsh detergent treatment (lane 3).

2.4   Discussion

Photosystem I is a multi-protein complex consisting of the PSI core and peripheral light-harvesting complex I that together form the PSI-LHCI supercomplex in

algae and higher plants. *C.reinhardtii* is acceptable model organism for the study of structure, function, and biogenesis of photosynthetic components. It contains 4 chloroplast-encoded PSI genes (*psaA*, *psaB*, *psaC*, and *psaJ*) and 10 nuclear-encoded PSI genes (*psaD*, *psaE*, *psaF*, *psaG*, *psaH*, *psaI*, *psaK*, *psaL*, *psaN*, and *psaO*) as well as 9 *Lhca* genes (*Lhca1-Lhca9*) and their respective proteins (Stauber et al., 2003; Takahashi et al., 2004; Merchant, 2007). Single particle analysis revealed that PSI complexes from *C.reinhardtii* are larger than those from higher plants and also shown the number of LHCI subunits are more ~14 (Germano et al., 2002; Kargul et al., 2003). However, X-ray structure is not determined so far since *C.reinhardtii* PSI-LHCI supercomplexes are in complex nature.

The best modeling mechanism known ever since is homology modeling in which the co-ordinates of a template with known structural data are used to predict and model a query sequence near accurately which in turn depends on the identity between the template and query sequence and also on the quality of the alignment of the sequences (Sali et al., 1995). The alignment was optimized by considering the alignments of sequences, as this is very critical step for final modelling. The quality of multiple alignment sequences were confirmed by relative secondary structures, thus minimizing the possibilities of errors in modelling (Figure 2.7). Higher plants were diverged from the unicellular organisms such as *C.reinhardtii* over one billion years ago (Merchant, 2007) which accounts the differences in sequence identity in some subunits as shown in Table 2.1. The structure of PSI core subunits that were represented in Figure 2.3 was not having the accountable differences in structure as well location of the most of the sub units. PsaA, PsaB, and PsaC were more than 80% identity with that of higher plants. PsaA and PsaB are the heart of PSI reaction center and acts as heterodimer where

charge separation takes place. PsaC, an apoprotein for the three Fe_4-S_4 clusters of PSI, essential for photochemical activity and this subunit has very similar function in all organisms (Nelson and Yocum, 2006). However, the small differences in some of the core subunits which have sequence identity of 50 to 80% such as PsaD to L and PsaN seems to play special role in the structural integrity or Fd-NADP reduction or interaction with the Lhca1-9 subunits and in electron transport reaction. PsaD, a stromal exposed subunit was known to interact strongly with Fd. The PsaE subunit in *C.reinhardtii* has an N-terminal extension of about 32 residues. Scheller et al., (2001) reported the existence of ~10 residues in *C.reinhardtii*. The extended region of PsaE interacts with PsaD subunit thus it helps $NADP^+$ reduction, mediating electron transport from PSI to Fd and it is also important for stabilization of PSI (Fromme et al., 2001; Jensen et al., 2007). PsaF has a role in docking of plastocyanin, in the absence of this subunit, it is observed that there is no stable complex formation between PSI and plastocyanin (Farah et al., 1995). It is also shown that efficient electron transfer from both plastocyanin and cytochrome c6 to PSI depends on PsaF (Hippler et al., 1997). Conserved region of N-terminal polypeptide of PsaF contains several positively charged residues thus, there might be strong interaction with negatively charged plastocyanin that leads to the formation of a stable plastocyanin-PSI complex responsible for fast electron transfer. PsaG has an extended N-terminal region containing ~25 amino acid residues when compared to the template and thus it helps in stabilization by interacting with PsaB, PsaF, Lhca1, Lhca4 subunits. Recently it was shown that PsaK and PsaG stabilize the association between PSI core and LHCI complexes in *C.reinhardtii* (Ozawa et al., 2010). PsaH subunit which is present on lumenal side thus under state transitions a mobile pool of Lhcb (PSII) interacts with this subunit. The structure of PsaL, which is

responsible for the trimerization of PSI in cyanobacteria (Jordan et al., 2001), lacks a short helix and the Ca(2+) binding site, which are essential for trimer formation indicating that the Galdieria PSI is a monomer (Fromme et al., 2001; Vanselow et al., 2009). Interestingly, the unique subunit of PsaO subunit in *C.reinhardtii* having three transmembrane helices and this subunit is closely associated with PsaH, PsaI, and PsaL. It was reported that PsaH, PsaI, and PsaL plays role in state transition and other abiotic stresses (Schluchter et al., 1996; Lunde et al., 2000). Thus, PsaO may play a role in stabilization of PSI core complexes as well in state transitions mechanism. PsaK associated strongly with PsaA (Figure 2.5) and to some extent with PsaL region, which is shown to play an important role in PSI trimer formation reported in cyanobacteria (Boekema et al., 1987) also in *C. reinhardtii* plays similar role. PsaN subunit located on lumenal side distantly than other core subunits (Figure 2.4), so this subunit may dissociate easily from PSI. PsaN subunit of *C.reinhardtii* has an extended region of amino terminal (data not shown), which may help in interaction with Lhca2, Lhca8 and Lhca9 of *C.reinhardtii* where additional Lhca's exist than higher plants.

Light harvesting complexes of *C.reinhardtii* differ with higher plants in number as well as structural arrangement, but function was same, that is harvesting the solar energy and then transferring to the core reaction center of PSI. The arrangement of *C. reinhardtii* LHCI subunits was clearly modeled in the 3D model and LHCI subunits were positioned as half moon shape at bottom of the PSI core. Lhca1, Lhca3, Lhca4, Lhca5, Lhca6 and Lhca7 were exactly matching to the predicted model of Stauber et al., (2009). Mozzo et al., (2010) reported another way of arrangement based on expression of LHCI apoproteins in bacteria and refolding *in vitro* pigment-protein complexes. These results were coinciding with LHCI polypeptide arrangement of Mozzo et al.,

(2010) in Lhca1, Lhca3, Lhca4, Lhca5 and Lhca8. The deviation may be due to the different approaches followed in building up of a predicted model in each case. The 3D model which is shown here is mainly based on energy minimization approach compared to proteomic approach of Stauber et al., (2009) and refolding of *in vitro* pigment-protein complexes of Mozzo et al., (2010). From Table 2.3, it is clear that Lhca1 interact with PsaF core subunit by 11 H-bonds and Lhca6 subunit by 14 H-bonds. Lhca2 does not have any H-bonding interaction with PSI core thus, it can disassociates easily from the core in any abiotic stress, but it has many H-bonds with other LHC subunits. Lhca3 strongly interact with PsaB core subunit by 5 H-bonds and Lhca4 by 3H-bonds. Since it has very few number of H-bonds when compared to other LHCI subunits this is also easily can be dissociated under stress conditions. Lhca4 interacts with PsaB core subunit by 4 H-bonds and with Lhca2 subunit by 7 H-bonds. Lhca5 and Lhca6 subunits have strong interaction with PsaB core subunit by 11H-bonds and 15H-bonds respectively and these two subunits have maximum number of H-bonding interaction with the PSI core subunit (Table 2.3). Lhca7 subunit has many strong interactions with PsaA core subunit among the LHCI subunits by 7 H-bonds. Lhca8 and Lhca9 were two LHCI subunits among which many number of H-bonds exist (Table 2.3). The PsaO subunit, which is unique to *C.reinhardtii*, has several interactions with other PSI core subunits such as PsaB by 29 H-bonds, PsaH by 5 H-bonds, PsaI by 4 H-bonds and PsaN by 2 H-bonds. Thus the interaction of PsaO subunit especially with PsaH and PsaI involved in state transition mechanism in *C.reinhardtii.* Thus, these hydrogen bonds may play role stabilization of PSI-LHCI supercomplexes.

The evaluation of 3D model data by various methods such as PROCHECK and RMSD values suggests that this could be the most preferential arrangement of light

harvesting complexes. Thus the 3D model of PSI-LHCI supercomplexes represented here provides detailed structural information for *C.reinhardtii* that could be useful for understanding the structural information and various biotechnological understanding applications. Further studies like crystallography and NMR studies may provide the exact location of these subunits.

The 3D model reveals that there are strongly non covalent interaction between all subunits (Figure 2.7). It is clearly shown that the interactions were stronger among the core subunits and as well as light harvesting complexes. Also these interaction were seen between core and Lhca, indicating that the complexity of the PSI-LHCI supercomplexes in *C.reinhardtii.* Thus, this may be of the reason why *C.reinhardtii* PSI-LHCI supercomplexes X-ray structure has not been solved. Interestingly, experimental results were agreeing with the 3D model (Figure 2.8). The experimental data reveals that even with harsh detergent treatment to PSI-LHCI supercomplexes, the LHCI protein cannot be separated from PSI core protein. However, in higher plants it is easy to separate core and light harvesting complexes by mild detergent because there is not much non covalent interactions between core and light harvesting complexes (Ben-Shem et al., 2003). This indicates that the non-covalent interaction between PSI core and LHCI plays a pivotal role to maintain the structural integrity of PSI-LHCI supercomplexes. A preliminary report of 3D model of PSI-LHCI supercomplexes from *C.reinhardtii* was published recently (Yadavalli et al., 2011).

Development of peptide tag antibodies against *C. reinhardtii* LHC I subunits

Chapter 3

3.1   Introduction

The unicellular green alga *C.reinhardtii* has been explored as a eukaryotic model organism for decades. In all eukaryotic oxygenic photosynthetic organisms, light harvesting chlorophyll *a*- or *b*-binding proteins (LHC proteins) function in the collection and transfer of light energy to the reaction centers of PSII and PSI (Dekker and Boekema, 2005). Additionally, these proteins are also involved in light dissipation through energy quenching. Therefore, light-harvesting proteins are important components of the photosynthetic machinery that optimize photosynthetic function and minimize photo-oxidative damage in response to light quantity and quality. Compared to higher plants LHCI (Ben-Shem et al., 2003; Amunts et al., 2010), which contains Lhca1, Lhca2, Lhca3 and Lhca4, *C.reinhardtii* have more than nine LHCI's which were identified by proteomic analysis (Hippler et al., 2001; Stauber et al., 2003; Stauber and Hippler, 2004; Dekker and Boekema, 2005; Mozzo et al., 2010). Electron micrographic studies revealed that there are more than 14 Lhca subunits in *C.reinhardtii,* showing the complexity of the light harvesting proteins (Germano et al., 2002). The arrangement of Lhca subunits in higher plants is Lhca 1, Lhca 4, Lhca2 and Lhca3 flanking the core subunits. In case of *C.reinhardtii* the sequential arrangement of nine Lhca's are not known (Takahashi et al., 2004). In view of the facts that the *C.reinhardtii* light harvesting complexes are unique (Germano et al., 2002) and the structural integrity of LHCI of PSI-LHCI supercomplexes are not known, it is difficult to isolate individual LHCI proteins to develop antibodies by direct method because of its complex structure.

Most biochemical analysis of PSI in various plants have been identified as four different LHCI proteins (Lhca1-4) with molecular masses determined to be between 20 and 25 kDa by fully denaturing gel electrophoresis (Haworth et al., 1983). By gentle separation of mildly solubilized PSI, two different sub-fractions of LHCI, named LHCI-680 and LHCI-730 (Lam et al., 1984), could be identified. LHCI-730 is composed of Lhca1 and Lhca4 (Lam et al., 1984; Bassi et al., 1985) and exists in a heterodimeric state (Jansson et al., 1996). For a long period, it was assumed that six to eight LHCI proteins (two copies of each protein) surround the core of PSI (Boekema et al., 2001). However, the 4.4 Å crystal structure of PSI from pea revealed only four LHCI proteins per PSI (Ben-Shem et al., 2003).

The PSI-LHCI supercomplex from *C.reinhardtii* is significantly larger than the corresponding complex from higher plants (Germano et al., 2002; Ben-Shem et al., 2003; Amunts et al., 2010). However, the assignment and function of individual LHCI polypeptides in the PSI-LHCI supercomplex remain to be elucidated. The structure of the PSI-LHCI supercomplex appears similar in *C.reinhardtii* and higher plants. The oligomeric structure of *C.reinhardtii* LHCI is rather stable compared to that of higher plants. This indicates that assembly of the LHCI is independent of the PSI complex and that the oligomeric form of the LHCI accumulates stably *in vivo* even in the absence of the PSI core complex (Wollman and Bennoun, 1982). In order to identify the LHCI proteins from *C.reinhardtii*, the specific antibodies are being required. The *C.reinhardtii* LHCI (Lhca 1-9) arrangement models represented by Stauber et al. (2009) is based on the proteomic profiling and another model represented by Mozzo et al. (2010) which is based on biochemical/spectroscopic properties are still not clear. Developing peptide tag antibodies could help in defining the structure as well as for biochemical studies and

functional roles of LHCI polypeptides in *C.reinhardtii*. In addition, using the peptide tag antibodies, the nature of abiotic stress effect on LHCI and their integrity with the PSI core could be elucidated.

In the present study, for the first time nine peptide tag antibodies against Lhca1 to 9 polypeptides were developed and used to detect the LHCI proteins from isolated PSI-LHCI supercomplexes of *C.reinhardtii*. This were tested in *C. reinhardtii* under iron deficiency conditions.

3.2 Materials and Methods

3.2.1 Designing peptides for the light harvesting complexes

The sequences used for designing the peptides were Lhca1 (GenBank: AAD03734.1), Lhca2 (GenBank: XP_001691031.1), Lhca3 (GenBank: BAD06919.1), Lhca4 (GenBank: BAD06918), Lhca5 (GenBank: XP_001702730) Lhca6 (GenBank: ABD37907.1), Lhca7 (GenBank: AAO16495.1), Lhca8 (GenBank: XP_001696202) and Lhca9 (GenBank: AAL87738) downloaded from gene bank at the NCBI (Appendix I). Peptides were designed using peptide antigen finder, a web based software based on empirical formula developed by Kolaskar and Tongaonkar (1990). Finally only one peptide chosen from each sequence based on the antigenicity nature, hydrophilicity. Conserved regions were excluded to avoid cross reactivity with other Lhca sequences. Most of the hydrophobic amino acid residues are present inside or core of the protein, which are not potential for developing the peptide tag antibodies. Presence of more number of hydrophilic residues in the peptide indicates that the residues are likely to be exposed on the surface of a folded protein, which was confirmed by checking with the

PyMol Molecular Graphics System, Version 1.2r3pre, Schrödinger, LLC. Cysteine was added to either C-terminal or N-terminal based on the location of the peptide in the protein sequence and composition of peptide for conjugation with keyhole limpet hemocyanin (KLH).

3.2.2.   Conjugation of the peptide to carrier molecule (keyhole limpet hemocyanin)

The peptides of Lhca2, to 5 and 8 were of kind gift from Arizona State University, USA and the peptides Lhca1, 6, 7 and 8 were purchased from G.L.Biochem, Shangai, China. The integrity and purity of the peptide was checked by MALDI-TOF-TOF. Protein carriers are frequently applied to induce immune responses against covalently attached low molecular weight peptide epitopes (Mezo et al., 2000). These peptides were conjugated with carrier molecule by using Indole 3-acetic acid N-Hydroxy succinamide ester (IAA-NHS) as coupling reagent by previously described protocol with slight modifications (Harlaow and Lane, 1988; Karlsen et al., 1990). Briefly, 5 mg of each peptide was dissolved in 50mM phosphate buffered saline (PBS) pH 7.2 and activated by adding 100 µL of 10mM Iodoacetic acid N-hydroxy succinamide ester. However, Lhca1 was dissolved by adding dimethyl sulfoxide as it contains more number of hydrophobic amino acid residues. Excess IAA-NHS ester was removed by dialyzing with 5mM PBS (pH 7.2). About 10 mg of maleimide activated-KLH (Pierce) was dissolved in one mL of sterile distilled water. Activated peptides and KLH were mixed and incubated for 8.0 h at 4°C with continuous gentle rotation. A pinch of $NaBH_4$ was added to stop the reaction. Then peptide-KLH conjugate was purified by gel filtration chromatography (Sephadex G-25) by collecting 1 mL fractions.

Peptide-KLH conjugate containing fractions were pooled based on absorbance at 280nm.

3.2.3. Development of polyclonal antibodies

Conjugate-adjuvant emulsion was prepared from 500 µL of conjugate and 500 µL of Freund's complete adjuvant (initial injection) or incomplete adjuvant (booster injection). Approximately 200 µg of conjugated peptide was injected at multiple sites subcutaneously to the adult New Zealand white rabbits. Similar doses were followed after two, four and six weeks with Freunds incomplete adjuvant. Immune sera were collected from the marginal ear vein before third and fourth booster dose. Permission was taken to carry out the experiments on rabbits from Institutional Animal Ethical Permission *i.e.,* 'Committee for the Purpose of Control and Supervision of Experiments on Animals', India, approval number: LS/IAEC/SRG/2010/12 Dated March 18th, 2010.

3.2.4 Affinity purification of crude sera with Affigel-10 coupled with peptide

Three mg of peptide was dissolved in one mL of coupling buffer (0.1 M $NaHCO_3$ pH 8.5) and then kept on the ice. Approximately, two mL of Affigel-10 (Bio-Rad) was transferred to a small disposable column, washed with thrice ice cold deionized water and finally, washed with ice cold coupling buffer. Both peptide containing buffer and Affigel-10 were mixed in coupling buffer and sealed with parafilm. Further, this mixture was rotated gently on a rocker for 4h at 4 ^{o}C for coupling peptide to the affinity matrix. Unreacted affigel-10 sites were blocked by adding one mL of 0.1 M glycine methyl ester per mL gel, followed by incubation for another one hour. Crude sera was diluted two times with 1X TBS pH 7.4 buffer and filtered through 0.4µm filter syringe before passing the serum through column. The filtered serum was

passed several times through affigel- 10 coupled peptide and then gel was washed with 20 volumes of TBST buffer (50 mM Tris-HCl, pH 7.4, 150 mM NaCl, 0.1% Tween 20). Peptide specific antibodies were eluted with 0.1 M Glycine pH 2.5 into the tubes containing Tris buffer (1M pH 8.8). Based on A_{280} values, antibodies containing fractions were pooled and dialyzed against 10mM PBS (pH 7.2).

3.2.5. Isolation of PSI-LHCI supercomplexes from *C.reinhardtii*

C.reinhardtii cells were grown in liquid culture by providing continuous light source with 50 µmol /m/s. Cells were allowed to grow until it attained one OD at 730nm. Cells were harvested with F10SX500 mL sorval rotor. Thylakoids and PSI-LHCI supercomplexes were isolated according to Subramanyam et al. (2006) and Yadavalli et al. (2011). Chlorophyll content estimated by taking 10 µL of thylakoids and 1.0 mL of acetone according to Arnon (1949). The final sample was suspended in PSI resuspension buffer containing 5mM Tris-HCl pH 8.0, 5mM $CaCl_2$, 10mM Mg_2Cl_2 and 0.03% β-dodecyl malotside at 2 µg/µL Chlorophyll concentration.

3.2.6. Gel electrophoresis and blotting

Five µg chlorophyll containing PSI-LHCI supercomplexes were loaded on the Tricine-SDS-PAGE. After the run, proteins were transferred to Polyvinylidene Fluoride (PVDF) membrane by western blotting apparatus as per manufacturer's instructions (Bio-Rad). PVDF membrane was removed from the sandwich and then made into two halves, one for testing the cross reactivity of crude sera and other half used for blotting with affinity purified peptide tag antibodies. Membranes were blocked with 2% bovine serum albumin (BSA) in TBST buffer with constant shaking for 1.0 h at room temperature. Later membranes were washed thrice with TBST buffer with

constant shaking. The blots were incubated with crude sera (1:1000 dilution) and affinity purified peptide antibodies (1:5000 dilution) respectively for 2.0 h with constant shaking (at 25 °C). Then blots were washed with TBST buffer thrice, followed by incubation in secondary antibody conjugated with horse radish peroxidase for 1.0 h with constant shaking. Further, the secondary antibody was decanted and then washed thrice with TBST. The blots were developed by enhanced chemiluminescence (ECL) reagents at 0.1 mL/cm^2 membrane (Bio-Rad) for three min. Excess reagent was drained off and the blot is placed between saran wrap. Signals were obtained by placing the blot in VersaDoc5000 (Bio-Rad) and exposed for couple of minutes in order to visualize the specific Lhca proteins by using peptide tag antibodies.

3.3   Results

3.3.1   Antigenic peptides designed for LHCI subunits

All LHCI sequences of *C.reinhardtii* were downloaded from NCBI GenBank. So far there are only nine Lhca sequences available. Here, peptide finder software was used to design the antigenic peptides based on the sequence submitted and results shows possible antigenic peptides. The choice of peptide sequence for antipeptide antibody production

is the single most important step in the process. In general, ideal antigenic epitopes are hydrophilic, surface orientated, and flexible. This is because in most natural environments, hydrophilic regions tend to reside on the surface, whereas hydrophobic regions are likely found hidden in the protein conformation. Antibodies can therefore only bind to epitopes found on the surface of proteins and tend to bind with higher

50

affinity when those epitopes are flexible enough to move into accessible positions. So, each peptide was analyzed for their antigenicity by Hopp-Woods scale and hydrophilicity nature. Among the peptides generated by peptide finder, only one peptide per each light harvesting complex was chosen which is good in antigenicity and hydrophilicity were shown in Figure 3.1 and Table 3.1 respectively. The peptides of Lhca1 to 9 were plotted in Hopp-Woods scale showing that strong antigenicity nature. The values on Y-axis (Hopp-Woods Scale) above zero line from traces of Figure 3.1 shows the antigenicity of the peptides. Also, Hopp-Woods Scale used for predicting potential antigenic sites which are likely to be rich in charged and polar residues (Hopp and Woods, 1983). Further, analyzed the exact location of the antigenic peptide by using PyMol structural view, which showed that all these antigenic peptides were at the surface of the protein, indicates that these peptide were more hydrophilic in nature (Figure 3.2).

Table 3.1 Antigenic peptides designed for the Lhca1 to 9 of *C.reinhardtii* and nature of the peptide

Sequence (kDa)	Peptide sequence	Length	Peptide Molecular weight (kDa)	Hydrophilic residues %
Lhca1 (25 kDa)	6 LPDDLPGNYGFDPL(C)	15	1.807	35
Lhca2 (27 kDa)	149 SEEMKLKELKNGRLA(C)	16	1.849	60
Lhca3 (32 kDa)	36 DRSKDQLYVGASQC	14	1.569	57
Lhca4 (28 kDa)	36 EAREWIDAWKSK(C)	13	1.518	58
Lhca5 (27 kDa)	137 (C)LMHWVEVRRWQDYK	15	1704	57
Lhca6 (27 kDa)	129 KNAVAARPSARSARR(C)	16	1.857	53
Lhca7 (28 kDa)	177 (C)GDAAKYAEYKQKEVK	16	1.517	53
Lhca8 (26 kDa)	6 KRSGVAARSASSRK(C)	15	1.563	64
Lhca9 (23 kDa)	57 (C)GQDEGRLKWYAEAE	15	1.755	50
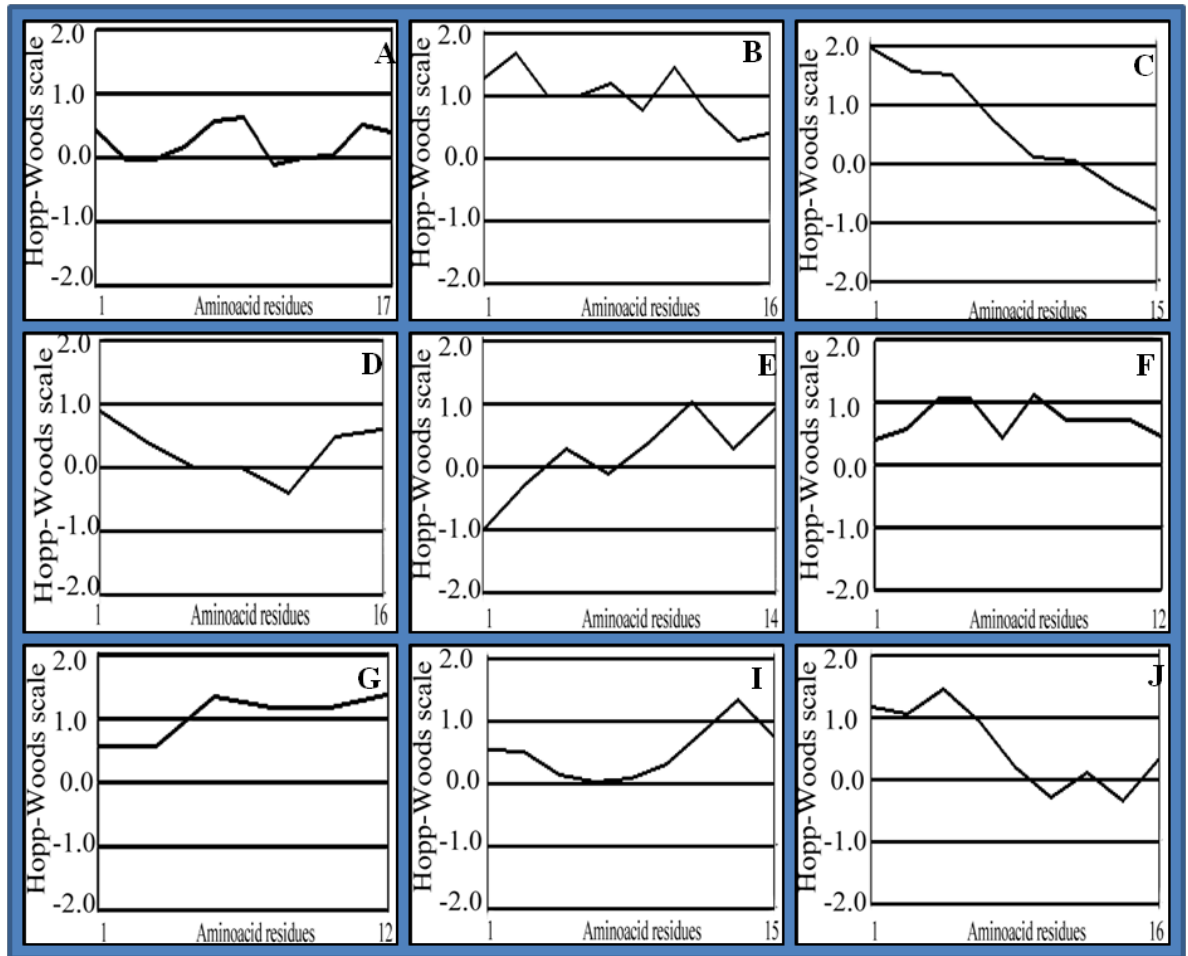
Figure 3.1 Antigenicity nature of the peptides plotted by using Hopp-Woods scale (Y-Scale). On X-axis amino acid residues of the peptide were shown. Values greater than zero are hydrophilic and thus likely to be exposed on the surface of a folded protein. A) Lhca1 peptide, B) Lhca2 peptide, C) Lhca3 peptide, D) Lhca4 peptide, E) Lhca5 peptide, F) Lhca6 peptide, G) Lhca7 peptide, H) Lhca8 peptide, I) Lhca9 peptide, and J) Lhca10 peptide.

A — Lhca1 peptide
B — Lhca2 peptide
C — Lhca3 peptide
D — Lhca4 peptide
E — Lhca5 peptide
F — Lhca6 peptide
G — Lhca7 peptide
H — Lhca8 peptide
I — Lhca9 peptide
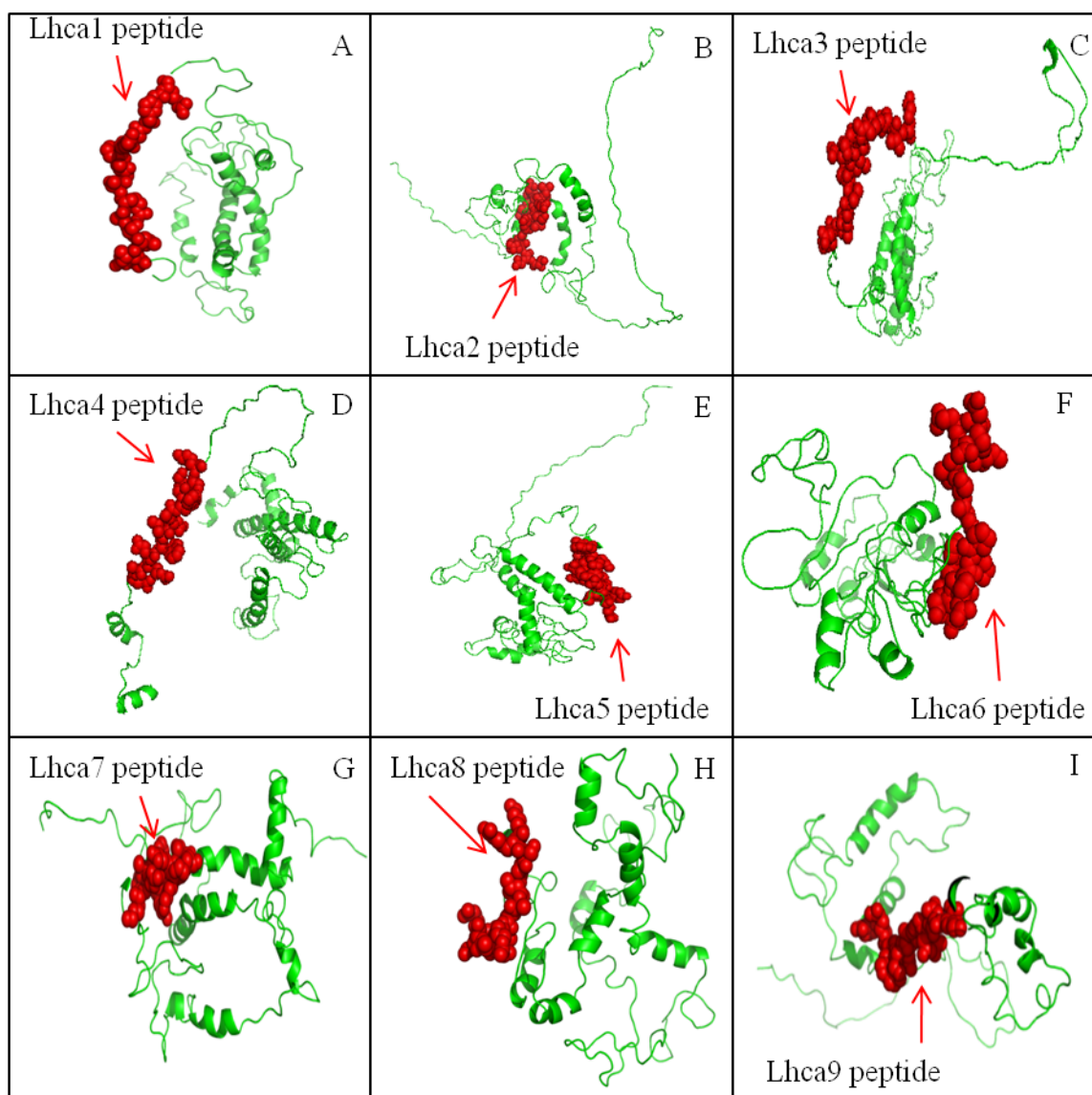
Figure 3.2 Location of antigenic peptide region (red spheres representation) of the corresponding LHCI subunit (green cartoon representation). A) Lhca1 protein, B) Lhca2 protein, C) Lhca3 protein, D) Lhca4 protein, E) Lhca5 protein, F) Lhca6 protein, G) Lhca7 protein, H) Lhca8 protein, I) Lhca9 protein, and J) Lhca10 protein. The peptide location was observed in PyMol viewing software.

3.3.2. Mass spectra analysis of peptides and gel filtration of the KLH-peptide conjugates

Intact nature and purity of the peptide is important since loss of any residues or fragmentation of the peptide that is chemically synthesized leads to the altered immunogenicity. So, Intact nature of the peptides were checked by MALDI-TOF-TOF. The total mass of the peptide designed (Table 3.1) matching with the total mass of the peptide analyzed with MALDI-TOF-TOF for all nine peptides as shown in Figures 3.3, 3.4, and 3.5. This indicates that peptides were intact in nature can be used for developing the peptide tag antibodies. The most prominent peak in each case shows the entire mass of the peptide. For developing peptide tag antibodies, the peptide should be at least 95% pure. All the peptides shown here are having 98% purity.

Figure 3.3 MALDI-TOF-TOF mass spectra of synthesized peptides showing intact nature of the peptides. A) Lhca1 peptide, B) Lhca2 peptide and C) Lhca3 peptide.
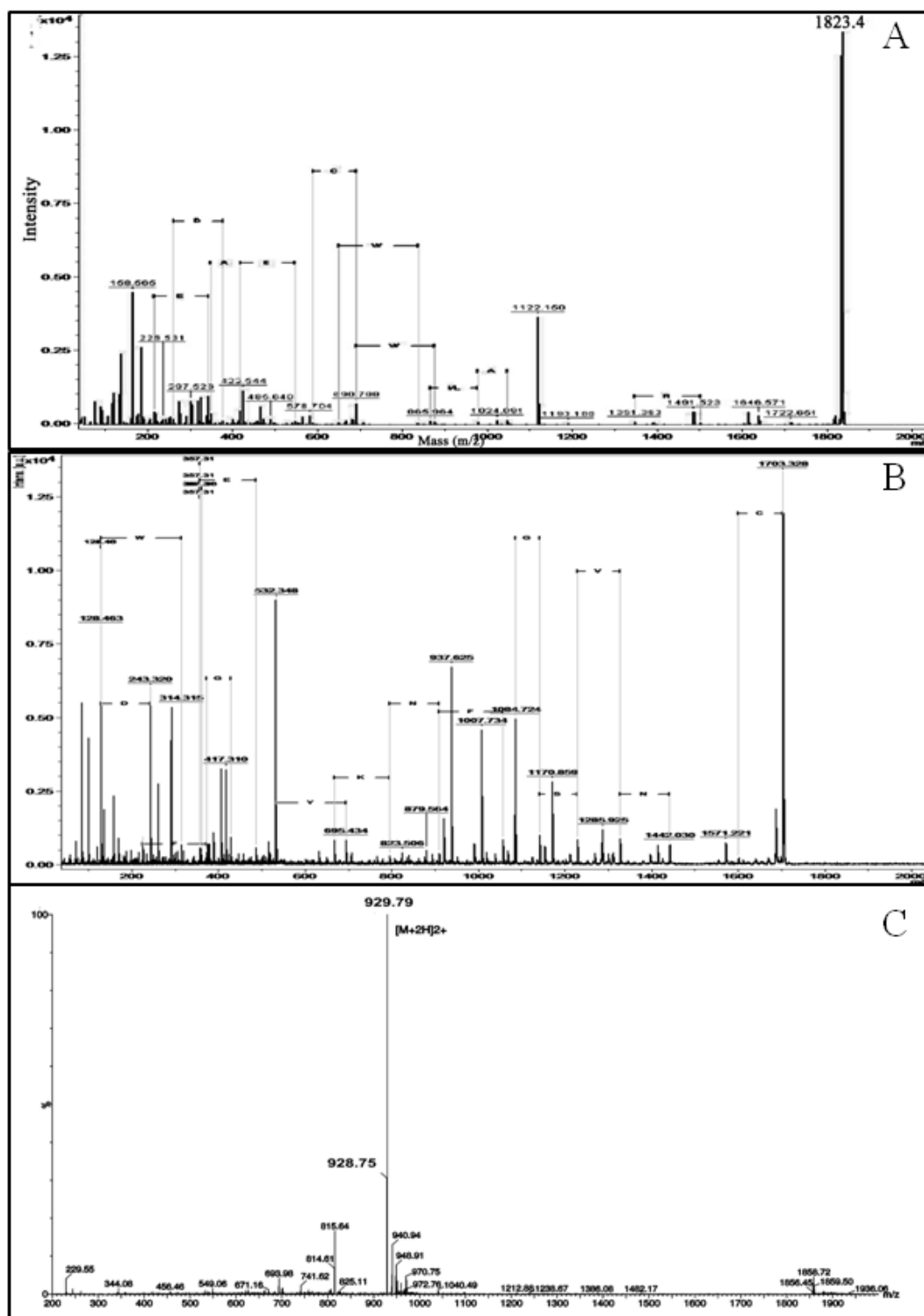
Figure 3.4 MALDI-TOF-TOF mass spectra of synthesized peptides showing intact nature of the peptides. A) Lhca4 peptide, B) Lhca5 peptide and C) Lhca6 peptide.

Figure 3.5 MALDI-TOF-TOF mass spectra of synthesized peptides showing intact nature of the peptides. A) Lhca7 peptide, B) Lhca8 peptide and C) Lhca9 peptide.
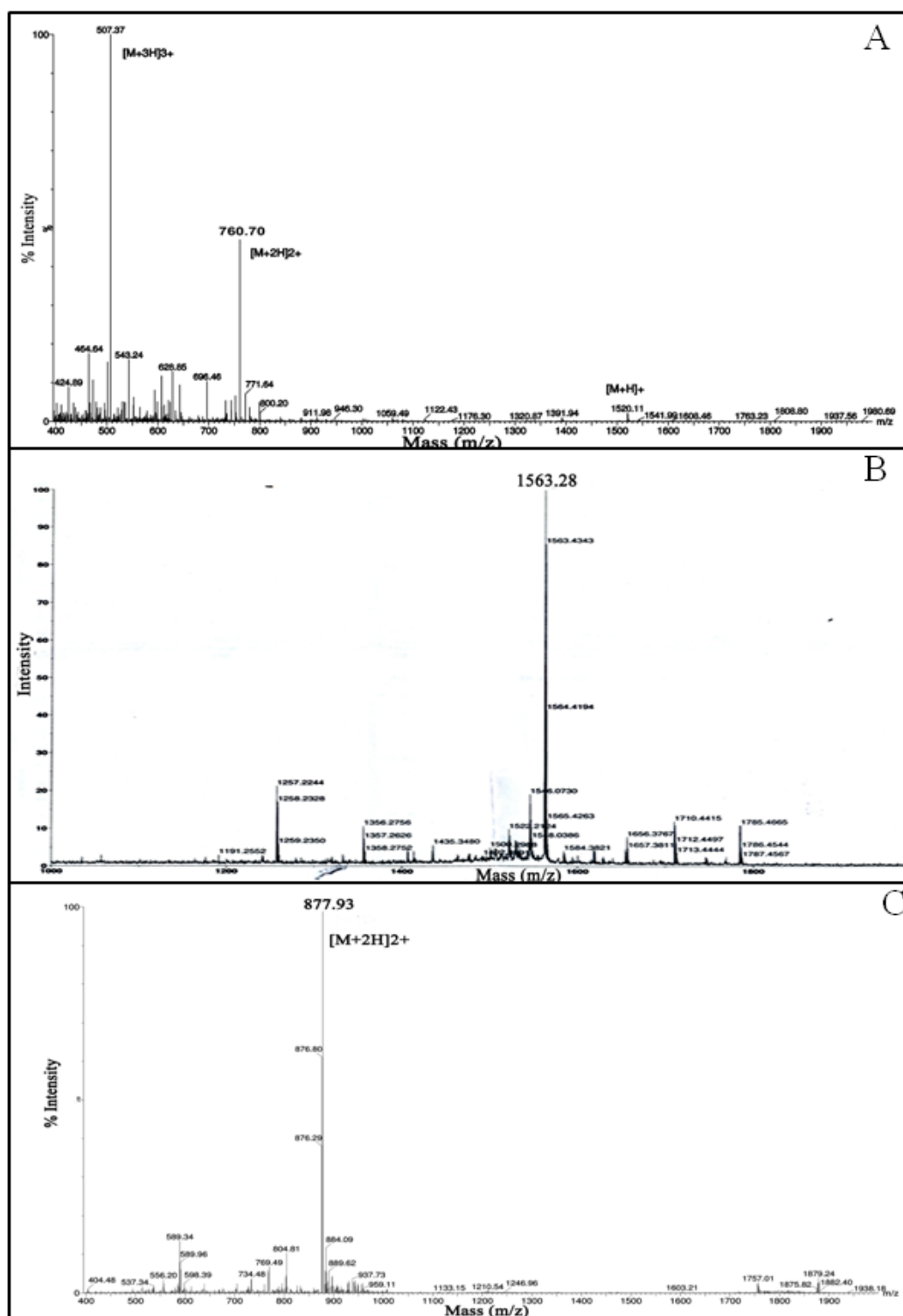
The results of KLH-Peptide conjugate based on A_{280} values of one ml fractions gel filtration chromatography indicates that the conjugated peptides eluted in the void volume. Only those fractions which shown maximum absorption at A_{280} were pooled and used for developing the anti-peptide antibodies (Figure 3.6).
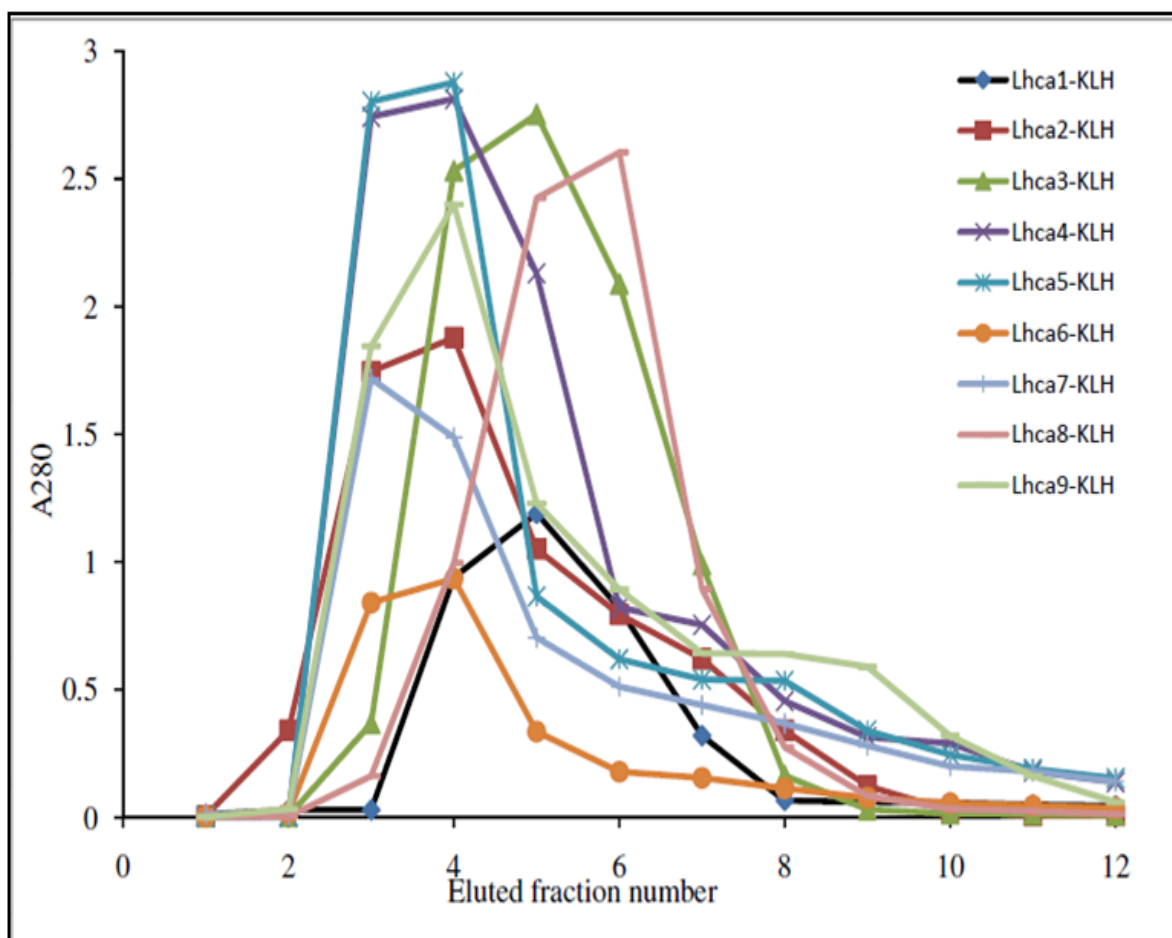
Figure 3.6 Eluted fractions of Peptide-KLH conjugates with A_{280} values. Peptide-KLH conjugate was found in the first 3 to 5 fractions.

3.3.3. Identification of Lhca1 to 9 proteins from *C.reinhardtii*

The affinity purified anti-peptide antibodies were tested by immunoblotting analysis from isolated PSI-LHCI supercomplexes of *C.reinhardtii* (Figure 3.7). Lane 1 shows the crude sera and lane 2 shows the affinity purified peptide tag antibodies of Lhca 1 to 9. Crude sera showed cross reactivity with many of the non relevant proteins because of the generation of a variable degree of anti-carrier response that influences mainly the quantity and affinity of the antibody produced (Tsuruta et al., 2006). The affinity purified peptide tag antibodies against Lhca1, Lhca6, and Lhca7 of purified PSI-LHCI supercomplexes from *C.reinhardtii* showed a single band upon exposure in VersaDoc imaging system (Figure 3.8). The cross reactivity of affinity purified antibodies with other proteins of PSI-LHCI supercomplexes were completely absent. The anti-peptide antibodies specifically recognized proteins of about 24kDa corresponds to Lhca1 (Figure 3.7A), 28.4 kDa corresponds to Lhca2 (Figure 3.7B), 30 kDa corresponds to Lhca3 (Figure 3.7C), 28.7 kDa corresponds to Lhca4 (Figure 3.7D), 28.2 kDa corresponds to Lhca5 (Figure 3.7E), 27.8 kDa corresponds to Lhca6 (Figure 3.7F), 26.2 kDa corresponds to Lhca7 (Figure 3.7G), 26 kDa corresponds to Lhca8 (Figure 3.7H), and 22.8 kDa corresponds to Lhca9 (Figure 3.7I) in *C.reinhardtii..* Also, the specific antibodies of Lhca1 to 9 were exactly matching to the molecular weight which has been reported previously (Takahashi et al., 2004) and thus the affinity purified peptide tag antibodies are pure.
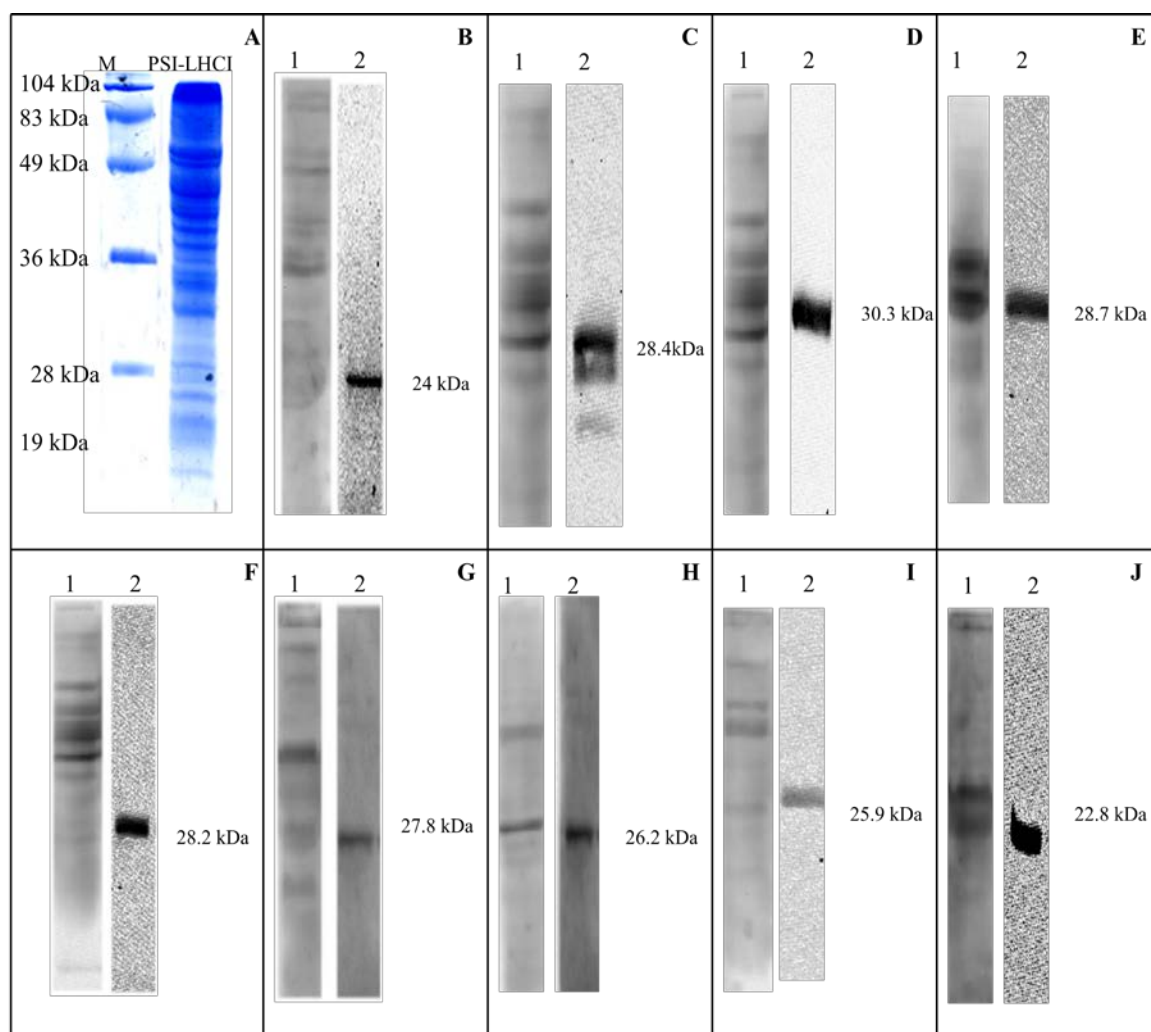
Figure 3.7 A) SDS-PAGE protein profile of PSI-LHCI super complexes of *C.reinhardtii*, B) Immunoblot of Lhca1, C) Immunoblot of Lhca2, D) Immunoblot of Lhca3, E) Immunoblot of Lhca4, F) Immunoblot of Lhca5, G) Immunoblot of Lhca6, H) Immunoblot of Lhca7, I) Immunoblot of Lhca8, and J) Immunoblot of Lhca9. In all immunoblots lane 1 probed with crude sera and lane 2 probed with affinity purified peptide tag antibodies. Each experiment was repeated thrice in identical samples and each time obtained similar results.

3.3.4. Discussion

The peptide selection is the first important point in developing the peptide tag antibodies since the peptide sequence contains amino acid residues which contain antigenic regions only could able to generate the antibodies against the peptide region. During peptide selection second priority has been given to the hydrophilic amino acid residues which ideally present on the surface of the protein thus it can detect the corresponding proteins without any difficulty. The peptides which are finally selected were good antigenicity nature and hydrophilic nature among the resulted peptides of the peptide finder (Figure 3.1 and Table 3.1).

Cross-reacting of the peptide tag antibodies with other proteins is due to the existence of the hemocyanin specific antibodies which is used for conjugation of the peptide to develop the antibodies. The hemocyanin is a huge molecule (approximately 400 kDa) containing many epitopes, thus presence of hemocyanin specific antibodies often leads to misinterpretation of the data. It is also reported that hemocyanin antibodies cross react with many of the proteins (May et al., 2003; Geyer et al., 2005). Affinity purification would help in eliminating the antibodies against hemocyanin (Dufau et al., 1975; Karlsen et al., 1990). It was clearly demonstrated that affinity purified anti-peptide antibodies developed against Lhca1 to 9 detected the corresponding proteins. Thus, such antibodies could help in understanding the structural details, localization of LHCI of PSI-LHCI supercomplexes in *C.reinhardtii*. In addition, using these antibodies one can study the physiology, structure, and functional organization of LHCI under abiotic stresses.

Proteomic and biochemical characterization of PSI-LHCI supercomplexes under iron deficiency *in C. reinhardtii*

Chapter 4

4.1 Introduction

Iron in aerobic soils and in water mostly found as insoluble form of Fe(III) oxides, while Fe(II) is typically not found in high concentrations in the environment under aerobic conditions. The Fe(III) oxides are accessed by organisms *via* an iron-limitation-inducible suite of physiological and biochemical mechanisms (Lynnes et al., 1998). There is now strong evidence that iron limitation controls algal productivity in some parts of the open ocean (Martin et al., 1994; Coale et al., 1996). Organisms have developed complex systems for iron acquisition and survival at low iron environments. The majority of iron in algae and plants is believed to be associated with the chloroplast (Briat et al., 2007). In oxygenic photosynthesis, iron is a cofactor in PSII, PSI, the cyt b_6/f complex, and (in algae), cyt c_6. The abundance of these proteins is reduced during iron-deficient growth (Singh et al., 2003).

On the molecular level, PSI is a prime target of iron deficiency, probably because of its high iron content (12 Fe per PSI). The ratio of PSI/PSII changes from 4:1 to 1:1 under iron deficiency in cyanobacteria (Straus, 1994), and a diatom evolved to low ambient iron has a constitutive PSII/PSI ratio of about 10:1 (Strzepek and Harrison, 2004). The mechanistic details of Fe stress response differ among phototrophs, but the various approaches seek to address similar physiological demands. Because of PSI's high Fe demands, Fe deprivation leads to a decrease in the number of PSI complexes, resulting in a bottleneck in the photosynthetic electron flow. Accumulation of reduced PSI can lead to the production of damaging singlet oxygen species via the Mehler reaction. To avoid oxidative stress, many species express auxiliary light-harvesting proteins which increase the absorption cross-section of PSI, allowing the cell to maintain a similar level of electron throughput with a smaller Fe investment. As Fe

stress becomes more severe, however, maintaining phototrophic growth becomes much more difficult and the cell's more pressing need is to prevent photodamage, often by utilizing uncoupled chlorophyll-binding proteins as excitation sinks that avoid the danger of singlet oxygen production.

Cyanobacteria also respond to iron deficiency by degradation of light-harvesting phycobilisomes (Guikema and Sherman, 1984) and expression of the "iron-stress-induced" operon *isiAB*. One of the proteins coded on this operon, IsiA, shows significant sequence similarity to CP43, a chlorophyll *a*-binding protein of PSII, and forms a ring of 18 molecules around a PSI trimeric reaction center, as shown by electron microscopy (Bibby et al., 2001; Boekema et al., 2001). The recent finding from Chauhan *et al.,* (2011) showed that PSI-*IsiA* supercomplexes with two layers of *IsiA* around PSI form during prolonged growth at nM Fe levels.

In the obligate photoautotrophic green alga *Dunaliella salina*, a chlorophyll *a*/*b*-binding protein homolog is induced by iron deficiency and functionally associated with PSI (Varsano et al., 2006). Iron deprivation in *Dunaliella* triggers extensive changes in chloroplast morphology, photosynthetic activities, and induction of a major 45 kDa chloroplast protein termed *Tidi* which resembles the chlorophyll *a*/*b*-binding proteins present in light-harvesting antenna complexes (Varsano et al., 2006). Single particle electron microscopy analysis revealed that PSI units from iron-deficient cells are larger (31 and 37 nm in diameter) than PSI units from control cells (22 nm) (Varsano et al., 2006). The 77 K chlorophyll fluorescence emission spectra of isolated complexes suggest that the Tidi-LHCI antenna are functionally coupled to the reaction centers of PSI. These findings indicate that Tidi acts as an accessory antenna of PSI.

In the green alga *C. reinhardtii*, iron deficiency leads not only to a pronounced degradation of PSI, but also to a remodeling of the PSI-associated LHCI, which precedes severe iron deficiency resulting in increased PSII antenna size (Moseley et al., 2002; Naumann et al., 2005; Naumann et al., 2007). These structural changes decrease the functional efficiency of excitation energy transfer between LHCI and PSI and minimize photo-oxidative stress to the thylakoid membrane. A similar effect has been observed in red algae (Desquilbet et al., 2003; Doan et al., 2003). However, the iron deficiency in plants or algae has not been studied very well in terms of photosynthetic apparatus organization.

The present study focuses on changes in the protein profile of PSI-LHCI supercomplexes by three approaches i) Biophysical methods such as HandyPEA analysis, low-temperature fluorescence spectrophotometry, circular dichroism (CD) and ultrafast fluorescence spectroscopy, ii) Biochemical methods such as green gel electrophoresis, immunoblotting, superoxide dismutase (SOD) activity assays and iii) Proteomic approach by using 2D gel electrophoresis and MALDI-TOF analyse the down regulated proteins.

4.2   Materials and Methods

4.2.1   Measurement of fluorescence with Handy PEA.

Chlorophyll *a* fluorescence transients were measured with the Plant Efficiency Analyzer (PEA). In the Handy PEA measurements, actinic light is provided by an array of three high intensity light-emitting diodes, which are focused *via* lenses onto the cells surface to provide even illumination. The diodes provide red light of a peak wavelength

of 650 nm, which is readily absorbed by chlorophyll. Cells were dark adapted for five minutes, followed by fluorescence measurements were taken according to Antal et al., (2006). There was no difference found in control cells which were grown for 24 h, 48 h and 72 h therefore, in all experiments, cells grown for 72 h are treated as control and compared with cells grown under iron deficient conditions after 24 h, 48 h and 72 h.

4.2.2 Chlorophyll estimation

The chlorophyll concentration of thylakoids was determined by adding 10 µL aliquot of the thylakoid to 1 mL of 80% (v/v) acetone. The aliquot was vortexed and then centrifuged for 2 min at room temperature in a microcentrifuge. The supernatant was collected into a fresh Eppendorf tube without disturbing the pellet, to take the absorbance readings.

Chlorophyll concentration was determined by measuring absorption with a spectrophotometer at 645 and 663 nm using the following equation (Arnon, 1949).

Chlorophyll b (mg/mL) = $(22.9 \times A_{645}) - (4.68 \times A_{663}) \times$ dilution factor.

Chlorophyll a (mg/mL) = $(12.7 \times A663) - (2.69 \times A645) \times$ dilution factor.

Total chlorophyll (mg/mL) = Chl a + Chl b = $(20.21 \times A645) + (8.02 \times A663) \times$ dilution factor.

4.2.3 Low-temperature emission fluorescence measurement

Steady-state fluorescence emission spectra of intact cells at 77K were measured with a LS 55 fluorescence spectrophotometer (PerkinElmer). Cells were resuspended in growth medium containing 60% glycerol. Chlorophyll was excited at 436 nm and the emission is recorded from 650-750nm. The emission and excitation slit width were 5 mm.

4.2.4 Circular dichroism measurements

Visible circular dichroism spectra were measured in a J-810 spectropolarimeter (Jasco Inc., Easton, MD, USA). The optical path length of the cell was 1 cm, and the distance of the sample from the photomultiplier was 5 cm. The spectra were recorded in 1 nm steps with an integration time of 0.3 s and a band pass of 2 nm. Equal Chl (10 µg/mL) concentration was used for measuring the CD.

4.2.5 Ultrafast fluorescence spectroscopy

The time versus wavelength fluorescence intensity surfaces were recorded on a system consisting of an ultrafast laser and a streak camera, as described previously (Liddell et al., 2008). Briefly, 130 fs light pulses at 800 nm were generated by a mode-locked Ti:S laser (Mira 900, Coherent Laser Inc., Santa Clara, CA, USA) pumped by a frequency-doubled $Nd:YVO_4$ laser (44% from an 18 W Verdi, Coherent Laser Inc.). The repetition rate of the Ti:S laser was reduced to 4.75 MHz by a pulse picker (Model 9200, Coherent Laser Inc.). The excitation light (800 nm) was frequency doubled to 400 nm and focused onto a sample cuvette with a 5 mm path length. Fluorescence was collected at a right angle to the excitation beam and focused on the entrance slit of a Chromex 250IS spectrograph which was coupled to a Hamamatsu C5680 streak camera with a M5675 synchroscan sweep unit. The streak images were recorded on a Hamamatsu C4742 CCD camera. Measurements were performed on 800 ps, 1.4, and 2 ns timescales, with 1,024 pixels of time resolution. The FWHM of the overall time response of this system was ~6 ps at the 800 ps timescale, ~12 ps at the 1.4 ns timescale, and ~20 ps at the 2 ns timescale. The spectral resolution was 0.124 nm in the spectral range of 650–777 nm (1,024 pixels). To avoid singlet–singlet annihilation, the pulse energy was reduced to 0.1 nJ using a neutral density filter. The probability of a single

supercomplex absorbing multiple photons in a single laser pulse was estimated using Poisson statistics (Cho et al., 1984) and it was found that less than 2% of emitted photons could have come from supercomplexes which had received multiple excitations. Global analysis was performed using locally written software in MATLAB. The 1,024 kinetic traces were binned, resulting in a spectral resolution of 1.24 nm. A Gaussian shaped instrument response function was used in the fitting.

4.2.6 Superoxide dismutase (SOD) activity measurements

Thylakoid membranes were suspended in 10 mM Tris–HCl (pH 7.5), 0.3 M sorbitol, 1.5 m M $CaCl_2$, 10 mM $MgCl_2$, and activity was assayed according to Beauchamp and Fridovich (1971). The required cocktail for SOD activity estimation was prepared by mixing 27 mL of 50 mM sodium phosphate buffer (pH 7.8), 1.5 mL of methionine (300 mg mL^{-1}), 1 mL of NBT (14.4 mg 10 mL^{-1}), 0.75 mL of Triton X 100 and 1.5 mL of EDTA. 10 μL of riboflavin (4.4 mg 100 mL^{-1}) and 50 μg of protein were then added to this mixture. After the contents were mixed in a cuvette, they were illuminated for 12 min using a Comptalux bulb (Philips, Eindhoven, The Netherlands) and the absorbance was measured at 560 nm.

4.2.7 Green gel electrophoresis

PSI-LHCI supercomplexes were solubilized in 50 mM Tricine, 5 mM EDTA pH 7.5, 50% Glycerol, and 0.5% β-dodecyl maltoside. Sample was resolved on 4 to 15% PAGE gels with 25 mM Tris, 250 mM Glycine, 0.005% SDS running buffer containing 0.05% Deriphat.

4.2.8   Isolation of PSI-LHCI supercomplexes

C. reinhardtii cells (obtained from the *Chlamydomonas* culture collection at Duke University) were grown following standard procedures (Subramanyam et al., 2006; Subramanyam et al., 2010a). Mother culture of *C. reinhardtii* cells were harvested and washed twice with media (Appendix II) which does not contain the iron and inoculated in to the one litre culture flask. Cells were grown under both control and iron stress conditions with continuous illumination (50 μmol m^{-2} s^{-1}) to a density where OD$_{730}$ nm ~ 1. Cells were then lysed and thylakoid membranes were isolated according to Fischer et al., (1997) and Yadavalli et al., (2011) and resuspended in 200 mM sorbitol, 5 mM Tris–HCl (pH 8.0), 5 mM CaCl$_2$. PSI-LHCI supercomplexes were isolated as previously described (Kargul et al., 2003; Subramanyam et al., 2006; Subramanyam et al., 2010b). Sucrose density gradients were prepared by step wise adding different concentration of the Sucrose (2 M, 1 M, 0.75 M, 0.5 M, and 0.25 M from bottom to top) and 5 mM Tricine pH 8.0, 0.5 M Betaine. Following sucrose density gradient centrifugation, the lowest band was collected and diluted with three volumes of 5 mM Tris–HCl pH 8.0, 0.05% DDM, 5 mM CaCl$_2$. The diluted samples were then concentrated using a Centricon-100 ultrafiltration device (Amicon, Beverly, MA, USA) at 4,000 g in a Sorvall SS-34 rotor at 4°C. For studying the gradual changes in PSI-LHCI supercomplexes during time course of under iron deficiency conditions, cells were harvested at 24, 48, and 72 h.

4.2.9 SDS-denaturing gel electrophoresis

For the analysis of the protein composition of PSI-LHCI supercomplexes from *C.reinhardtii,* samples were size-fractionated by gradient SDS-PAGE (15–23%) as described earlier by Subramanyam et al., (2010b). Equal amounts of protein (100 μg) were loaded on each lane. The PSI-LHCI supercomplexes were solubilized in 2% SDS and 0.1 M dithiothreitol, and the gel was stained with Coomassie brilliant blue R250.

4.2.10 Immunoblotting of PSI-LHCI supercomplexes

PSI-LHCI polypeptides were separated by polyacrylamide gel electrophoresis (PAGE). Electrophoresis was performed on a 12% separating and 4% stacking gel of polyacrylamide. Equal quantities of protein were loaded onto each lane. An equal volume of 2× buffer was added to the aliquots. To identify and quantify the polypeptides contained in the PSI-LHCI supercomplex, immunoblotting was carried out essentially as described by Towbin et al., (1979). Immunoblotting was performed by electrophoretic transfer of proteins to PVDF membranes. The membrane was incubated with polyclonal antibodies raised in rabbits. Primary antibodies against PsaA, PsaB, PsaC, PsaD, PsaE, and PsaG were purchased from Agrisera (Vännäs, Sweden). Peptide tag antibodies of Lhca were raised for identification of LHCI subunits (see Chapter II). Subsequently, secondary antibodies ligated to horseradish peroxidase were applied. Chemiluminescence reagents (Bio-Rad) were used as substrate for secondary antibody. The images were recorded on a VersaDoc 5000 CCD camera (Bio-Rad).

4.2.11 Sample preparation for Isoelectric focussing of PSI-LHCI supercomplexes

400 µg of protein was precipitated by following method. A volume of 400 µL of methanol was added to the sample and vortexed thoroughly (Yadavalli et al., 2011). To this solution, 400 µL of water-saturated chloroform was added and the solution was vortexed. To the above fraction, 200 µL of deionized water was added, and the solution vortexed and centrifuged for 6000 xg in a microcentrifuge. The protein precipitate was formed between the interphase. The upper and lower phases were carefully removed and discarded. The protein precipitate was washed with 300 µL of methanol and then with another 300 µL of 95% methanol. The pellet was air dried until methanol evaporated. The pellet was solubilized with 400 µL of rehydration buffer (7 M urea, 2 M thiourea, 2% 3-[(3-Cholamidopropyl) dimethylammonio]-1-propanesulfonate (CHAPS), 1% Biolyte pH 3-10NL (Bio-rad), 50 mM DTT, 0.01% Triton (v/v) X-100, 0.05% (w/v) β-dodecyl maltoside, and bromophenol blue) by vortexing for 2 h. The solubilized pellet solution was centrifuged at 20000 xg for 15 min at room temperature. The supernatant was saved in a fresh microfuge tube without disturbing the pellet.

The 17-cm immobilized pH gradient (IPG) strip was rehydrated with 300 µL of sample containing ~400 µg of protein. The IPG strip was placed with the gel side facing down on the sample from one end without forming any air bubbles. The sample was allowed to stand for 5 min and then 3.0 mL of mineral oil was added on the backside of the strip and covered with a lid. The sample was left with the mineral oil for at least 14 h to rehydrate the strip. Two electrode wicks were placed on electrodes of the focusing tray by wetting with 8 µL of nano-pure water and placed in the PROTEAN IEF Cell system (Bio-rad). The strip was carefully removed from the rehydration tray by holding one side of the strip with a forceps, and the mineral oil was drained. The IPG strip that

has been rehydrated was loaded into the focusing tray by placing the gel side down and overlaying it with 3.0 mL of mineral oil and covering with the lid. The following program was followed to run the isoelectric focussing at 20 °C.

Step 1: 250 V, 20 min, linear

Step 2: 10,000 V, 2.30 h, linear

Step 3: 10,000 V, 40,000 V-h, rapid.

4.2.12 Second dimension gel electrophoresis of IPG strips

After completion of isoelectric focussing, the IPG strip was carefully removed and the mineral oil was drained. The IPG strip was placed in the rehydration tray by facing the gel side up. A volume of 6 mL of equilibration buffer I (375 mM Tris–HCl, pH 8.8, 6 M urea, 2% (w/v) sodium dodecyl sulphate (SDS), 20% (v/v) glycerol, and 2% (w/v) DTT) was added to the tray and IPG strip was incubated on the rocker with slow motion for 15 min. The equilibration buffer I was discarded by slanting one side and then 6 mL of equilibration buffer II (375 mM Tris–HCl, pH 8.8, 6 M urea, 2% (w/v) SDS, 20% (v/v) glycerol, and 2.5% (w/v) Iodoacetamide) was added and the tray was incubated for 15 min on the rocker.

The glass plates were assembled according to the instructions of the manufacturer and the resolving gel (12%) was poured allowing 1-cm gap for placing the IPG strip. Water-saturated butanol was overlaid; this ensures that a flat top gel surface is achieved when the gel polymerizes. The top of the gels should be thoroughly washed with distilled water to remove all traces of butanol and unpolymerized acrylamide. Agarose used for overlaying on the gel was melted in a microwave. The equilibrated IPG strip was immersed twice in 1x running buffer (25 mM Tris–HCl, pH 8.3, 192 mM glycine, and 0.1% SDS) to ensure that excess equilibration solution has been removed.

The plastic backing was placed along a big glass plate with forceps and the strip was gently pushed down onto the top of resolving gel. Overlay agarose was added to the well and the strip was slowly pushed into the well to ensure full contact between the IPG strip and the resolving gel. In order to reduce the heat, a circulating water bath was connected to the Protean II xi (Bio-rad) 2D cell by setting the temperature to 15°C. The electrophoresis chamber was filled with 1x running buffer and connected to the power supply. The initial run was for 20 min at 80 V and then increased to 200 V. Colloidal coommassie stain method was followed to detect 2D spots (Neuhoff et al., 1988) and gel was scanned using Amersham gel scanner. The gel spots were identified using PDQuest basic 8.0.1 imaging software

4.2.13 Trypsin digestion

The SDS gel was washed twice with distilled water. The spots were picked up manually with a clean scalpel, made into small 1-mm^3 pieces, and transferred into sterile 1.5-mL eppendorf tubes as previously reported by Yadavalli et al., (2011). Washed the gel particles with water and 50 mM NH_4HCO_3/acetonitrile 1+1 (v/v) for 15 min. The remaining liquid was discarded and enough acetonitrile was added to cover the gel particles. After adding acetonitrile, the gel pieces shrink and stick together; the excess acetonitrile was subsequently removed. The gel particles were air dried. Protein disulfide bridges were reduced by adding reduction buffer and incubating the gel for 45 min at 50°C. After cooling to room temperature, excess liquid was removed and replaced quickly with the same volume of freshly prepared alkylation buffer. The gel particles were incubated for 30 min at room temperature in the dark and the iodoacetamide was removed. The gel particles were washed with 50 mM NH_4HCO_3/acetonitrile in 1:1 (v/v) for 15 min, twice. The gel particles were completely

covered with acetonitrile. Extra acetonitrile was removed once the gel particles finished shrinking, and then the gel particles were allowed to air dry. To this, enough freshly prepared trypsin enzyme solution (25 mM NH_4HCO_3 with 10 ng/µL trypsin) was added and the solution was incubated for overnight at 37°C. The trypsin solution can be added to cover the gel pieces. The excess solution was carefully transferred to sterile 0.5-mL tubes and the gel pieces were extracted twice with 50% acetonitrile and 5% triflouroacetic acid. These two extracts were combined with the earlier one and concentrated with Speedvac. The ZipTipc18 was wetted by depressing a pipette plunger to a dead stop, using the maximum volume setting of 10 µL, and aspirating the wetting solution into the tip. This procedure was repeated twice. The ZipTipc18 was equilibrated with equilibration solution and dispensed to waste. This procedure was repeated two times. To bind peptides and/or proteins to ZipTipc18, the pipette plunger was depressed to a dead stop into the sample. The sample was aspirated and dispensed using seven to ten cycles for maximum binding of complex mixtures. The wash solution was aspirated into the tip and dispensed to waste. The peptides and/or proteins were eluted with 4 µL of elution solution into a clean vial using a standard pipette tip.

4.2.14 MALDI-TOF-TOF measurements.

Aliquots of the sample measuring 2 µL were mixed with 1.5 µL of matrix (a saturated solution of α-cyano-4-hydroxycinnamic acid in 50% acetonitrile/0.1% trifluoroacetic acid) and a droplet of the mixture (about 1.5 µL) was spotted on the sample plate and allowed it to air dry for 5 min (Subramanyam et al., 2006). Mass spectra were collected on Bruker's autoflexIII mass spectrometer and analyzed with Flux analysis. From the monoisotopic masses obtained, the amino acid sequences of

matching tryptic fragments of *C. reinhardtii* thylakoid proteins were obtained using the MASCOT and Expasy server.

4.3   Results

4.3.1   Analysis of Chl and photochemical activity

Under iron deficiency conditions cells showed a decrease in chlorophyll content (Figure 4.1A) over time. The culture changed its color from greenish to the yellow-greenish color after 72 h. Chlorophyll content decreased by 83 % compare to the control under iron deficient conditions after 72 h (Figure 4.1B). The cell growth rate was also decreased under iron stress relative to the control culture, as determined by the wet weight of the cell pellet. Upto the 48 h, the cells were not severely affected but it is clear after 72 h where cells were almost completely deployed of iron and forced to change in the metabolic activities to adjust the environment. This may be due to utilization of cells reserved iron (Ferritin) for normal physiological functions. After exhaustion of the reserved iron the cells were severely affected due to lack of any alternative source for metabolic process of the organism. The decrease in chlorophyll content is an indication of the corresponding LHCI subunit downregulation, as each Lhca subunit binds at least 14 chlorophyll molecules. Since the loss of chlorophyll molecules leads to the inefficient light harvesting and there by casing decline in photochemical activities.
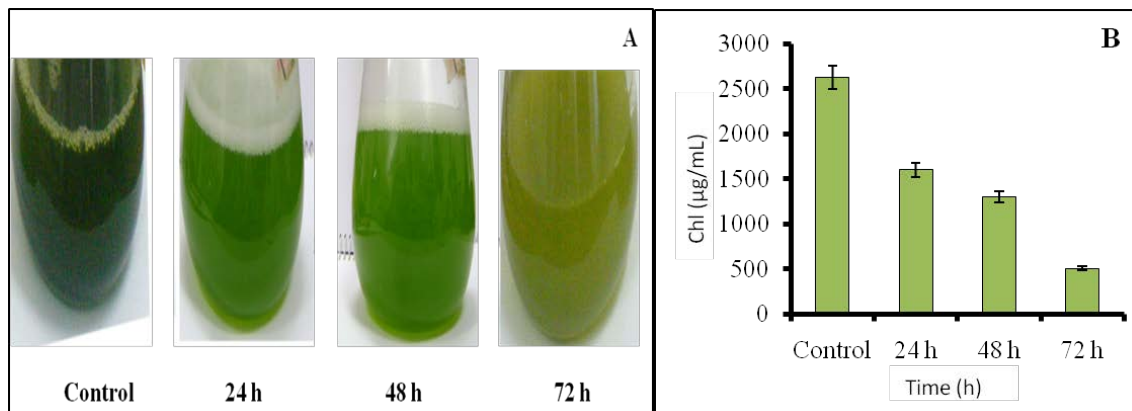
Figure. 4.1 *C. reinhardtii* **culture under iron deficiency conditions at different time intervals (A) shows the phenotype of the cultures and (B) Indicates a decrease in chlorophyll content (n=5).**

4.3.2 Analysis of Chl fluorescence transient

The Chl florescence transients are sensitive to various abiotic stresses which can be analyzed by the JIP test (Strasser and Strasser, 1995; Strasser et al., 2000; Strasser et al., 2004). When dark-adapted photosynthetic cells are exposed to strong saturating light, for one second, the Chl *a* fluorescence transient shows complex kinetics termed as the OJIP transient, which reflects mainly the stepwise closure of PS II centers, *i.e.,* the accumulation of Q_A state. Three-phase kinetics of the PS II closure following J, I, P steps during OJIP rise is determined by the successive establishment of the equilibrium between the reduction and
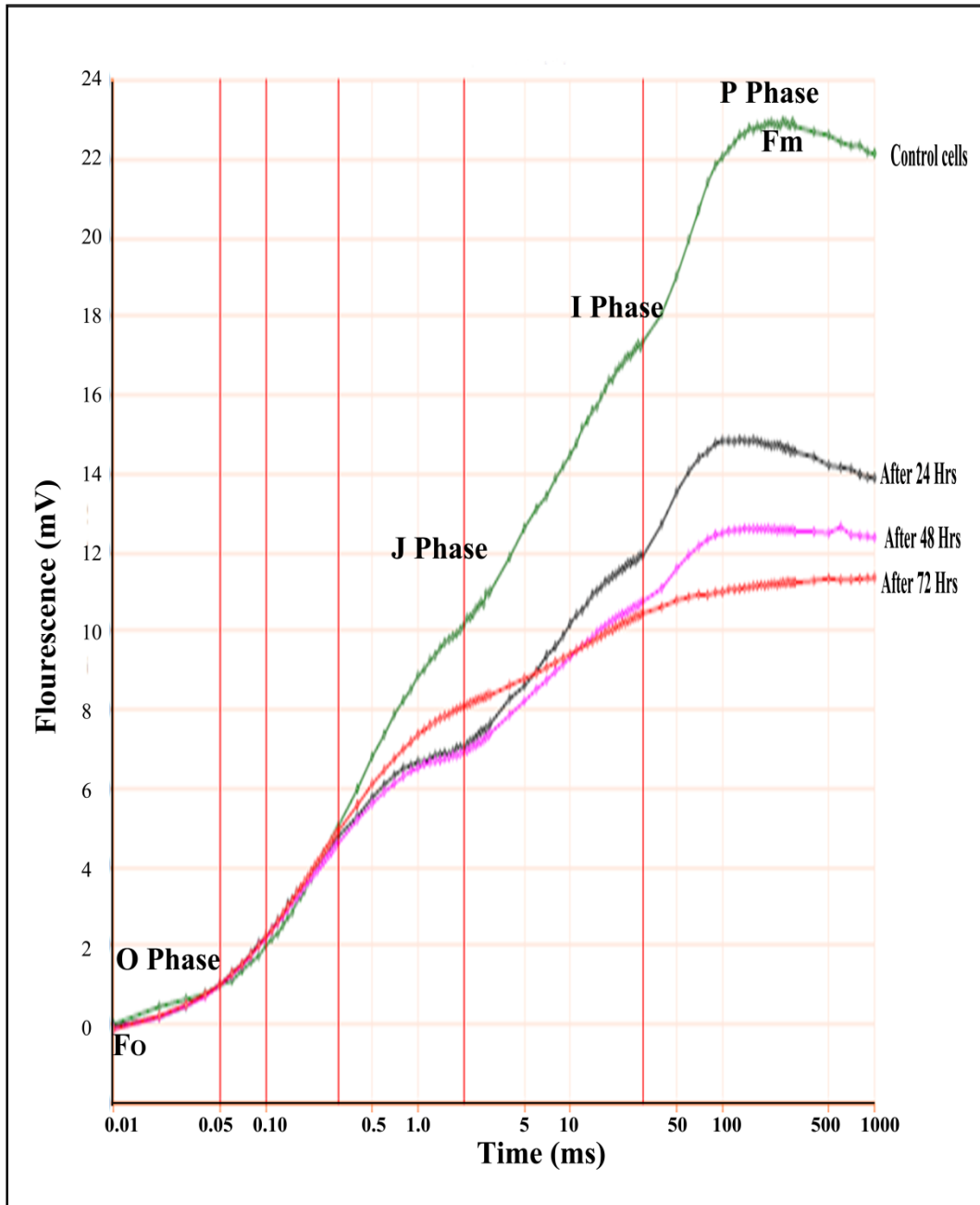
Figure 4.2 Fast Chlorophyll *a* fluorescence transients of control and iron deficient cultures of *C.reinhardtii* cells at different time intervals. The curves were normalized at F_0.

re-oxidation of the PS II acceptor side (OJ), PQ pool (JI), and intermediates beyond the Cyt b_6/f complex (IP) (Antal and Rubin, 2008). The O–J phase is largely attributed to the reduction of Q_A. As a whole, the O–J–I–P transient is associated with changes in the redox state of electron carriers in PSII and non-photochemical quenching processes (Lazar, 2003).

When fluorescence data was normalized at F_1, significant differences were observed between the control and iron deficient cultures (Figure 4.2). In cells from the control culture, the three phases of OJIP are very clear and have maximum florescence indicating the efficient electron transport in the Z-scheme. Under iron deficient conditions the maximal fluorescence was decreased about 50% indicating decline in electron transport in the Z-scheme. Even though the maximal fluorescence was reduced to 50% the three phases were still clear after 24 h of iron deficiency; longer periods of Fe stress led to additional amplitude decrease and blurring of the three observed maxima. The fluorescence yield decreased by 20% at J phase, 41% at I phase, and 52% at P phase (Fm) after 72 h under iron deficient conditions. Among these three phases the P phase shows the PSI florescence (Franck et al., 2002; Papageorgiou et al., 2007), which is completely lost under iron deficiency conditions, indicating that the iron deficiency response in *C. reinhardtii* targets the PSI reaction centre. Similar results were obtained when *C. reinhardtii* cultures were deprived of sulphur (Antal et al., 2006).

4.3.3 Analysis of Fluorescence emission

Figure 4.3 shows the steady state room temperature fluorescence emission data of *C. reinhardtii* cells grown under control and iron limited conditions. Room temperature fluorescence (Figure 4.3a) data shows little difference in the fluorescence maxima at 680 nm between control and iron stress cells under equal Chl concentrations.

The 77 K emission spectra is dominated by a small number of red-shifted chlorophyll sites, and is a more sensitive monitor of changes in both PSI and PSII. The 77K emission spectra reveals the
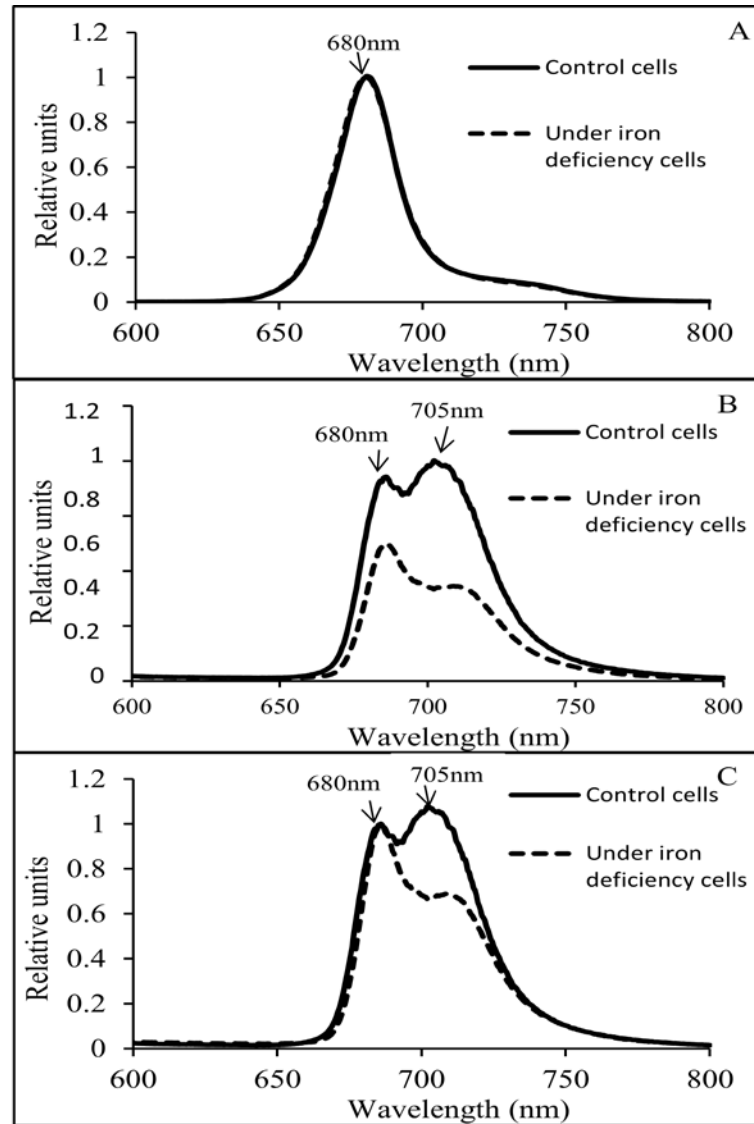
Figure 4.3   Fluorescence spectra of control and iron stress *C.reinhardtii* cells. A) room temperature emission spectra B) 77K spectra emission spectra C) normalized at 680 nm of 77K emission spectra

fluorescence maxima at 680 and 705 nm which are attributed to PSII and PSI, respectively (Hwang-Schweitzer et al., 1992; Thangaraj et al., 2011). The amplitudes of these two peaks change dramatically under Fe stress; this can be seen most easily by normalizing the two spectra at 680 nm (Figure 4.3c). This data indicates that both PSII and PSI were damaged; however, the impairment of PSI is more after 72 h of cell grown under iron deficiency.

4.3.4 Sucrose gradient analysis of PSI-LHCI supercomplexes

PSI-LHCI supercomplexes were isolated using sucrose density gradient centrifugation. The detergent extracts of the thylakoid membranes were loaded onto the gradient at equal chlorophyll levels (0.8 mg/ml Chl). After the centrifugation, three distinct bands were observed in both the control and the iron stress samples (Figure 4.4); the fractions corresponded to F1 (LHCII), F2 (PSI-LHCI and PSII), F3 and F3' (Both contains PSI-LHCI supercomplexes) (Subramanyam et al., 2006).

For this study, PSI-LHCI supercomplexes (F3 and F3') were collected from the sucrose gradient. Significant differences were observed between the control and iron stress samples in the banding pattern. The intensity of the F3 band was reduced in iron stress conditions, while the F3' band was completely absent (Figure 4.4), further underscoring PSI's sensitivity to Fe stress.
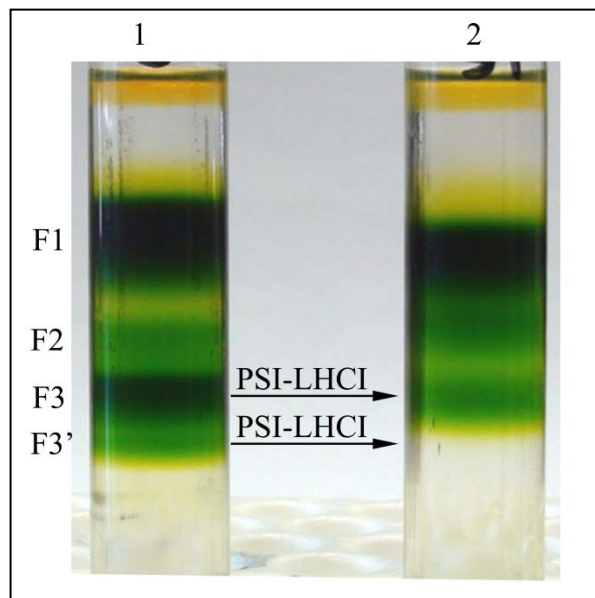
Figure 4.4 Separation of PSI-LHCI supercomplexes from solubilized thylakoid membranes by sucrose density centrifugation. F1 (LHCII), F2 (PSI-LHCI and PSII), F3 and F3' (Both contains PSI-LHCI supercomplexes).

4.3.5 Visible CD data analysis

Visible CD spectroscopy is a sensitive technique to monitor the excitonic pigment–pigment and pigment–protein interactions. In the Q_y region, there are two negative peaks at 641 and 675 nm and one positive peak at 656 nm (Figure 4.5), similar to the previous report (Subramanyam et al., 2006; Subramanyam et al., 2010b). The two major bands at 656 and 675 nm are due to Chl dimers caused by the excitonic interaction of Chl *a* in PSI–LHCI supercomplexes, while the negative peak at 641 nm is characteristic of Chl *b* (Bassi and Simpson, 1987; Subramanyam et al., 2006; Subramanyam et al., 2010b). In the Soret region, the positive peak at 443 nm originates from Chl *a*, while the negative peak at 460 nm is characteristic of Chl *b*. The visible CD spectrum of PSI-LHCI supercomplexes isolated from *C. reinhardtii* cells grown under iron stress conditions shows an increase in the amplitude of the major peak at 675 nm

and a blue shift of about 5 nm. The negative peak at 641 nm showed an increase in amplitude relative to the control, along with a blue shift of about 4 nm. The Soret band peaks at 443 and 460 nm also increased in intensity. The differences in the peak intensity indicate significant differences in pigment interactions in PSI-LHCI complexes; it is also possible that there may be macro- aggregation of pigment-proteins or pigment-pigment from iron stress cells (Subramanyam et al., 2005).
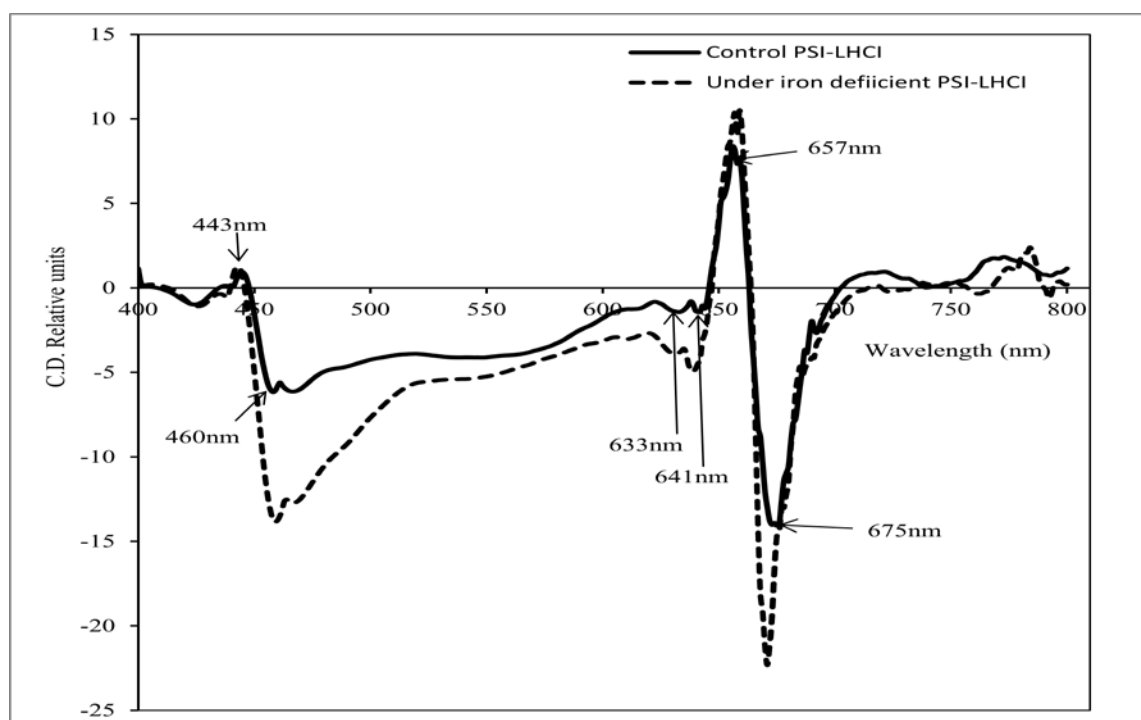
Figure 4.5 Visible CD spectra of isolated PSI–LHCI supercomplexes from control and iron-stressed *C. reinhardtii* cells. The Chl content of the samples was adjusted to 10 μg/ml. CD was measured in absorbance units. However, for easier comparison, the data are plotted in relative units. CD was repeated 3 times in different samples and each time identical spectra were obtained.

4.3.6 Pigment protein complex analysis

Green gel was performed in order to see the pigment-pigment interactions. Figure 4.6 shows a clear separation of pigment complexes of PSI core, PSI-LHCI complexes and LHCI complexes, respectively. In which, LHCI complexes content was lower when compare to the control. This indicates that pigment-pigment complexes were disturbed in iron deficiency cells. CD data is in agreement with the green gel data.
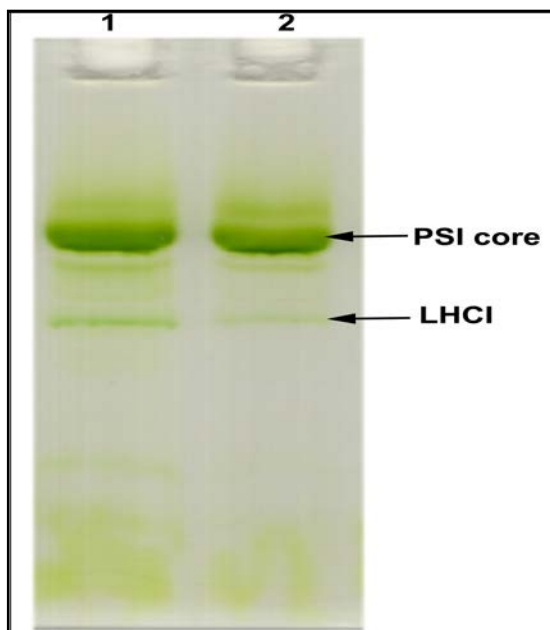
Figure 4.6 Green gel of PSI-LHCI supercomplexes. Lane 1- Control PSI-LHCI supercomplexes, and Lane 2-PSI-LHCI supercomplexes isolated from iron deficient culture. LHCI content was decreased under iron deficient conditions.

4.3.7 Streak camera data analysis

Fluorescence decay spectra were measured using an ultrafast streak camera setup for PSI-LHCI supercomplexes isolated under iron stress, and for control conditions. For each sample, kinetics were measured on 800 ps, 1.4, and 2 ns timescales and fit to three decay components. The component with the shortest lifetime was very consistent across

samples and timescales, with a lifetime of ~33 ps. This is consistent with the behaviour previously observed for *C. reinhardtii* PSI-LHCI under salt stress conditions. (Subramanyam et al., 2010b). Based on comparison with previous studies of excitation trapping in PSI (Gobets and Van Grondelle, 2001), this component of the fluorescence decay can be attributed to the trapping of excitons originating within the PSI core. The second component, which has previously been associated with the trapping of excitons originating in the peripheral LHCI complexes (Ihalainen et al., 2005), is more heterogeneous. As is shown in Table 4.1, however, the variations between samples measured at different time scales are more significant than the differences between the three samples. Although fitting the fluorescence decay with three exponentials provides a convenient description of the kinetics, it must be kept in mind that the real process being measured is far more complicated—the lifetimes found by global analysis merely provide characteristic time scales for various decay processes. Variation of the lifetime found by global analysis with measurement timescale can be attributed to heterogeneity within this decay phase.

Only the lifetimes of the first two components are presented; the third was typically fixed at 4 ns during fitting and does not represent functional antenna pigments. Values are mean ± SE ($n = 8$). Far more insight into the nature of these decay phases can be obtained by examining the spectral shapes of the three decay components. The shape of the first (~33 ps) component is extremely consistent among the samples measured (Figure 4.7a).
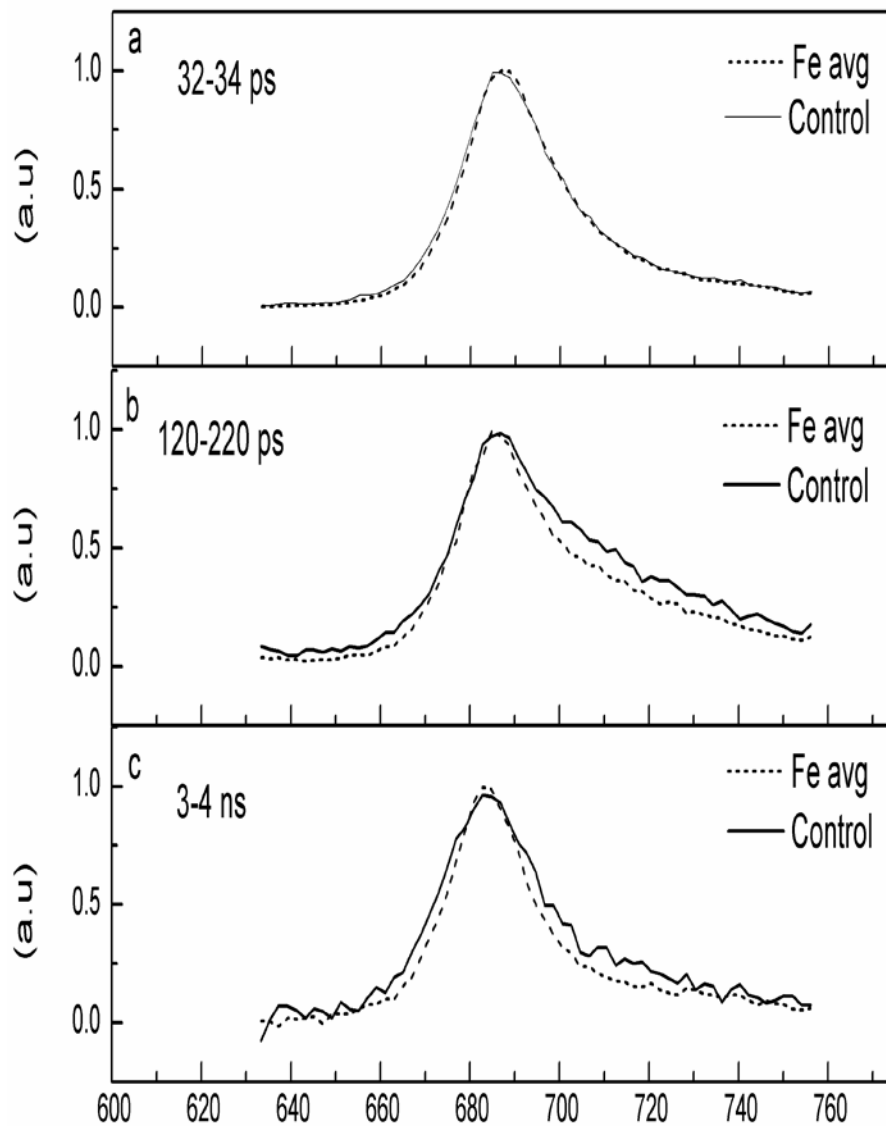
Figure 4.7 Representative fluorescence decay-associated spectra (FDAS) obtained from fluorescence streak camera measurements from isolated PSI-LHCI supercomplexes obtained from *C.reinhardtii* grown under control and iron stress conditions. Fluorescence decay lifetimes are 35–38 ps (a), 22–211 ps (b), and 2–4 ns (c). Each curve shown is the average of the fitted curves from the three data sets collected for each sample

Given that the PsaA and PsaB proteins, which bind the bulk of PSI's core antenna, appear based on immunoblotting results to be largely unaffected by iron stress, this suggests strongly that only pigments bound to the PSI core contribute to this component. This is consistent with structural studies (Jordan et al., 2001; Amunts et al., 2007) that show that the PSI core is a stable, tightly integrated complex.

Similar conservation can be seen in the spectral shapes of the third component (3–4 ns); such lifetimes are typically attributed to detergent-solubilized Chl that is not coupled to PSI (Figure 4.7c). It should be noted that the amplitude of the nanosecond component was much lower in the control sample than in the stress samples and the spectral shapes could only be compared after normalization. This indicates that the PSI-LHCI from iron stressed cells contains more uncoupled pigments. The major difference in the decay-associated spectra of the control and iron-stress samples can be seen in the spectral shape of the 120–220 ps component (Figure 4.7b). While the decay lifetimes are relatively unchanged by cell growth under iron stress conditions, this component shows a decrease in emission intensity on the red side of the peak in the iron-stressed samples. Red emission in *C. reinhardtii* PSI has previously been associated with strongly coupled pigments bound by the LHCI proteins (Gibasiewicz et al., 2001; Gibasiewicz et al., 2002; Gibasiewicz et al., 2005) and so this loss of red emission can be attributed to a disruption of the LHCI antenna system. Similar results were observed in salt stress conditions, suggesting that LHCI is liable to be lost under a variety of different stress conditions (Subramanyam et al., 2010b).

Table 4.1 Trapping lifetimes obtained from streak camera measurements

Sample	τ_1	τ_2
Control	32.1 ± 3.6 ps	172.26 ± 42.4
Fe stress	34.4 ± 1.4 ps	165.0 ± 5.8
Timescale		
800 ps	29.8 ± 3.4 ps	136.1 ± 23.6
1.4 ns	33.4 ± 2.4 ps	161.1 ± 13.2
2 ns	34.9 ± 1.7 ps	196.5 ± 21.2

4.3.8   Effect of iron stress on the protein content of PSI core subunits

The PSI-LHCI supercomplexes were separated by SDS-gel electrophoresis and protein profile was shown in Figure 4.8. Immuno blotting was carried out to determine the changes of protein level in both PSI and LHCI. Figure 4.9 shows immunoblotting of PSI core subunits. There was no change in the central core proteins of PSI (PsaA and PsaB). The core proteins PsaA, B, C, D, and E are almost stable after 24 h of growth under iron deficiency conditions. More importantly, levels of PsaC and PsaD were reduced in expression, and PsaE was completely disassociated (Figure 4.9) after 72 h of continuous iron deficiency conditions. Of all the PSI subunits, PsaE is the most sensitive and completely depleted by iron stress (Figure 4.9). Similar results were obtained when cyanobacteria adopted to low-iron aquatic environments (Chauhan et al., 2011).

4.3.9   Analysis of LHCI protein subunits under iron deficiency conditions

The Lhca subunits show varying susceptibility to iron deficiency conditions (Figure 4.10). After 24 h of iron deficiency conditions, Lhca1 is the first to be disassociated completely from the core complexes, Lhca9 degraded by 80%,, Lhca2, LHca7 and Lhca8 were degraded by 50%. Lhca3, Lhca4, Lhca5, Lhca6, were unchanged.
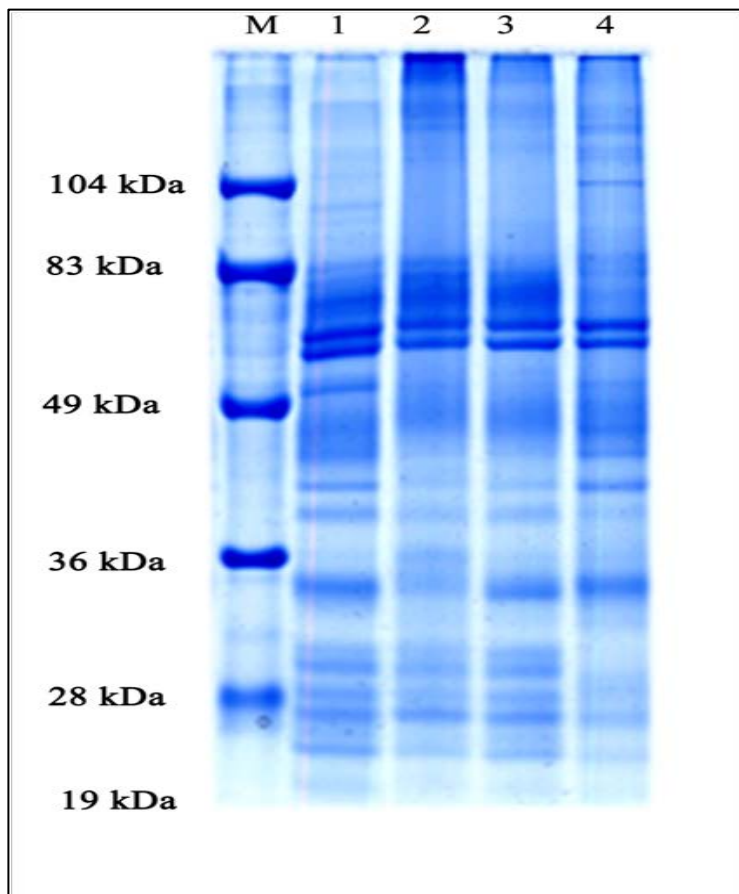
Figure 4.8 SDS-PAGE protein profile of PSI-LHCI supercomplexes. Cells were grown at different days under iron deficiency, lane 1 (control), lane 2 After 24 h under iron deficiency, lane 3 After 48 h under iron deficiency, lane 4 After 72 h under iron deficiency. All the experiments were compared with the 72 h cells and this one treated as control. However, in all the lanes equal Chl (10 μg) concentrations were maintained.

After 48 h of iron stress, Lhca2 suffers more damage than the rest of the subunits. When Fe stress conditions were continued up to 72 h, the remaining Lhca subunits were disassociated from the PSI core, with the exception of Lhca6, which remain stable with 50% damage. Each LHCI protein lost from the PSI-LHCI supercomplex results in a loss of 10-14 chlorophyll molecules; this leads to a dramatic

decrease in PSI absorption cross-section and is likely to be a component of stress-induced chlorosis.
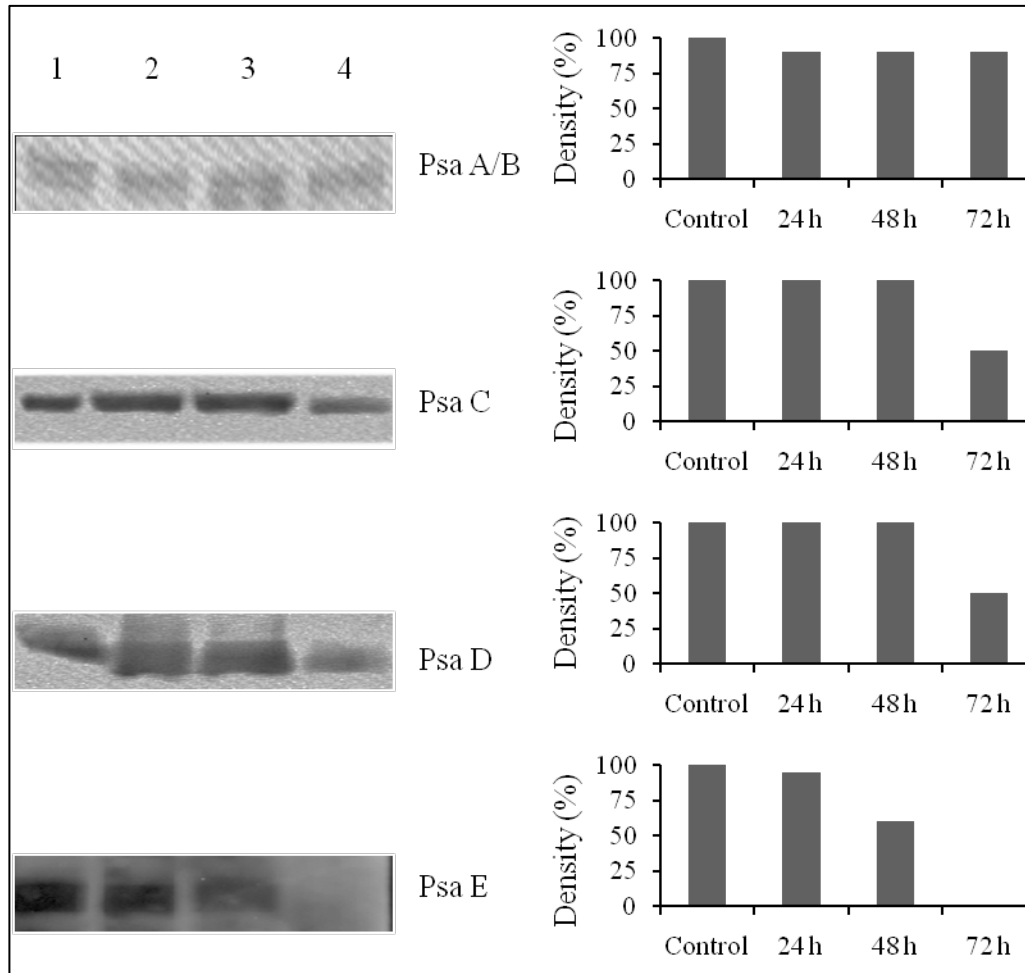
Figure 4.9 Immunoblot of PSI core subunits were identified from isolated PSI-LHCI supercomplexes. PsaA, PsaB and PsaD were more stable under iron deficiency conditions compare to PsaC and PsaE. Right panel shows the density of the each PSI core proteins obtained from western blots (left panel).
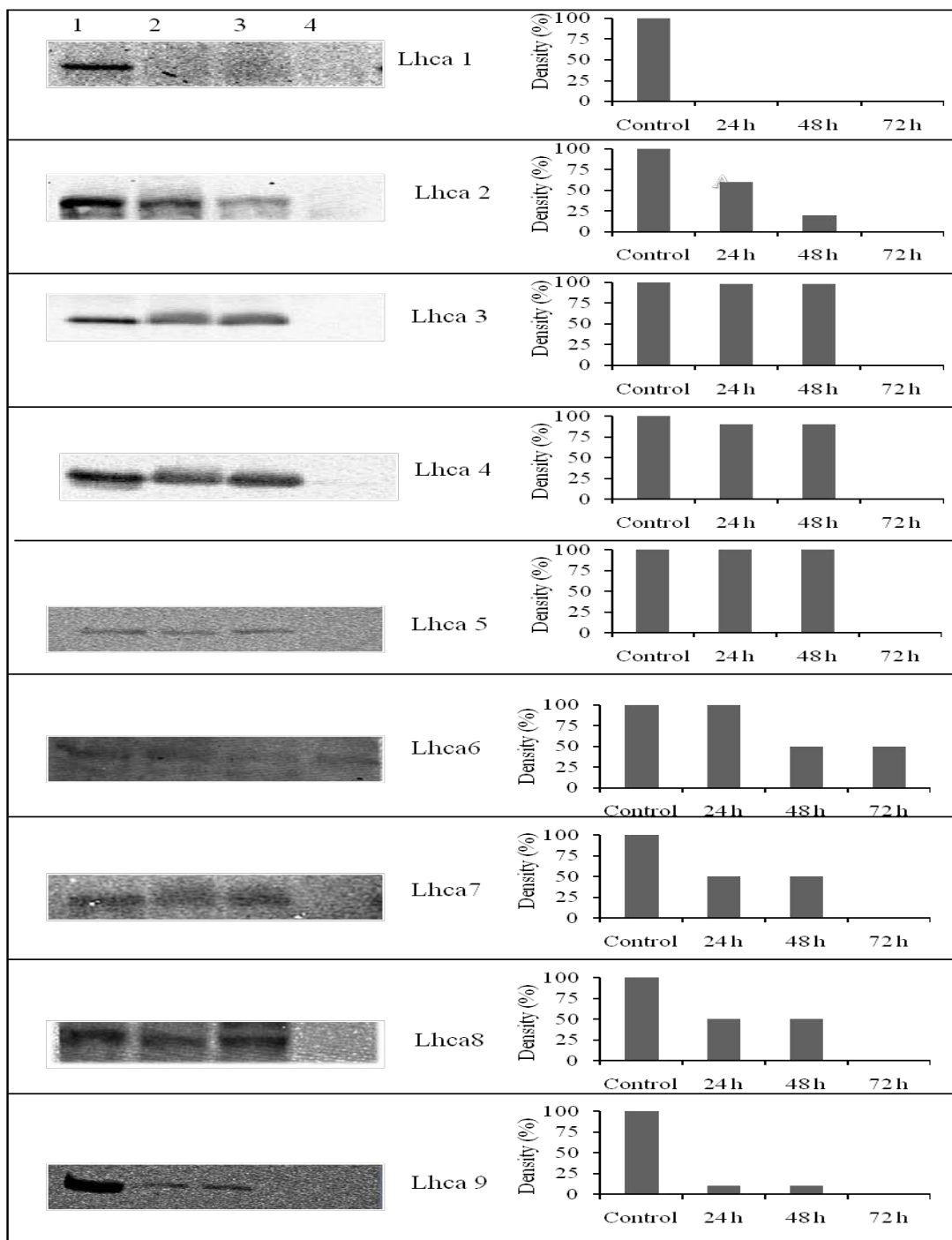
Figure 4.10 Immunoblot of Lhca 1-9 polypeptides were identified from isolated PSI-LHCI supercomplexes. Lhca 1 and Lhca 9 were more susceptible to iron deficiency conditions. Lhca 6 was more stable compare to all other LHCI subunits. Right panel shows the density of the each LHCI proteins obtained from western blots (left panel).

91

4.3.10 SOD activity analysis.

The expression of SOD genes are involved in the environmental stress responses of many species, including both animals and plants (Chen and Pan, 1996). Electrophoretic pattern of SOD isolated from thylakoids was shown in Figure 4.11.
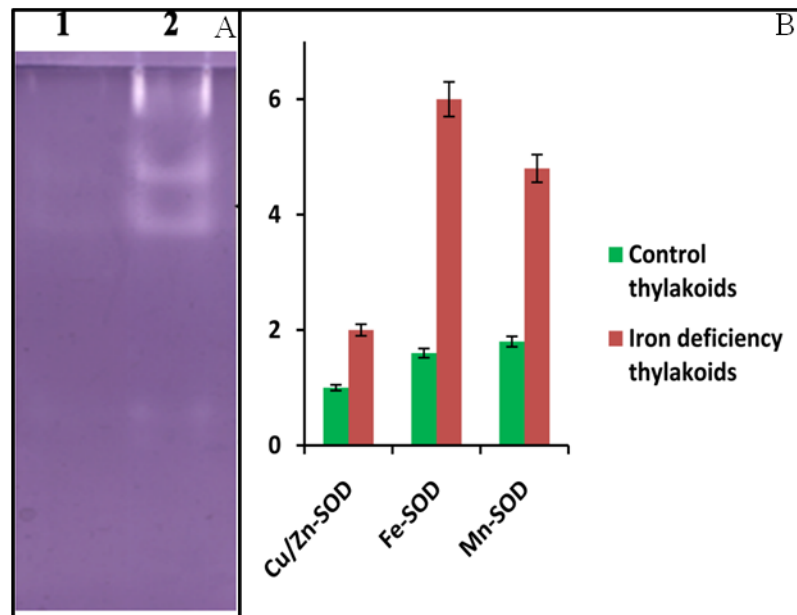
Figure 4.11 A) Identification of SOD isoforms by electrophoresis under native staining and B) SOD isoforms activity of thylakoids. Lane 1 shows control thylakoids and lane 2 shows thylakoids isolated from cells under iron deficiency.

The sensitivity of Cu/Zn-SOD to cyanide (KCN) has been used as a diagnostic tool to distinguish Cu/Zn-SOD from Fe-SOD and Mn-SOD that are unaffected by cyanide. Likewise, Fe-SOD is irreversibly inactivated by H_2O_2, whereas Mn-SOD is resistant to both inhibitors (Baum and Scandalios, 1979). The SOD detected in the present study is thought to be Fe-SOD. These results shows that all SOD forms (Cu/Zn-SOD, Fe-SOD and Mn-SOD) are overexpressed in Fe stress condition in thylakoids,

indicating that Fe deprivation and oxidative stress are intimately connected in *C. reinhardtii*. Thus, changes observed in PSI and PSII may be due to oxidative damage.

4.3.11 2D gel electrophoresis analysis

From the 2D gels, number of proteins were separated based on their isoelectric point, in which there are several changes were observed from PSI-LHCI supercomplexes in Fe deficiency cells after 72 h. However, a number proteins altered especially LHCI subunits (Figure 4.12). Most of these altered LHCI subunits were subjected to MALDI-TOF and analysis in Mascot server to identify their proteins. The LHCI subunits such as Lhca2, Lhca3, Lhca4, Lhca5, and Lhca7 were almost completely down regulated under iron deficiency conditions. Lhca6 showing 50% loss in the protein quantity under iron deficiency conditions (Table 4.2). The peptide fragments obtained by MALDI-TOF-TOF were theoretically matched with the 'PepMAPPER peptide digest tool' of expasy server. The fragments matched were indicated in the Table 4.2.
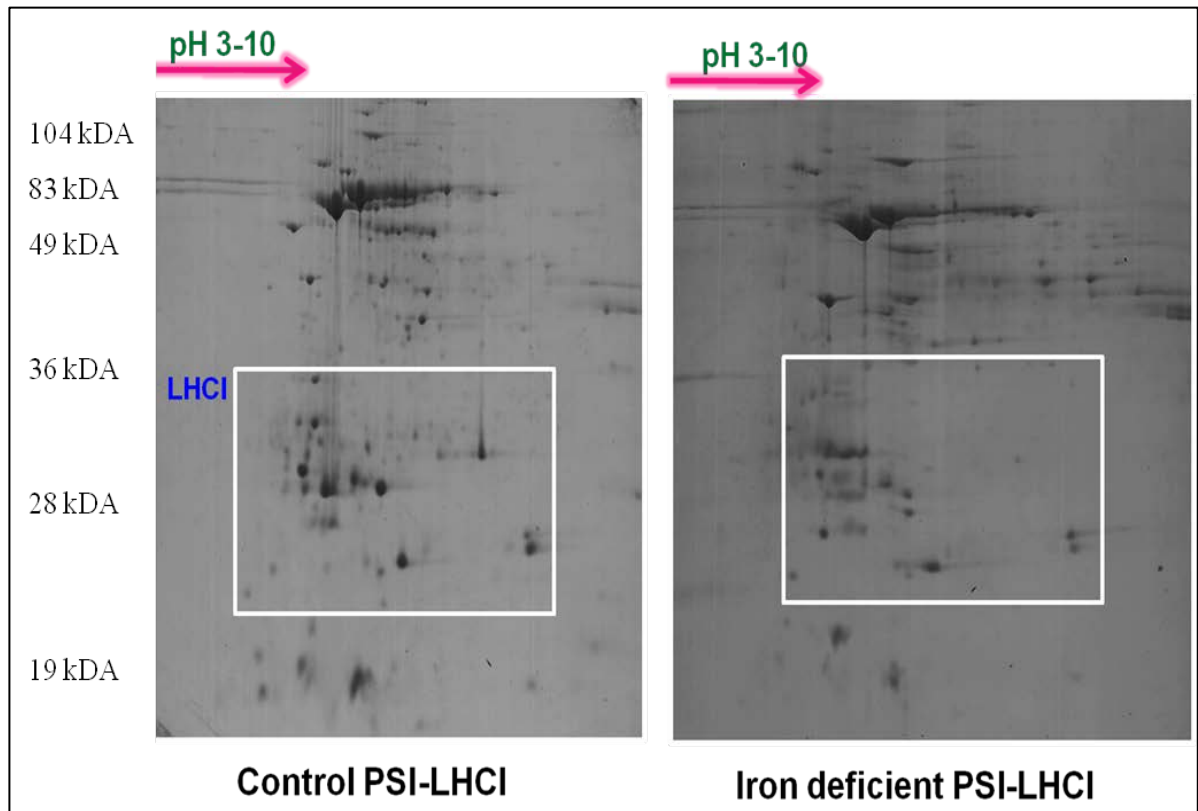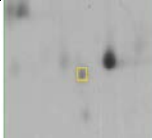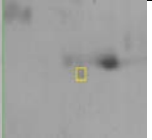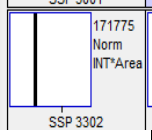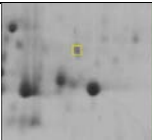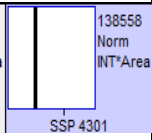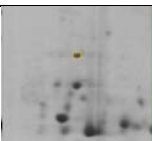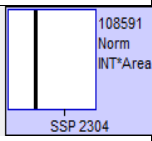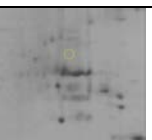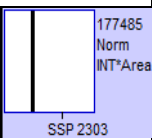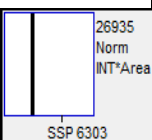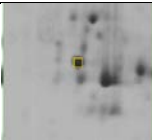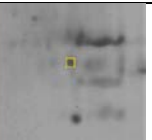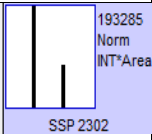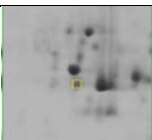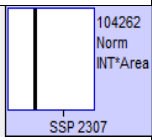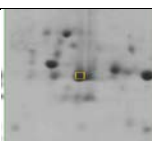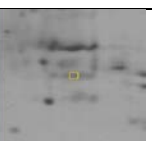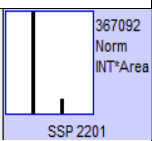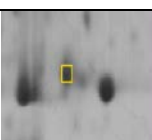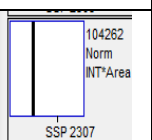
Figure 4.12 2D Gel electrophoresis of Control and iron deficient PSI-LHCI supercomplexes. The box area represents LHCI subunits, which were down regulated under iron deficiency conditions.

The LHCI subunits were mostly effected as seen in the Figure 4.12 indicated in the white border box area, both in the number as well as the quantity of the expression of the proteins. Among the spots analyzed within the box were found to have light harvesting complex I subunits of *C. reinhardttii.*

Table 4.2 MALDI-TOF analysis of differentially expressed LHCI polypeptides.

Mascot search match: protein ID	Corresponding protein	No. of fragments matched	PSI-LHCI		Quantity level
			Control	Fe deficient	
AAD03734	Lhca1 (23.9 kDa)	1			171775 Norm INT*Area SSP 3302
XP_001691031	Lhca2 (28.4 kDa)	2			138558 Norm INT*Area SSP 4301
BAD06919.1	Lhca3 (30.3 kDa)	2			108591 Norm INT*Area SSP 2304
BAD06918	Lhca4 (28.7 kDa)	1			177485 Norm INT*Area SSP 2303
XP_001702730	Lhca5 (28.2 kDa)	1			26935 Norm INT*Area SSP 6303
ABD37907	Lhca6 (27.8 kDa)	2			193285 Norm INT*Area SSP 2302
AAO16495	Lhca7 (26.2 kDa)	1			104262 Norm INT*Area SSP 2307
XP_001696202	Lhca8 (25.9 kDa)	2			367092 Norm INT*Area SSP 2201
AAL87738.1	Lhca9 (22.8 kDa)	1			104262 Norm INT*Area SSP 2307

4.4   Discussion

The primary objective of this work was to evaluate the effects of iron stress on PSI-LHCI supercomplexes from *C. reinhardtii*, in an effort to understand the effects of stress on PSI function. Previous research has shown that many types of abiotic stress affect PSII, but the extent of damage for PSI is less studied. The results indicate that stress-related damage to PSI is also significant and may be an important part of the organism's overall stress response.

C. reinhardtii cells were grown under complete iron less media, reaching an OD of ~1 at 730 nm. The control cells reached maximumm growth within four days; growth in iron deficient medium did not reach this level due to Chl associated proteins degradation. The fluorescence transient showed that there were alterations is PSII, however, the electron transfer is reduced from Q_A to PSI after 72 h grown cells, which indicate that PSI is prone to Fe stress. Also, the low temperature 77K emission spectra showed that the PSI is damaged more than PSII (Figure 4.3B). Iron stress conditions clearly impair cell growth; the goal of this study is to establish the degree to which this growth impairment results from damage to PSI-LHCI. The electron transfer activity was decreased (Figure 4.2), but levels of the subunits PsaA and PsaB, which form the core of PSI and bind the majority of the cofactors of the electron transfer chain (ETC) (P700, A, A_O, phylloquinones (A_1) and the 4Fe4S clusters, F_X) (ETC), were unchanged. This suggests that the impairment may lie in energy transfer from LHCI to PSI core, or in damage to the acceptor side of PSI (terminal Fe-S clusters $F_A + F_B$), rather than to the oxidizing side of the ETC.

In keeping with these results, the fluorescence decay component associated with trapping in the PSI core was virtually unchanged between the control and iron stress

samples (Figure 4.7a). The 32–34 ps compound arises from the PSI core (Gobets and Van Grondelle, 2001) but there is no difference in fluorescence lifetime in the control and iron stress samples (Figure 4.7a) indicating that the PSI core antenna is not affected. Differences were quite apparent in the second component (Figure 4.7b), which decays on the 120–220 ps timescale. The curves look similar on the blue side of the emission peak, but the stressed samples show significantly less emission on the red side than the control sample. Red-shifted pigments in photosynthetic systems typically arise from strongly coupled dimers of Chl molecules and may exert a significant influence on the exciton trapping dynamics. Previous spectroscopic studies of green algal PSI (Gibasiewicz et al., 2001; Gibasiewicz et al., 2002; Gibasiewicz et al., 2005) have indicated that the PSI core in *C.reinhardtii* does not contain any pigments with transition energies lower than that of P700-longer-wavelength pigments are associated only with the peripheral LHCI complexes. The loss of red-shifted emission in the iron samples can therefore be attributed to the change in pigment–pigment interactions of LHCI complexes under iron stress conditions. Green gel results also support this conclusion. Similar results have been obtained for *Chlamydomonas* grown under salt stress (Subramanyam et al., 2010b), where a decrease in the red side of the LHCI-related decay component was observed. The disruption of the red sites probably results from an overall decrease in the quality of PSI-LHCI coupling, which would cause more energy to be lost as fluorescence rather than being delivered to the core. In general, partially disrupted LHCI proteins would lead to the formation of more chlorophyll triplet states, exacerbating the production of reactive oxygen species (ROS) production during iron stress. Thus, in iron stress it may be different excitation energy distribution from LHCI to PSI core.

The visible CD data show an increase in amplitude at 675 and 656 nm, which can be attributed to a loss of tightly coupled Chl *a* in the LHCI antenna due to macro aggregation of the pigments. The peak associated with Chl *b* shifts from 641 to 638 nm under iron deficient conditions (Figure 4.5), suggesting a change in pigment–pigment interactions and may arise, for example, from a change of the Chl *a*–Chl *b* distance. The green gel data also supporting this with CD data that the pigment complexes were lost under Fe deficiency conditions. In addition, under UV-B stress also showed similar report that CD signals were increased due to change in pigment-pigment interaction or macro-aggregation of pigments (Rajagopal et al., 2005).

The immunoblot studies of LHCI subunits reveals that these were more prone to damage in iron deficient conditions than the core subunits. This may be because of existence of LHCI subunits surrounding the PSI core in half-moon shape, thus the free radicals generated under stress conditions first targets LHCI subunits. Thus, it also was hampering the light harvesting capacity of LHCI. The most susceptible LHCI subunits in order targets were Lhca1, Lhca9, Lhca2 and followed by Lhca4, Lhca5, Lhca7 and Lhca8. However, Lhca6 was more stable even after 72 h gown cells in Fe deficiency. These results suggest that Lhca1 and 9 subunits seem be to exposed to the surrounding environments which can be targeted first. The remaining subunits may exists close to the PSI core subunits, however, the Lhca6 subunits may be very closely associated with core where it protected very well. Based on the 3D model (Chapter II Figure 2.2 and Figure 2.5), it is evident that Lhca6 was embedded inside and closely to the core subunits and Lhca1 and 9 are exists closely to lumen where these are exposed to outside environments. This indicates that Lhca6 polypeptide able to harvest the light energy 50% of its maximal efficiency under iron deficiency conditions.

The stromal acceptor side of the PSI reaction center proteins were damaged by iron deficiency conditions. Figure 4.9 shows a clear reduction in the membrane-extrinsic PsaC and PsaE subunits of PSI. The crystal structure of *Thermosynechococcus* PSI shows that PsaE stabilizes the stromal hump and the interaction between the PsaA/B heterodimer and PsaC (Jordan et al., 2001; Jensen et al., 2007). From this data, it is clear that the degradation of the PSI stromal ridge begins at PsaC and PsaE. Complete loss of PsaE was reported in *C. reinhardtii* under salt conditions (Subramanyam et al., 2010b). The PsaE protein is located at the reducing side of photosystem I (PSI) and stabilizes the stromal hump that is involved in docking the soluble electron acceptors, particularly ferredoxin/flavodoxin (Lelong et al., 1996; Jordan et al., 2001; Jensen et al., 2007). While PsaC binds the terminal electron acceptors F_A and F_B and is essential for the function of PSI (Oh-oka et al., 1988), PsaD and PsaE stabilize PsaC and the stromal hump that is involved in ferredoxin binding (Chitnis et al., 1995; Sétif et al., 2002).

The damage to PSI-LHCI subunits is associated with an increase in SOD activity; thus scavenging the higher levels of reactive oxygen species generated under stress conditions. Similar results have been observed in *Arabidopsis* under cadmium or copper stress (Drazkiewicz et al., 2007), and in winter wheat sprout leaves under the effect of exogenous hydrogen peroxide (Batsmanova, 2008) and in sacred lotus under chilling and oxidative stresses (Li et al., 2009). The loss of PsaE at the reducing side of PSI may cause electron leakage to oxygen in the light (Mehler reaction), resulting in the formation of reactive oxygen species which could in turn damage the Fe–S clusters. These results agree with a report of a deletion mutant of *psaE* in the cyanobacterium *Synechocystis sp.* strain PCC 6803, which shows increased photo damage due to

formation of oxygen radicals (Jeanjean et al., 2008). As a result, the ferredoxin-docking site near the stromal Fe–S clusters destabilized, crippling electron transfer through PSI.

Mutagenesis studies have indicated that the subunits on the reducing side of PSI assemble in a well-defined order: PsaC first, followed by PsaD and PsaE (Zhao et al., 1993; Yu et al., 1995). Under iron-stress conditions, the decrease in levels of PsaC (Figure 4.9) results in the near-elimination of PsaE (Figure 4.9); this correlation supports a scheme in which the presence of PsaD is a prerequisite for PsaE binding (Lüneberg et al., 1994). Immunoblotting results also indicate that the levels of PsaC are considerable reduced under iron stress conditions (Figure 4.9); this is consistent with an assembly pathway in which PsaC binds first (Jolley et al., 2006) and is removed last when the complex is disassembled. PsaD has been proposed to play a role in the structural stabilization of the otherwise labile PsaC (Li et al., 1991; Chitnis et al., 1996), and the magnetic properties of the terminal Fe-S clusters F_A and F_B, which bind to PsaC, are affected by the presence of PsaD (Golbeck, 1999; Vassiliev et al., 2001). Under salt conditions, the PsaE was missed completely, however, the PsaD was partially damaged in *C.reinhardtii* (Subramanyam et al., 2010b).

In summary, these results indicate that the iron deficiency rapidly induced reduction of the photosynthetic pigments and further, Chl *a* fluorescence transient data indicated a substantial reduction in photochemical electron transport in iron deficient cultures. Apparently, the acceptor side of PSI is strongly affected by iron stress and the electron transfer capabilities of F_A and F_B could be severely impacted. Furthermore, it is known that the LHCI proteins attach to PSI near PsaF (Ben-Shem et al., 2003; Amunts et al., 2007), so the decrease of PsaC under iron stress could explain the loss of LHCI-associated red emission observed in the fluorescence decay-associated spectra

(Figure 4.7). Further, immunoblot results revealed that LHCI subunits are disassociated during iron deficiency. Also, The 2D electrophoresis and the MALDI-TOF data showed that the down regulation of LHCI proteins are most prominent. All of these results appear to be triggered by the accumulation of ROS damage in the absence of effective protection from SOD; this supports the idea that accumulation of SOD in response to iron, salt, drought and cold stress plays a crucial role in helping the cell to survive under environmental stress conditions. SOD is influencing the changes in PSI organization. However, PSII was also damaged and thus the *C.reinhardtii* cell growth was impaired due to the change in both PSII and PSI.

Based on this results we proposed a schematic representation of the PSI-LHCI supercomplexes under iron deficiency condition at different stages (Figure 4.13). In the first 24 h Lhca1 and Lhca9 were completely damaged. Lhca6 is the only LHCI subunit remains withstand even after 72 h under iron deficiency conditions. Effect of Reactive oxygen species (ROS) are more on PSI-LHCI supercomplexes which are under iron deficiency conditions after 72 h (indicated by number of arrows).
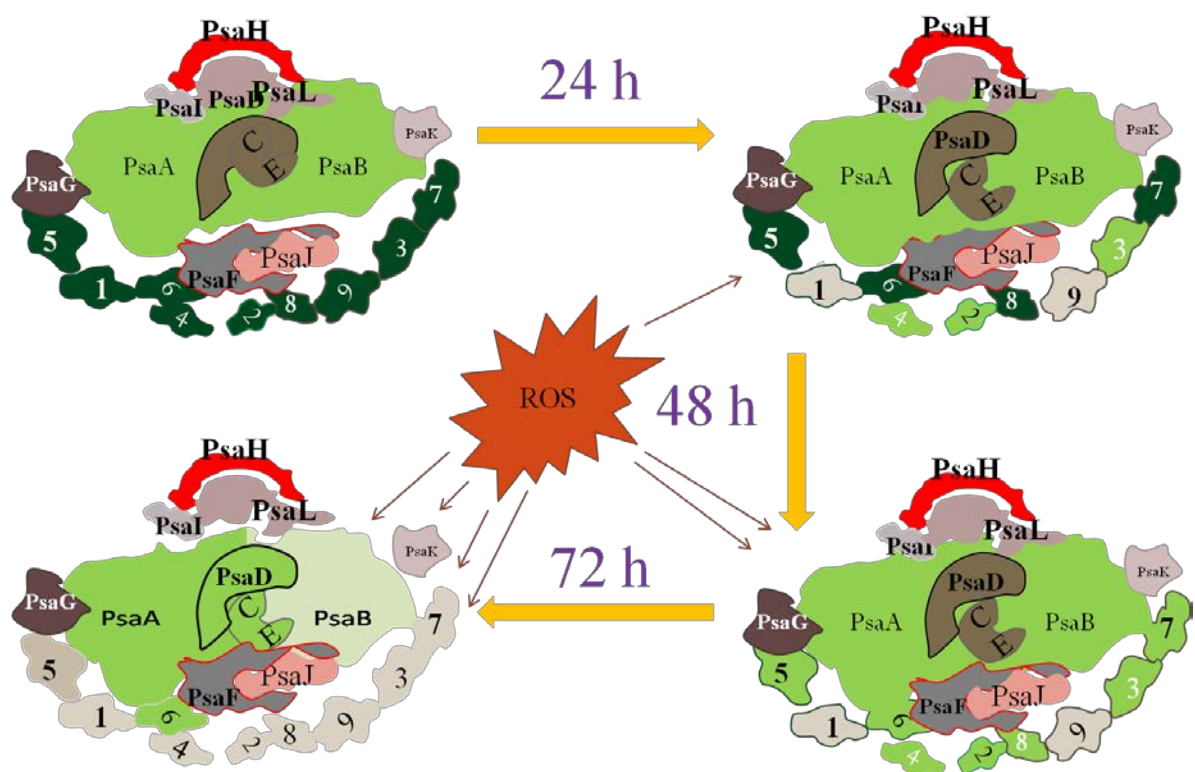
Figure 4.13 Proposed Schematic representation of PSI-LHCI supercomplexes under iron deficiency.

Protein level changes of photosystem I under iron deficiency in *Oryza sativa*

Chapter 5

5.1   Introduction

Iron (Fe) is an essential nutrient for all plants. The prevalence of iron deficiency is estimated to be about 30% of the world population (Lucca et al., 2002). Iron deficiency is a widespread agricultural problem that manifests as chlorosis, leading to reduced plant growth and crop yield, especially in calcareous soils, in which the solubility of iron is extremely low because of the high pH (Mori, 1999; Kobayashi et al., 2009). Higher plants utilize various mechanisms to maintain iron homeostasis. To acquire sparingly soluble iron from the rhizosphere, graminaceous plants synthesize natural iron (III) chelators known as mugineic acid family phytosiderophores (MAs) (Kobayashi et al., 2010). Higher plants have evolved two major strategies for iron acquisition under conditions of low iron availability. Non-graminaceous plants utilize strategy I, which requires the reduction of Fe(III) chelates at the root surface and the subsequent uptake of generated Fe^{2+} ions. Graminaceous plants use strategy II, which is mediated by the synthesis and secretion of natural Fe chelators, MAs. The secreted MAs solubilize Fe(III) in the rhizosphere and the resulting Fe(III)-MA complexes are absorbed into the root cells through YS1/YSL transporters in the plasma membrane (Curie et al., 2001).

As a transition metal, its ability to gain and lose one electron confers important properties for redox reactions, taking part in proteins essential for photosynthesis, respiration and many other cellular functions, including DNA synthesis and hormone production. Although abundant in soil, iron is mainly present as oxidized Fe^{3+} compounds, which are poorly soluble in neutral-to-alkaline soils. Consequently, plants grown in calcareous soils often exhibit severe chlorosis and decreased protein content in shoots due to Fe deficiency (Marschner, 1995; Sperotto et al., 2007). Fe-deficiency is a

serious nutritional problem for virtually all forms of life. Roots of iron-deficient plants show morphological and physiological changes. In dicots and non-grass monocots, Fe-deficiency is associated with inhibition of root elongation, increase in root tip diameter and abundant formation of root hairs (Chaney et al., 1992; Schmidt et al., 2000). Young rice plants are highly susceptible to low iron supply, being different from other cultivated grass species, such as oats, due to lower phytosiderophore production (Mori et al., 1991; Takahashi et al., 2001). Severe iron deficiencies can lead to lower productivity and even to plant death, resulting in complete crop failure (Guerinot and Yi, 1994). Senescence and subsequent death are terminal phases in the development of all plant organs, including leaves, stems, flowers and roots. Senescence is a highly regulated, ordered series of events involving the decline of photosynthetic activity, disintegration of chloroplasts, breakdown of biomolecules, loss of chlorophyll, decrease in cellular metabolic activities and recycling of valuable nutrients to other parts of the plant, rather than a passive process that simply leads to death.

The field of proteomics is gaining recognition as a reliable and reproducible high-throughput approach in understanding biological processes (Rakwal and Agrawal, 2003) and abiotic stresses (Ahsan et al., 2009; Nwugo and Huerta, 2011) would help in understanding the mechanism of alteration (upregulation or downregulation) at protein level.

In the present study, I have chosen a rice cultivar, Raasi, and subjected to iron deficiency conditions. This variety has been growing in many drought prone areas because of its tolerant nature under drought conditions. Since there are no iron deficiency resistant rice varieties are available so far, therefore, I have chosen this

variety for identifying the protein and functional changes in PSI complexes under iron deficiency conditions.

5.2   Materials and Methods

5.2.1   Growing of rice seedlings

Seeds of Raasi rice variety were obtained from Directorate of Rice Research (DRR), Hyderabad (A.P). The seeds were sterilized in 10% H_2O_2 for 10 min and 70% ethanol for 5 min, followed by a thorough washing five times with sterile distilled water. The seeds were equally spread in the petri dishes. Hoagland's Solution which normally contains iron at 5ppm referred to as control (Hoagland and Arnon, 1938; Hothem et al., 2003) and without iron were separately prepared and kept at 4 $^{\circ}$C. An equal volume of Hoagland solution (with iron and without iron) was poured on to the seeds and then covered with lid. The seeds were kept in dark until the germination. Germinated seeds were kept under 16 h light and 8 h dark photoperiod and ~100 µmol of photons m^{-2} s^{-1} supplied by fluorescent tubes for growing of seedlings in the growth chamber at 25 $^{\circ}$C. Media was regularly added to the seedlings and grown for a month under laboratory conditions.

5.2.2   Measurement of fluorescence with Handy PEA

Chlorophyll a (Chl a) fluorescence transients measured by dark-adapting (10min) second leaf of rice seedlings using Handy PEA fluorimeter.

5.2.3 Chlorophyll estimation

Chlorophyll content of the rice leaves measured as per the Chapter 4.2.2.

5.2.4 Protein extraction and SDS-PAGE

Protein was isolated from 30 days old grown leaves about 200 mg of leaves were homogenized in a pre-chilled mortar and pestle using 3mL of sodium phosphate buffer (50 mM, pH 7.4) containing 1 mM EDTA, 1% polyvinylpyrrolidone and proteinase inhibitors. This homogenate was centrifuged for 20 min at 18,000 xg. Protein was estimated by Bicinchoninic acid method (Smith et al., 1985). Protein extraction was carried out as per method described by Shine et al. (2011) with some modifications. Briefly an aliquot of 500 µL of buffered supernatant was used for protein extraction. The soluble proteins were precipitated by adding equal volume of 5% chilled trichloroacetic acid and kept in -20 °C for 2.0 h. The supernatant was discarded after centrifugation at 7800 xg for 10 min and the pellet was dissolved in sample buffer by adding an equal volume of 2× sample buffer containing 62.5 mM Tris–HCl (pH 6.8), 10% glycerol, 2% sodium dodecyl sulphate (SDS), and 0.5% β-mercaptoethanol, containing traces of bromophenol blue, and heated for 5 min at 95 °C. Solubilized proteins (50 µg) were resolved on 12% Tricine-SDS–polyacrylamide gel (Schagger, 2006) under reducing conditions in vertical gel electrophoresis unit (Bio-Rad).

5.2.5 Immunoblotting of PSI and LHCI specific antibodies

Immunoblotting was performed with PSI core and Lhca1 to 4 specific antibodies (Agrisera, Sweden) as per the Chapter 4.2.9.

5.2.6 Super oxide dismutase (SOD) activity measurements

SOD activity was measured as per the chapter 4.2.5

5.2.7 Sample preparation for 2D gel electrophoresis

Sample preparation for 2D gel electrophoresis was carried out according to the method described by Nwugo and Huerta (2011) with certain modifications. The leaf proteins were precipitated by adding 3 mL of chilled solution A (90% (v/v) acetone, 1% (v/v) trichloroacetic acid (TCA), 0.0007% (v/v) β-mercaptoethanol). The mixture was incubated for 2.0 h at -20 °C followed by centrifugation at 4 °C for 10 min at 36000xg. The supernatant was decanted, and the pellet was washed twice until the supernatant was clear by adding 3 mL of chilled solution B (98.53% (v/v) acetone, 1 mM polymethylsulfonylfluoride (PMSF), 2 mM EDTA, 0.0007% (v/v) β-mercaptoethanol), incubating at -20 °C for 10 min, and centrifuged at 4 °C for 10 min at 19000 xg. The whitish pellet was air dried to remove any remaining acetone. The pellet was suspended in 200 μL of rehydration/isoelectric focusing (IEF) buffer (9 M Urea, 50 mM dithiothreitol (DTT), 4% (w/v) CHAPS, 0.2% (v/v) 3/10 ampholytes, 0.002% (w/v) bromophenol blue) by incubating at room temperature for 60 min. Insoluble material was removed by centrifugation at 14000 xg for 15 min at room temperature and the protein content of the supernatant was determined by using RC-DC protein assay kit (Bio-Rad). First dimension IEF and second dimension SDS-PAGE was carried out as mentioned in the previous Chapter 4.2.10.

5.2.8 Immunoblotting of PSI core and LHCI proteins

2D gel proteins were transferred onto the PVDF membrane by western blotting and then probed with PsaA, PsaB, PsaC, PsaD, PsaE, Lhca1, Lhca2, Lhca3, and Lhca4

primary antibodies (Agrisera, Sweden). PSI core antibodies are common for any organism since there is not much difference in the protein sequence. LHCI subunit primary antibodies are different for higher plants and *C.reinhardtii.* Western blotting and probing with different antibodies were same as mentioned in previous chapter 4.2.10.

5.2.9 Trypsin Digestion and Mass Spectrometry

Carried out as per the earlier Chapter 4.2.12

5.3 Results

5.3.1 Chlorosis and stunted growth under iron deficient conditions

It is found that when the seedlings under iron deficient conditions shown the symptoms of yellowing or chlorosis of the interveinal areas of the leaves and entire leaf turns yellow. Iron deficiency majorly affecting the emerging leaves first than the rest of plant part. The stem and root length were decreased under iron deficiency by 20 and 50%, respectively indicating that the roots are most sensitive parts than above ground part. The decrease in root length also indicates that inefficiency of absorption of nutrients from rooting zone under iron deficiency conditions (Figure 5.1).

Chlorophyll content has been decreased by 42% within 30 days after germination in iron deficient grown seedlings compare to the control (Figure 5.2). It indicates that the chlorosis is due to decrease in content of chlorophyll synthesis under iron deficient conditions. The primary photochemistry (Light reactions) also effects due to decrease in chlorophyll content because of weak harvesting capacity of the chlorophyll.

Figure 5.1 Raasi rice variety seedlings growth pattern after 30 days germination under complete Hoagland nutrient solution and Hoagland nutrient solution without iron in the growth medium.
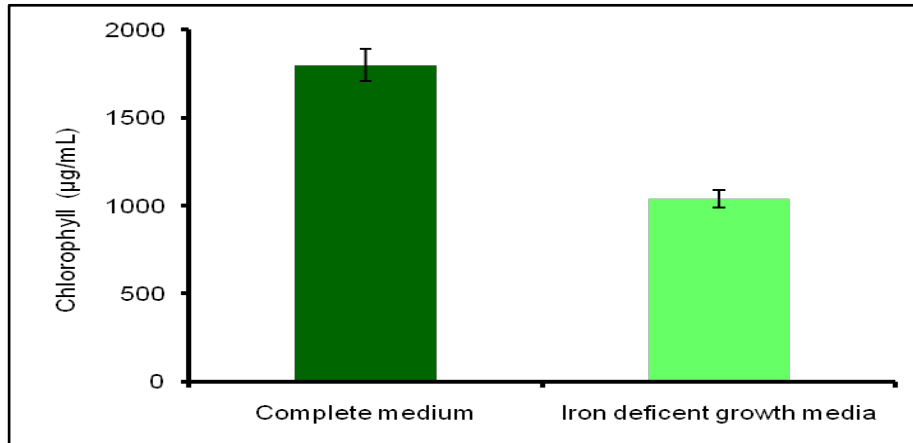
Figure 5.2 Chlorophyll content of the seedlings which are grown in control and in iron deficient growth media (n=5).

5.3.2 Photosynthesis efficiency under iron deficient conditions

Polyphasic chlorophyll *a* fluorescence (OJIP) transients were analyzed according to the JIP test (Strasser et al., 2000) (Figure 5.3). Measured parameters (F_O, F_J, F_I, F_m,) led to calculation and derivation of a range of parameters (Strasser et al., 2000; Strasser et al., 2004). Quantum efficiencies were calculated such as (1) the maximum quantum yield of primary photochemistry (*Fv/Fm*), 0.82 in case seedlings grown in control, and 0.7 in case of iron deficiency medium, and (2) the performance index on an absorption basis (PIabs), is the performance of the overall energy flow which was obtained in rador plot (Figure 5.4) and pipeline models (Figure 5.5) analysed with Biolyzer HP 3 software, Bioenergetics Laboratory, University of Geneva, Switzerland. PIabs is a function of the maximal and minimal fluorescence levels (Fm and Fo), the intermediate step J and the slope at the origin of the fluorescence rise.
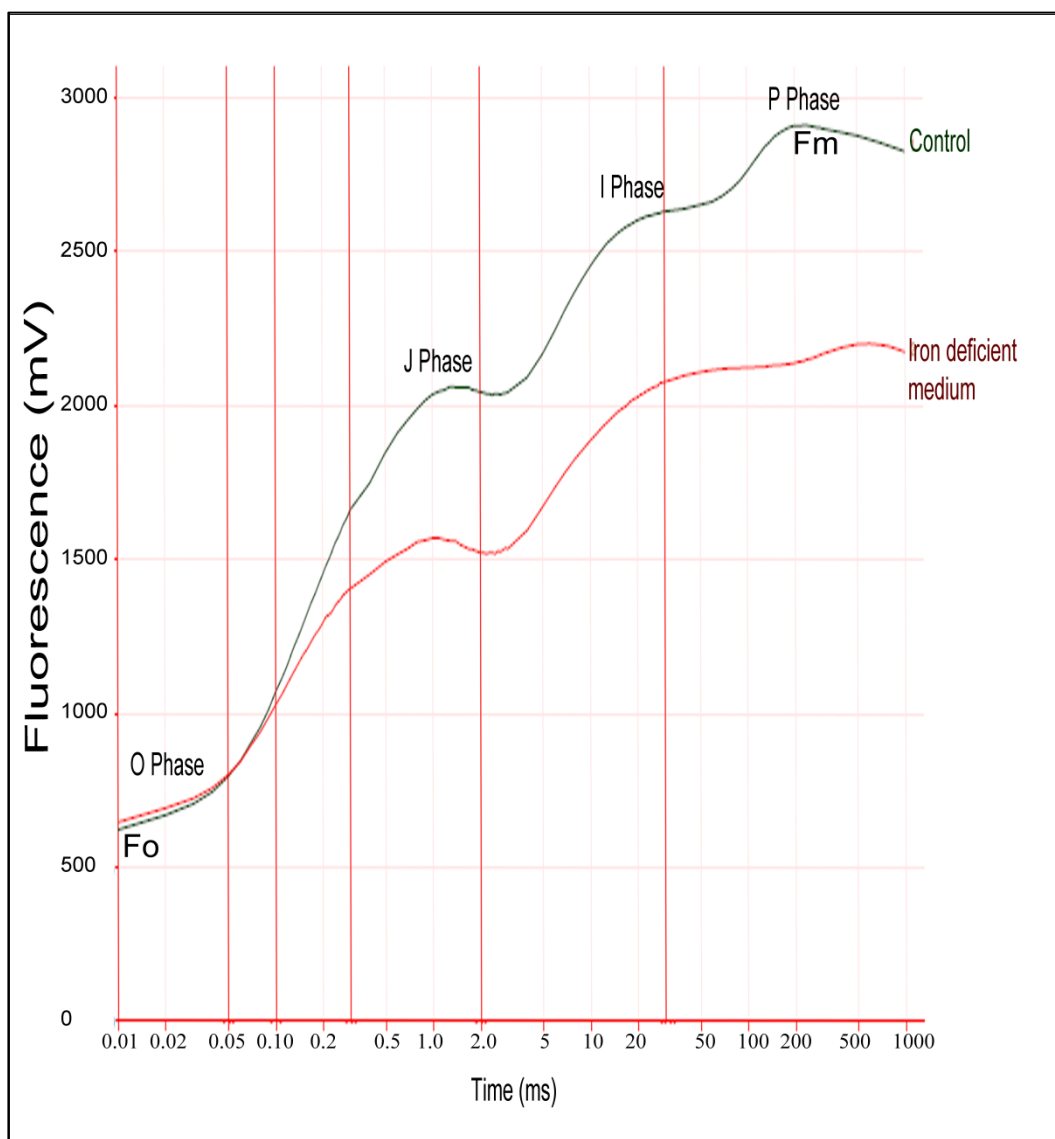
Figure 5.3 Changes in polyphasic chlorophyll *a* fluorescence (OJIP) transient curves in Raasi rice seedlings grown under control (Green curve) and iron deficient (Red curve) medium of Hoagland growth medium. O–J–I–P are fluorescence yield at 20 µs, 2 ms, 30 ms, and maximum fluorescence, respectively.

The results of the HandyPea fluorescence indicates that J phase, I phase, and P phase fluorescence reduced and these three phase were not clearly demarcated as that of

seedlings grown under control (Figure 5.3). The fluorescence maxima (Fm) decreased by 20% in iron deficient medium compare to control. This suggests that electron transport activity under iron deficient conditions (Z-scheme of photosynthesis) has been impaired under iron deficient conditions leading to the lower levels of photosynthesis efficiency. The fluorescence yield decreased by 16% J phase, 15% at I phase, and 22% at P phase (Fm) in plants under iron deficient conditions. There was also a significant decrease in quantum efficiencies like TRo/CSm, RC/CSo, TRo/CSo, RC/CSm, Fm, PIabs and ABS/CSm under iron deficient conditions compare to control seedlings (Figure 5.4). The energy pipeline model was prepared using a chlorophyll fluorescence analyzing program (Biolyzer HP 3 software, Bioenergetics Laboratory, University of Geneva, Switzerland). The contribution of the light reactions to primary photochemistry is estimated according to the JIP test (PIabs), reflecting the performance of the overall energy flow. PIabs, which is an indicator of sample vitality, significantly decreased by 32.7% under iron deficiency conditions (Figure 5.5).
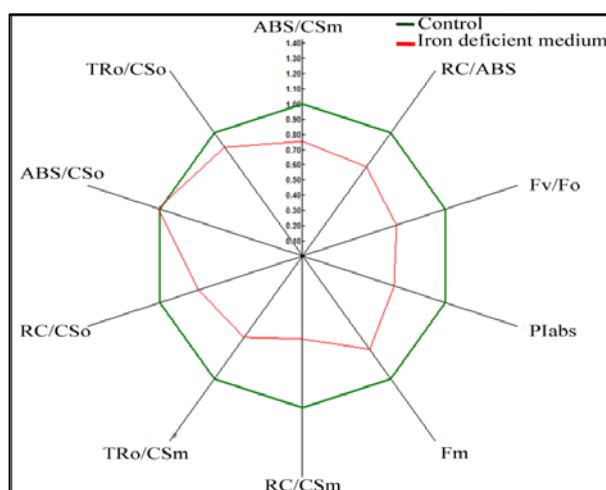
Figure 5.4 Rador plot showing the various parameters by taking seedlings grown in control as reference sample.

	Specific (membrane) model	Phenomenological(Leaf) model
Control	A — ABS/RC, TRo/RC, ETo/RC, DIo/RC, PI abs = 4.83	B — ABS/CSo, TRo/CSo, ETo/CSo, DIo/CSo
Iron deficent medium	C — ABS/RC, TRo/RC, ETo/RC, DIo/RC, PI abs = 3.10	D — ABS/CSo, TRo/CSo, ETo/CSo, DIo/CSo
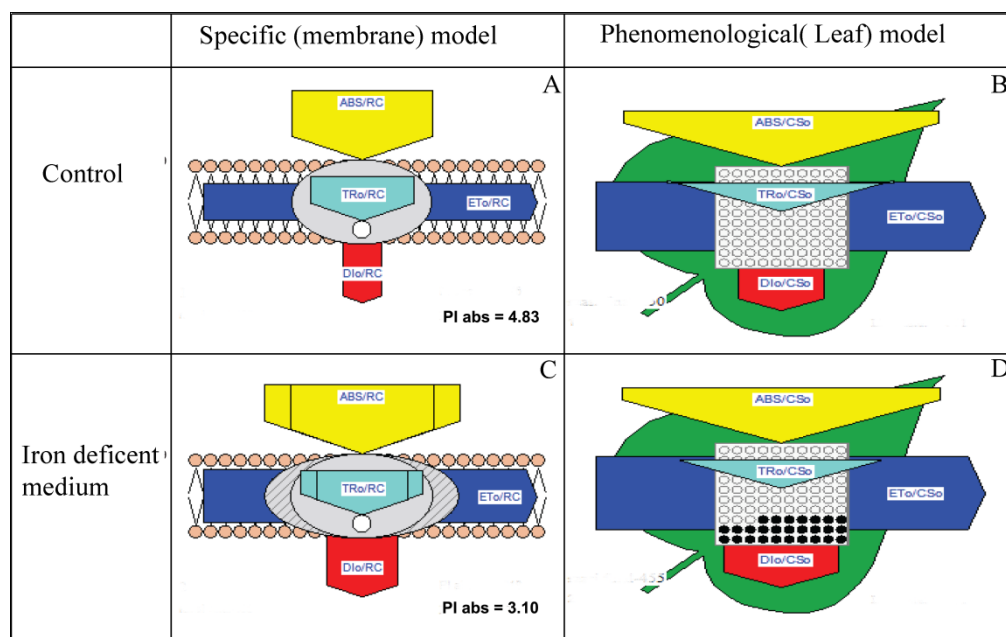
Figure 5.5 Pipeline models showing Raasi rice seedlings grown in control (A and B) and iron deficient medium (C and D). Two different representation were shown here with parameters. One is Specific (membrane) models of control (A) and iron deficient culture (C), and other is Phenomenological yield models of control (B) and iron deficient culture (D). Phenomenological energy fluxes per excited cross-section (CS) of rice seedling leaves. ABS/RC=absorption per reaction centre; Each relative value is represented by the size of the proper parameters (arrow), empty circles represent reducing QA reaction centers (active), full black circles represent non-reducing QA reaction centers (inactive or silent).

5.3.3 Protein profile and immunoblot of leaf extracts grown under control and iron deficient medium

Tricine SDS-PAGE results shows the alteration of many proteins under iron deficiency conditions (Figure 5.6). In the protein profile the decrease in the expression of light harvesting complexes I subunits (LHCI) which ranges from 21 to 25 kDa are prominent. The proteins which are down regulated were checked with PSI core and LHCI subunit specific antibodies (Figure 5.7).
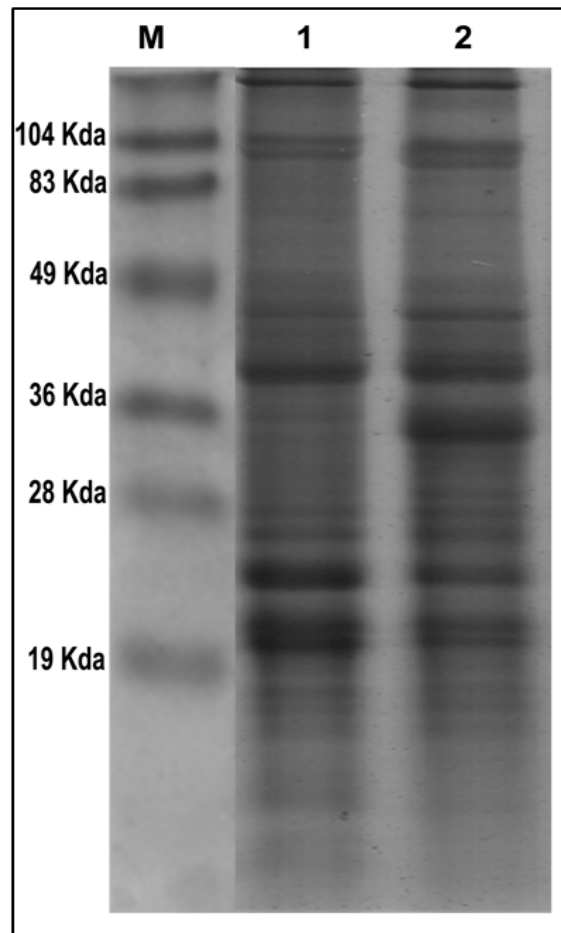
Figure 5.6 Protein profile of Raasi rice seedlings. M-Marker, lane 1- control, and lane 2-grown in iron deficient conditions.
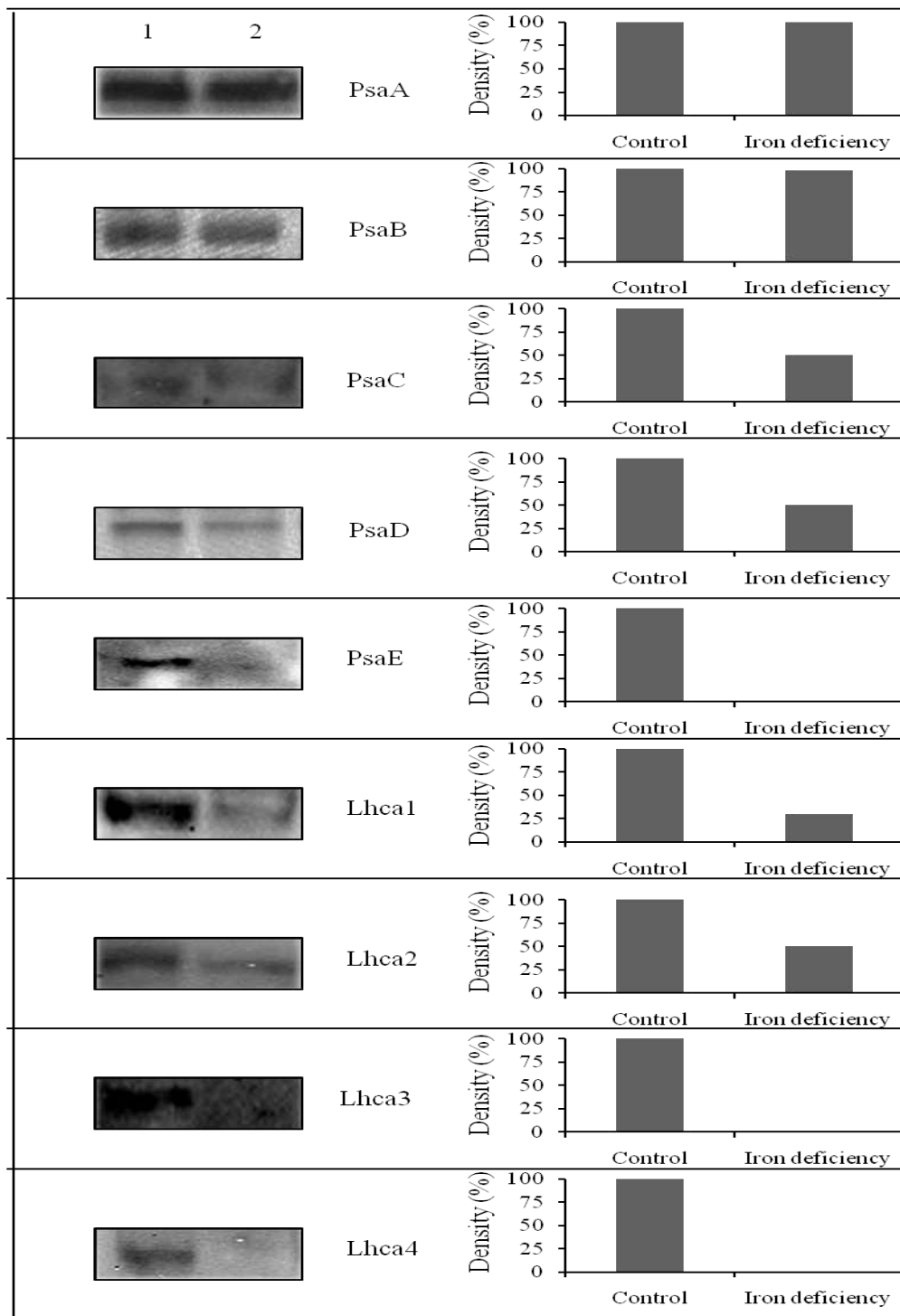
Figure 5.7 Immunoblot of PSI core and LHCI specific antibodies. lane 1- control, and lane 2-grown in iron deficient conditions. Right panel shows the density of the each protein obtained from western blots (left panel).

PsaA, and PsaB were remain stable under iron deficiency conditions where as PsaD and PsaC degraded more than 50% and PsaE is completely degraded under iron deficiency conditions. The alteration of PSI core proteins of rice is similar to the changes in *C. reinhardtii* under iron stress (See Chapter 4.3.8). The immunoblot results of LHCI subunits under iron deficiency shows that Lhca3 and Lhca4 were completely degraded and Lhca1 and Lca2 were shown 25 and 50% of abundance, respectively with that of control.

5.3.4   Leaf Proteomic analysis

2D gel electrophoresis pattern of control and iron deficient total leaf proteome were shown in Figure 5.7. This suggests that iron deficiency induces alterations (down regulation, up regulation) in many proteins. By using PDQuest gel analysis software (Bio-Rad), over 300 spots were detected in control and 260 spots in seedlings grown under iron deficient conditions. Since this is a total proteome, it has been found that many of the proteins along with the thylakoid membrane proteins. To know the the upregulated and downregulated proteins of interest (encircled in Figure 5.8) were digested with Trypsin and MALDI-TOF was carried and results were shown in Appendix IV which are majorly of Rubisco subunits, one of the most affecting enzyme under any of the abiotic stress conditions.
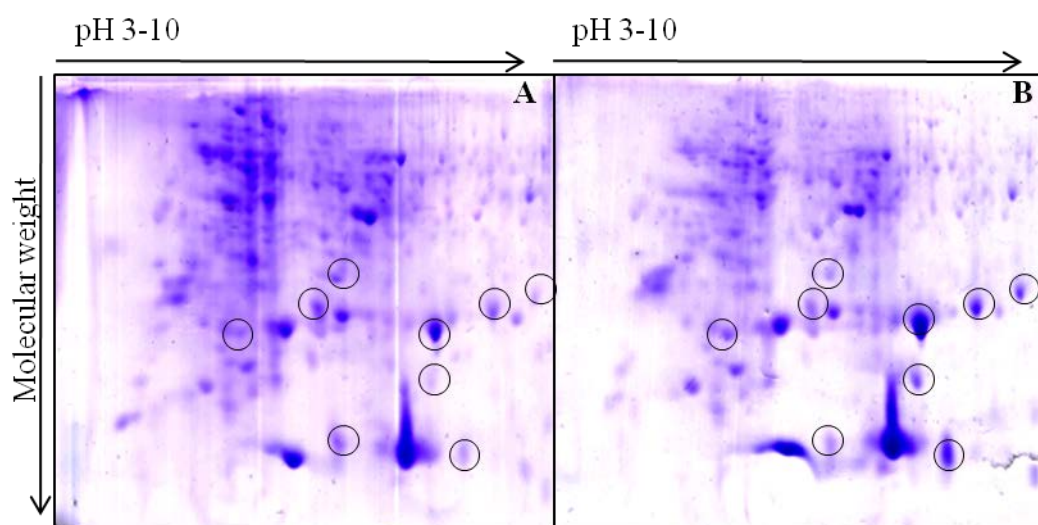
Figure 5.8 2D Gel electrophoresis of leaf proteins grown with A) control, and B) iron deficient medium.

5.3.5 2D immunoblot analysis of PSI core subunits

In order to see the photosynthetic protein level changes of isoforms, I have performed the 2D immunoblot against PSI core. The results of immunoblot results of PSI core were shown in the Figure 5.9. It is found that PsaA subunit has two isoforms. The two isoforms are stable under iron deficiency conditions (Figure 5.9). PsaB to E were found to have single protein without any isoforms. Among the core subunits, PsaC and PsaD were degraded almost to 50% where as PsaE subunit lost completely under iron deficiency conditions. These results were agreement with the SDS-PAGE immunoblots (Figure 5.7).
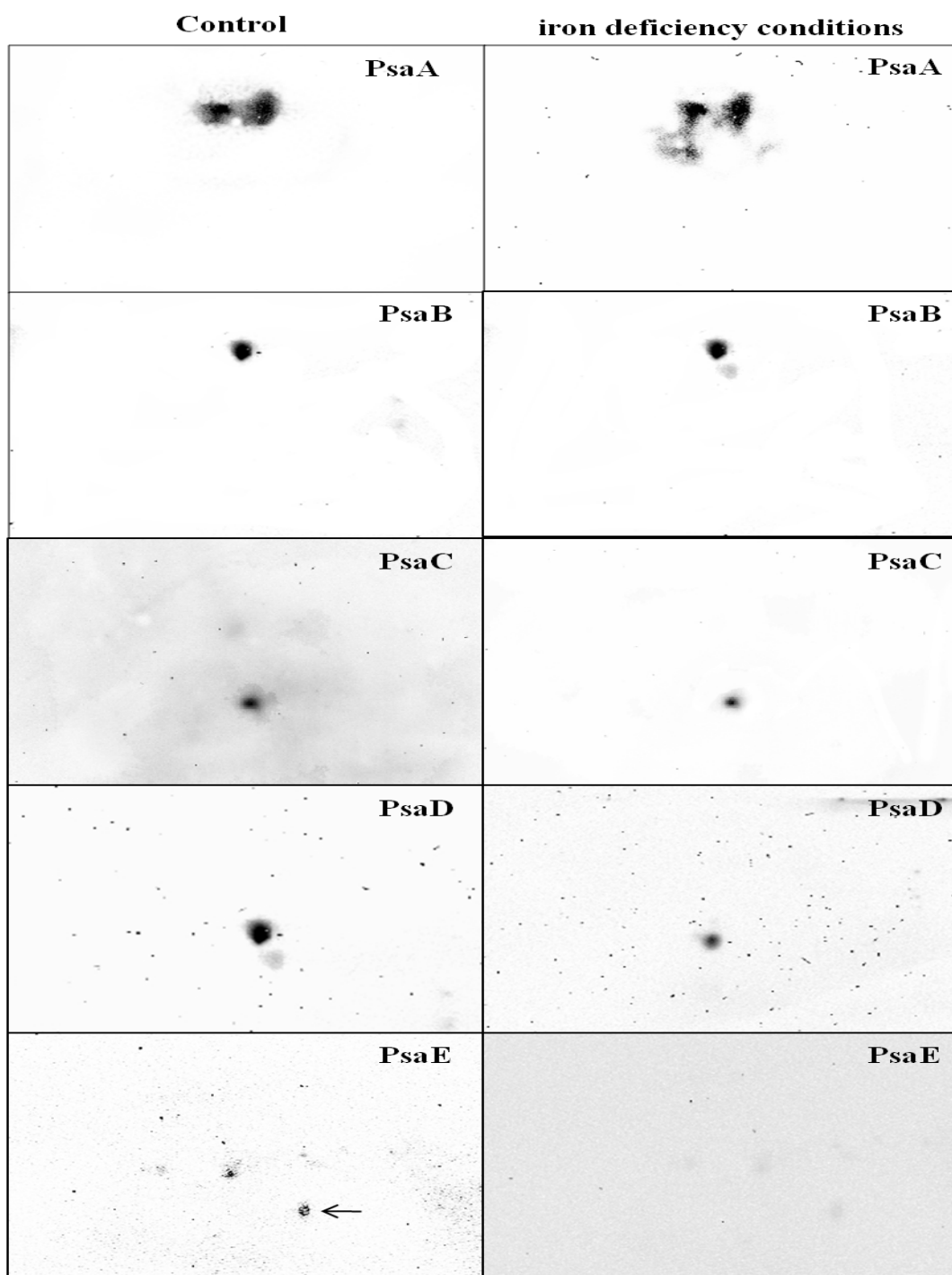
Figure 5.9 2D Immuno blots of seedlings grown in control (left panel) and iron deficient conditions (right panel) probed with PsaA, PsaB, PsaC, PsaD, and PsaE.

5.3.6 2D immunoblot analysis of LHCI subunits

It is known from the proteomic data that each LHCI have a number of isoforms and thus, it is important to perform the 2D immunoblot by using LHCI antibodies to identify the specific changes in the their respective isoforms under iron deficiency. Figure 5.10 shows the results of immunoblots probed with Lhca1 to 4 specific to the higher plants. LHCI subunits found to contain more number of isoforms compare to the core subunits (Figure 5.10). Lhca1, 22 kDa and Lhca4, 21 kDa each has one isoform, while Lhca2, 24 kDa has two isoforms and Lhca3, 25 kDa has three isoforms. Lhca1 subunit degraded by 70%. Among the two isoforms of Lhca2, one of the isoform was degraded about 50% while the second isoforms remain stable. The three isoforms of Lhca3 and one isoforms of Lhca4 which are expressed in control were completely degraded under iron deficiency conditions (Figure 5.10).
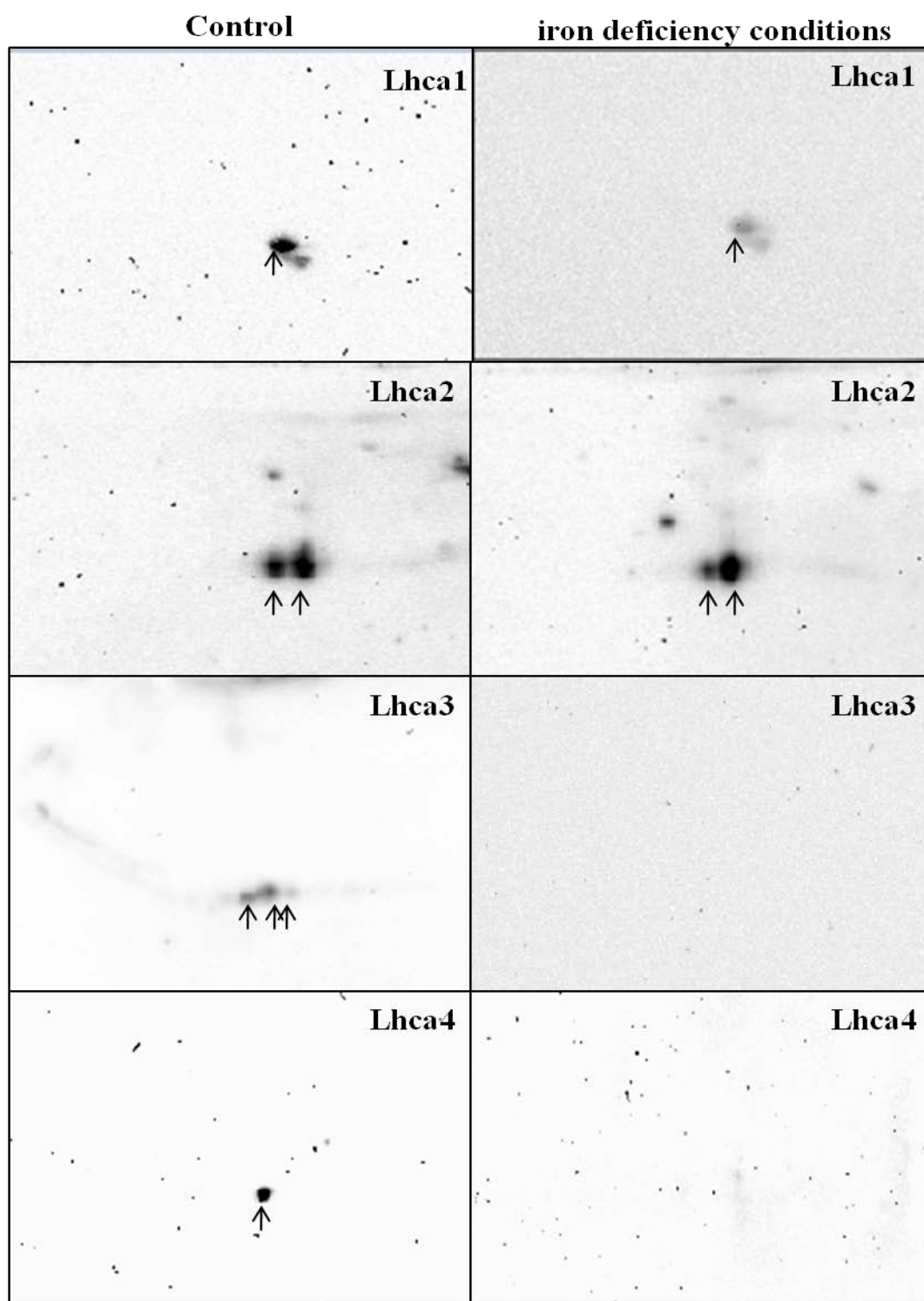
Figure 5.10 2D Immuno blots of seedlings grown in control (left panel) and iron deficient conditions (right panel) probed with Lhca1, Lhca2, Lhca3, and Lhca4.

5.3.7   SOD activity analysis

SOD activity was found to increased 36% compare to the control (Figure 5.11). This indicates reactive oxygen species (ROS) generated under iron deficiency conditions. The increase in the total SOD level is an indication of super oxides dismutase scavenging activity under stress conditions.
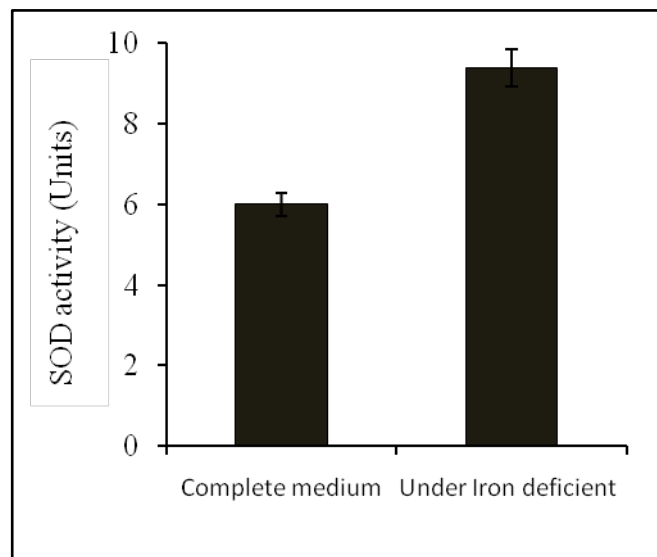
Figure 5.11 Total SOD activity of seedlings grown under control and iron deficient conditions (n=5).

5.4   Discussion

Chlorophyll is the pigment of plant photosynthesis. Its content generally reflects the level of photosynthesis. The decreased chlorophyll concentration in rice leaves under iron stress directly effected the photosynthesis, and thereby affected overall rice plant growth. The decrease of chlorophyll concentration occurs at the early stage of leaf senescence, which was regarded as a reliable measure of leaf senescence. It is additionally used as a bio-indicator reflecting plant photosynthesis and plant growth status as well as pollution stress. It is reported that the chlorophyll oxidation by free hydroxyl radicals in rice leaves resulted in early leaf senescence

(Dunford, 1987). This is due to various stress conditions. The photosynthetic system in higher plants is highly susceptible to abiotic stresses, leading to inhibition of photosynthetic CO_2 assimilation. The energy imbalance between light harvesting and CO_2 assimilation leads to an over excitation of the photosynthetic apparatus, increasing the potential for photoinhibition and photooxidative damage. To avoid the energy imbalance resulting from abiotic stress, plants are able to down-regulate genes associated with photosynthetic light harvesting to reduce the light energy absorbed (Huner et al., 1998). The LHCI subunits which are decreased under iron deficiency is one of the mode to balance the light energy absorbed.

The JIP test provides adequate information about the function of the photosynthetic apparatus. Since shape changes in OJIP fluorescence transients can be translated to quantitative changes of several parameters, JIP parameters are very useful for *in vivo* investigation of photosynthetic apparatus (Strasser et al., 1995). Since the decrease in chlorophyll could be linked to the decline of photosynthetic parameters of JIP test. The decrease in performance index (PIabs) is related to the decrease in productivity of photosynthetic metabolites there by reducing the biomass production capability (Figures 5.4 and 5.5). Results on chlorophyll a fluorescence reported here reveal that leaves of rice seedlings that are under iron deficiency conditions had low reducing power with lower efficiency of electron transport and less active reaction centers (Figure 5.5). The less active reaction centres have lower in capacity of generating ATP or NADP(H) under iron deficiency conditions.

It has been identified that rice bHLH protein OsIRO2 is an essential regulator of the genes involved in iron uptake under iron-deficient conditions which secretes more MA there by absorbs iron more efficiently under unavailable iron conditions such as calcareous soils where high pH results in insoluble iron which is unavailable to the plant (Ogo et al., 2007). The protein band found around 34 kDa in Figure 5.6 may be the transcript of OsIRO3 which is expressed in transcript profiling of rice under iron deficiency up-regulated from 25- to 90-fold in both root and shoot respectively that plays important role in iron homeostasis (Zheng et al., 2010). There

is another report of up-regulation of Alb3 gene under Fe-deficiency in rice shoots (Sperotto et al., 2007). The Alb3 protein is required for the integration of the light-harvesting complex (LHC) protein into the thylakoid membrane and loss of Alb3 in *C. reinhardtii* leads to reduction (>10-fold) in the amount of LHCI and LHCII and about 70% reduction in total chlorophyll (Dolcini and Carobi, 1971; Gohre et al., 2006). Degradation or dissociation of LHCI subunits in this case may be due to the up-regulation of Alb3 gene. Along with LHCI subunits the PSI core proteins such as PsaC, D and E levels have been altered under iron stress (Figures 5.7 and 5.9).

All LHCI subunits functions as a light receptor, it captures and delivers excitation energy to photosystems with which it is closely associated. Each LHCI subunit binds at least 14 chlorophylls (8 Chl-a and 6 Chl-b) and carotenoids such as lutein and neoxanthin. Lhca2 and Lhca3 present in monomeric, while Lhca1 and Lhca4 found in dimeric pigmet-protein fractions (Lam et al., 1984). In addition Lhca3 channels the protons produced in the catalytic Mn center of water oxidation into the thylakoid lumen (Morishige et al., 1993). Thus the alteration in Lhca3 lead to the ineffective oxidation of water besides impairing light harvesting capacity. It is reported that LHCI is sensitive to excess light (Hui et al., 2000), senescence (Humbeck and Krupinska, 2003) and chilling stress conditions (Scheller and Haldrup, 2005).

2D gel electrophoresis technique allowed resolution of isoforms with different pI values for Lhca1-4. Detection of four to five isoforms resolved in tomato at different isoelectric points (Storf et al., 2004). In tomato three isoforms of Lhca1, four isoforms of Lhca2, and two isoforms of Lhca4 has been reported under normal conditions (Storf et al., 2004). The distinct Lhca isoforms are caused by posttranslational modifications, protein processing, or even charge heterogeneity that occur in the protein segments, which have not been detected. The isoforms differ from one species to another species

and vary depending upon the environmental conditions. The isoforms reported here (Figure 5.10) are specific to the *Oryza sativa* L. are different from that of *Lycopersicon esculentum.*

In summary, one isoform of Lhca2, Lhca3 and Lhca4 downregulated under iron deficiency conditions were hampering the light harvesting capacity to minimize the balance the light harvesting capacity. The reactive oxygen species generated under iron deficiency conditions is also one of the factor for degradation or dissociation of LHCI subunits from the PSI core.

Summary

Summary

The physiological function of Photosystem I (PSI) as a sunlight energy converter, catalyzing one of the initial steps in driving oxygenic photosynthesis in cyanobacteria, algae, and higher plants. The *Chlamydomonas reinhardtii* PSI structure was not known since it contains a unique structure having additional light harvesting complex I (LHCI) subunits, which play a major role in transfer of sun light energy to the reaction center. Here, individual subunits of LHC and core subunits are built the model based on the plant PSI templates from the PDB 2WSC taken from RCSB Protein Data Bank. The results of PROCHECK analysis showed that most of the amino acid residues lie in the allowed regions. R-factor of the model stand at -0.87 Å deviation indicate that the present model is better existence. The results shown that arrangement of *C.reinhardtii* LHCI polypeptides in sequence as Lhca5, Lhca1, Lhca6, Lhca4, Lhca7, Lhca8, Lhca2, Lhca9, and Lhca3 based on spatial restraints by taking coordinates of the template. The modelled arrangement of Lhca1 to Lhca9 subunits in a sequential manner was entirely different from that of higher plants. Most of the PSI core subunits were at the same position as that of higher plants. PsaO subunit of *C.reinhardtii* built by threading model is located at PsaH, PsaI and PsaL core subunits. The location of PsaO subunit among the core subunits suggests that it may play a major role in state transition mechanism in *C.reinhardtii* and stabilization of PSI core. Results obtained by PDBsum structural tool showed several protein-protein interactions among the PSI-LHCI subunits. These non-covalent interactions among PSI-LHCI subunits were much stronger compare to higher plants proved by biochemical studies. It is surprising that these interactions were stronger with PSI core to LHCI. Thus, existence of much stronger interactions is one of the reason making difficulties in purifying individual

LHCI subunits in *C.reinhardtii*. This has been proved by experimentally by harsh treatment of PSI-LHCI supercomplexes with detergent (n-Dodecyl-beta-D-maltoside), but there was no disturbance observed in the integrity of PSI-LHCI supercomplexes. The nature of the H-bonding pattern among the LHCI subunits and with the core signifies the strong interaction between PSI core subunits and LHCI subunits. However, it is very easy to separate the PSI core and LHCI antenna from PSI-LHCI supercomplexes of higher plants , due to that crystal structure of pea at 3.3 Å has been resolved by Amunts et al. (2010). Consequently, the separation of individual LHCI subunits is highly difficult because of its strong protein-protein interactions in *C.reinhardtii*. Thus, the 3D model would gives structural information which can be useful to study the physiological importance of PSI-LHCI supercomplexes in different a biotic stress.

I have developed 9 Lhca (1 to 9) antibodies from Rabbit against light harvesting complex I. The affinity purified anti-peptide antibodies were tested by immunoblotting analysis from isolated PSI-LHCI supercomplexes of *C.reinhardtii*. Crude sera showed cross reactivity with many of the non-relevant proteins. The affinity purified peptide tag antibodies against Lhca1 to 9 of purified PSI-LHCI supercomplexes from *C.reinhardtii* showed a single band upon exposure in VersaDoc imaging system. The peptide tag antibodies specifically recognized proteins of about 24 kDa corresponds to Lhca1, 28.4 kDa corresponds to Lhca2, 30 kDa corresponds to Lhca3, 28.7 kDa corresponds to Lhca4, 28.2 kDa corresponds to Lhca5, 27.8 kDa corresponds to Lhca6, 26.2 kDa corresponds to Lhca7, 26 kDa corresponds to Lhca8, and 22.8 kDa corresponds to Lhca9 in *C.reinhardtii.* The specific antibodies of Lhca1 to 9 were exactly matching to

the molecular weight which has been reported previously (Takahashi et al., 2004) and thus peptide tag antibodies are pure.

Such antibodies could help in understanding the structural details, localization of LHCI of PSI-LHCI supercomplexes in *C.reinhardtii*. In addition, using these antibodies one can study the physiology, structure, and functional organization of LHCI under abiotic stresses.

Iron is abundant on earth, but is often present in the insoluble ferric state, leaving many surface environments Fe-limited. Iron is an essential micronutrient for all organisms because it is a component of enzyme cofactors that catalyze redox reactions in fundamental metabolic processes. Structural and functional changes in PSI-LHCI supercomplexes to iron deficiency was studied in *C.reinhardtii* and *Oryza sativa*. In *C.reinhardti,i* when fluorescence data was normalized at F_1, significant differences were observed between the control and iron deficient cultures which were harvested at 24 h, 48 h, and 72 h. In case of control culture the three phase of OJIP are very clear and have maximum florescence indicating the efficient electron transport in the Z-scheme. The fluorescence yield decreased by 20% at J phase, 41% at I phase, and 52% at P phase (Fm) after 72 h under iron deficient conditions. Among these three phases the P phase shows the PSI florescence (Franck *et al.*, 2002; Papageorgiou *et al.*, 2007), which is completely lost under iron deficiency conditions indicating the main target of iron deficiency at PSI reaction centre. The fluorescence emission data at 77K shows remarkable differences between control and iron stress samples at fluorescence maxima. These differences were more in PSI and clearly seen when the spectra were normalized at 680nm. This data indicates that both PSII and PSI were damaged; however, the impairment of PSI is more after 72 h of cells grown under iron deficiency. The visible

129

Circular dichroism (CD) spectrum of PSI-LHCI supercomplexes under iron stress conditions shows an increase in the amplitude of the major peaks in the red region at 675 and, 641 nm and peak shift about 4 and 3 nm, respectively. The soret band peaks at 443 and 460 nm also increased in intensity. The differences in the peak intensity indicate significant differences in pigment interactions in PSI-LHCI complexes and also possible that there may be macro-aggregation of pigment-proteins or pigment-pigment from iron stress cells. The streak camera (ultra fast spectroscopy) data shows the shape of fluorescence decay spectra in the first (~33 ps) component is extremely consistent among the samples measured. Given that the PsaA and PsaB proteins, which bind the bulk of PSI's core antenna, appear based on immunoblotting results to be largely unaffected by iron stress, this suggests strongly that only pigments bound to the PSI core contribute to this component. This is consistent with structural studies (Jordan et al., 2001; Amunts et al., 2007) show that the PSI core is a stable, tightly integrated complex. Similar conservation can be seen in the spectral shapes of the third component (3–4 ns); such lifetimes are typically attributed to detergent-solubilized Chl that is not coupled to PSI. The major difference in the decay-associated spectra of the control and iron-stress samples can be seen in the spectral shape of the 120–220 ps component. While the decay lifetimes are relatively unchanged by cell growth under iron stress conditions, this component shows a decrease in emission intensity on the red side of the peak in the iron-stressed samples.

Immunoblot results shows that levels of PsaA and PsaB were stable while PsaD and PsaC were reduced in expression. PsaE protein was completely lost after 72 h of continuous iron deficiency conditions. Among LHCI subunits, Lhca1 and Lhca9 were most susceptible and Lhca6 shown 50% of its expression and rest LHCI subunits were

completely lost after 72 of continuous iron deficiency conditions. The damage to PSI-LHCI subunits is associated with an increase in superoxide dismutase (SOD) activity; thus scavenging the higher levels of reactive oxygen species generated under stress conditions. 2D gel electrophoresis and MALDI-TOF of 2D spots were carried out as per the method published (Yadavalli et al., 2011). MALDI-TOF-TOF and Immunoblot results indicates that all LHCI subunits except Lhca6 were completely lost under iron deficiency after 72 h under continuous iron deficiency conditions.

The uptake of iron by rice is by strategy II mechanism unlike *C. reinhardtii* where it is strategy I. It is found that when the seedlings under iron deficient conditions shown the symptoms of yellowing or chlorosis of the interveinal areas of the leaves and entire leaf turns yellow. The decrease in root length also indicates that inefficiency of absorption of nutrients from rooting zone under iron deficiency conditions. Chlorophyll content has been decreased by 42% within 30 days after germination in iron deficient grown seedlings compare to the seedlings that are grown in the complete Hoagland nutrient solution (Control). It indicates that the chlorosis is due to decrease in content of chlorophyll synthesis under iron deficient conditions. Polyphasic chlorophyll *a* fluorescence (OJIP) transients were analyzed according to the JIP test. The performance index on an absorption basis (PIabs), was obtained in pipeline models by the three independent steps contributing to photosynthesis (Strasser *et al.*, 2000; Strasser *et al.*, 2004). The fluorescence yield decreased by 16% J phase, 15% at I phase, and 22% at P phase (Fm) in plants under iron deficient conditions. PIabs, which is an indicator of sample vitality, significantly decreased by 32.7% under iron deficiency conditions.

1D and 2D electrophoresis shows that there are several proteins were altered in rice soluble samples. Further, the protein subunit content was checked with PSI core and

131

LHCI subunits by using specific antibodies. PsaA, and PsaB were remain stable under iron deficiency conditions where as PsaC and PsaD degraded to 50% and PsaE almost completely degraded under iron deficiency conditions which is closely matching to the *C.reinhardtii*. The immunoblot results shows that LHCI subunits such as Lhca3 and Lhca4 were completely lost (degraded) and Lhca1 and Lca2 were shown 25% and 50% expression, respectively.

Thus, this study would provide the insights on the nature of structural and functional alterations of PSI by Fe stress in Chlamydomonas and Rice. In Chlamydomonas and Rice not only damage the PSII, however, PSI is more susceptible as it have more Fe content. These changes in the number and composition of PSI-LHCI supercomplexes may be caused by reactive oxygen species, which increase under iron deficiency conditions.

Appendix

APPENDIX I   *C. reinhardtii* LHCI subunits amino acid sequences

Lhca1

MALSMRTLSARTAAPRGFSGRRVAAVSNGSRVTMKAGNWLPGSDAPAWLPDDLPGN
YGFDPLSLGKEPASLKRFTESEVIHGRWAMLGVA   GSLAVELLGY   GNWYDAPLWA
VNGGKATWFGIEVPFDLNALLAFEFVAMAAAEGQRGDAGGVVYPGGAFDPLGFA
KDSSKSGELKLKEIKNGRLAMVAFLGFVAQHAATGKGPIAALGEHLANPWGANFA
TNGISVPFF

Lhca2

MAMLLKSRVSAGVSRPSRATVRVSASTRPMWYPGATAPAHLDGSMLGDYGFDPLRLG
VNKDNLKWFREAELTNGRWAMAAVVGILFTDAVGLPKFWTAGAEKYALDNQTLALI
EVAVFAVLEGKRYEIYKKTGETGFLSFAPFDPMGMKSEEMKLKELKNGRLAMLAFLGF
CSQAAVYGKGPIETLQLHLADPGHNNIYTSSVGPETAVTVAVLCVLPMIIEATKTLNPG
KESVPYFPWNEPWNKV

Lhca3

MMLTKSAQAAFSGKVARPAKANRARLVCRAEEKSIAKVDRSKDQLYVGASQSSLAYL
DGSLPGDFGFDPLGLLDPVNSGG   FIEPKWLQYS   EVIHARWAMLGAAGCIAPEV
LGAAGLIPDATNIKWFESGVIPPAGSYNGYWADPYTIFFVEIVAMQFAELRRLQDFR
YPGSMGQQYFLGLEAIFKGSGDAAYPGGPFFNLFNLGKTEAAMKELKLKEIKNGRL
AMLAMLG YGAQAVMTGKGPFQNLVEHLADPVNNNILTNFGKLVA

Lhca4

MAFVLAKSSAFGVAAKPVSRRSSVAVKASAVPENVKAREWIDAWKSKSGGAKRDAA
LPSWMPGADLPGYLNGTLPGDFGFDPLYLGQDPVKLKWYAQAELMNARFAMLAVAG
ILVPELLSNIGFSWPGAGVAWYDAGKFEYFAPASSLFGVQMLLFAWVEIRRYQDFVKP
GSANQDPIFTNNKLPDGNEPGYPGGIFDPFGWSKGDIKSLKLKEIKNGRLAMLAFAGFIG
QAYTTGTTPLKNLSTHLADPWSTTVWQNDLARL

Lhca5

MAALMQKSALSRPACSTRSSRRAVVVRAAADRKLWAPGVVAPEYLKGDLA   GDYG
WDPLGLGADPTALKWYRQSELQHARWAMLGVAGVLVQEIVKPDVYFYEAGLPQN
LPEPFTNINMGGLLAWEFILMHWVEVRRWQDYKNFGSVNEDPIFKGNKVPNPEMG
YPGGIFDPFGFSKGNLKELQTKEIKNGRLAMIAYMAFILQAQATGKGPLAALSAHLS
NPFGNNILKNIGTCTVPHSVDVQGLTIPLT CLWPGSQ

Lhca6

MMLVAKNAVAARPSARSARRSVVAKASSRPLWLPGSTPPAHLKGDLPGDFGFDPLG
LGANAESLKWFKESELVHSRWAMAAVAGILVQEIVRPDVFWYNAGKEVESPLGPLGL
LAVEFFLMHWVEVRRWQDLRKPGSVDQDPIFSQYKLPPHEVGYPGGVFAPFIPGDLA
ELKVKEIKNGRLAMLAFVGF   VMAAQVTGKG   PIAALQEHLA   DPWGTTIFSK
AAVVPGQAVA PPCKIPASVSYKGIEIPTPCFLQGLWP

Lhca7

MALSMIAQRRAGAFSARQAPRAVRAQALTRPVWFPGNPAPAHLDGTLAGDYGFDP
LFLGQEKETLRWYVQAELVHGRFAMLGAAGIILTSIGAKVGLGFP   EWYDAGKVVV
EKNNIDFPTLIVIQFYLMGWAETKRWYDFKNPGSQADGSFLGFTEEFKGLENGYPGGRF
FDPMGLSRGDAAKYAEYKQKEVKNGRLAMIA   CLGFAAQYAA   TGKGPLDNLS
DHLADPNHIN FATNGVSIPIA

Lhca8

MALTMKRSGVAARSASSRKSVVTCVARQSWLPGSQIPAHLDTPAAQALAGNFGFD
PLGLGKDPVALRWYQQAELIHCRTAMAGVAGILIP   GLLTKAGALN   VPEWYDAGKV
AIENSFAPWGSLLAVQLFLCGFVEAKRWQDIRKPGSQGEPGSFLGFEASLKGTSELGYP
GGPFDPLGLSKEADKWADWKL   KEVKNGRLAM   LAFLGFVAQK   YATGAGPVDN
LAAHLKDPWH VNYATNGVSLPFL

Lhca9

MIAAKSQVALGRRAPVRGQRVVAAASARPTWLPGLNPPAHLKGALAGDNGFDPLG
LGQDEGRLKWYAEAEKTNGRWAMMAVAGILGQELLGVTPAWWEAGAKEYDIPAQA
LTPIEFIVMGFLEIKRYQGFKQTGTSGFINSFPFDPAGMNSPSMATKEVKNGRLAMVAFI
GFCVQALATRTQPIEGLTAH LADPFGKNIT YYLTHLPETL GSAKRLPQPV WG

Appendix II   Growing *Chlamydomonas reinhardtii*

Preparation of Hutner's Trace Elements

Each compound as specified below were dissolved in distilled water.

1. Compound	2. g salt	3. mL H_2O
EDTA, disodium salt	50	250
$ZnSO_4\text{-}7H_2O$	22	100
H_3BO_3	11.4	200
$MnCl_2\text{-}4H_2O$	5.06	50
$CoCl_2\text{-}6H_2O$	1.61	50
$CuSO_4\text{-}5H_2O$	1.57	50
$(NH_4)_6Mo_7O_{24}\text{-}4H_2O$	1.10	50
$FeSO_4\text{-}7H_2O$	4.99	50

All solutions were mixed except EDTA. After heating all the solutions, EDTA solution was added. When everything is dissolved, adjusted the pH to 6.7 while at temperature 70°C with about 80-90 mL of hot KOH (20%). Finally solution was makeup to one litre. Stoppered with a cotton plug to breathe and allowed it to stand for two weeks by shaking it once a day. The solution turned eventually to a rusty purple with precipitate which was removed by sending through two layers of Whatman #1 filter paper. Repeated the filtration until the solution is purple and clear and stored at 4°C.

Preparation of CC10X

4. Compound	5. For one litre:
Tris base	25 g
Glacial acetic acid	10 mL
NH_4NO_3	5 g
$MgSO_4\text{-}7H_2O$	1 g
$CaCl_2\text{-}2H_2O$	0.2 g
KCl	1 g
Hutner's Trace Elements	10 mL

The final growth media for one litre constitutes

100 mL of CC10X

1 mL of a 1 M stock of KH_2PO_4

1 g of yeast extract

Autoclaved it for 30 minutes.

About 1 OD (730 nm) mother cells of about five mL inoculated to one liter of medium. Grown them on a shaker (115 rpm) under 24 hours of light (50 μmol m^{-1} s^{-1}). Grown for about 4-5 days (1 OD at 730).

Appendix III Hoagland's Solution   (Plant Nutrient Solution)

Following stock solutions were prepared for each compound and than mixed as indicated in the third column to make 1000 mL of Plant nutrient solution.

Component	Stock Solution (g/L)	mL Stock Solution/1L
2M KNO_3	202	2.5
2M $Ca(NO_3)_2$ x $4H_2O$	472	2.5
Iron (Sprint 138 iron chelate)	15	1.5
2M $MgSO_4$ x $7H_2O$	493	1
1M NH_4NO_3	80	1
Minors elements		
H_3BO_3	2.86	1
$MnCl_2$ x $4H_2O$	1.81	1
$ZnSO_4$ x $7H_2O$	0.22	1
$CuSO_4$	0.051	1
H_3MoO_4 x H_2O or	0.09	1
Na_2MoO_4 x $2H_2O$	0.12	1
1M KH_2PO_4 (pH to 6.0 with 3M KOH)	136	0.5
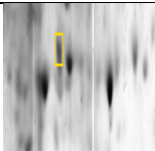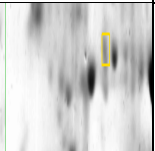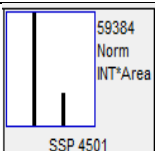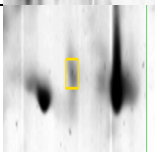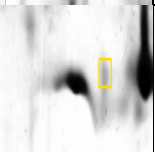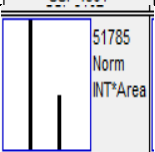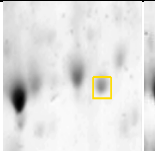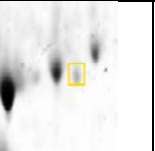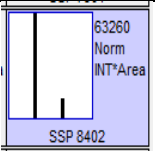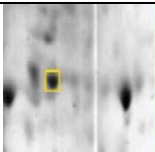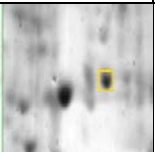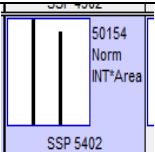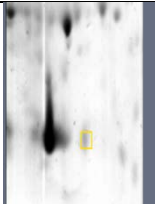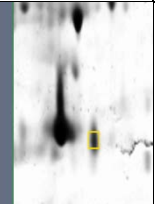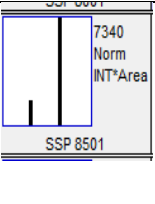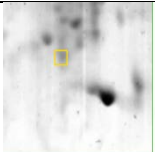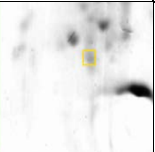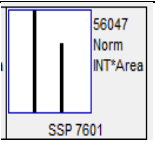
All stock solutions are stored in separate bottles.

Appendix IV Differential expression levels of the rice leaf proteins under iron deficiency conditions

To check the abundance of other proteins, 10 spots were picked for MALDI-TOF analysis and analysed the quantity of expressed protein levels shown in Table A .1. The results of the MALDI-TOF indicates that the changes occurred mostly in Rubisco enzyme and photosystem complexes.

Rubisco is the most abundant protein on earth and contributes up to 50 % of the soluble proteins and up to 30 % of total leaf nitrogen in leaves of C3 plants. Therefore, the degradation of Rubisco and the reutilization of the amino acids liberated are important for the nitrogen budget of plants. It is reported that iron deficiency in sugar beet decreases RuBP carboxylation capacity, through reduced Rubisco enzyme activation (Taylor and Terry, 1986; Winder and Nishio, 1995; Larbi et al., 2004), down-regulation of Rubisco gene expression and decrease in light harvesting, electron transport and carbon fixation (Winder and Nishio, 1995). Iron deficiency leads to down-regulation of Rubisco (EC 4.1.1.39) activity (Terry, 1980). Moreover, proteomic studies under abiotic stresses in rice already reported degradation of Rubisco subunits (Agarwal et al., 2002; Yan et al., 2006). Rubisco activase (RAC) is a low-molecular weight ATP-binding protein that modifies the conformation, facilitates the dissociation of inhibitors (tightly bound sugar phosphates) from active sites and increase the enzymatic activity of Rubisco. The induction of RAC transcripts and protein have been shown to be responsive to several stress conditions such as iron deficiency in sugar beet (Winder and Nishio, 1995) high temperature in wheat leaves (Law and Crafts-Brandner, 2001), low temperature (Yan et al., 2006), drought (Salekdeh et al., 2002; Ali and Komatsu, 2006), high salinity (Parker et al., 2006) in rice leaves.

Table A. 1. Differential expression levels of the leaf proteome under iron deficiency condition in rice seedlings

Spot no	Match to, score and Details of hit	Complete Iron deficient	Spot quantity
1	Match to: gi|1398999 Score: 52 Expect: 0.91 23 kDa polypeptide of photosystem II [Oryza sativa (japonica cultivar-group)]		59384 Norm INT*Area SSP 4501
2	Match to: gi|115451919 Score: 36 Expect: 31 Os03g0249400 [Oryza sativa Japonica Group] Found in search of peaklist.xml Nominal mass (M_r): 14064; Calculated pI value: 9.51		51785 Norm INT*Area
3	Match to: G6PIA_ORYSJ Score: 39 Expect: 0.4 Glucose-6-phosphate isomerase, cytosolic A OS=Oryza sativa subsp. japonica GN=Os03g0776000 PE=2 SV=2 Found in search of peaklist.xml Nominal mass (M_r): 62712; Calculated pI value: 6.80		63260 Norm INT*Area SSP 8402
4	Match to: gi|290585768 Score: 99 Expect: 1.6e-05 ribulose-1,5-bisphosphate carboxylase/oxygenase large subunit [Oryza sativa] Nominal mass (M_r): 26496; Calculated pI value: 7.00		50154 Norm INT*Area SSP 5402
5	Match to: BRE1A_ORYSJ Score: 41 Expect: 0.29 E3 ubiquitin-protein ligase BRE1-like 1 OS=Oryza sativa subsp. japonica GN=BRE1A PE=2 SV=3 Nominal mass (M_r): 101280; Calculated pI value: 7.97		7340 Norm INT*Area SSP 8501
6	Match to: CIPKP_ORYSJ Score: 34 Expect: 1.4 CBL-interacting protein kinase 25 OS=Oryza sativa subsp. japonica GN=CIPK25 PE=2 SV=1 Nominal mass (M_r): 57400; Calculated pI		56047 Norm INT*Area SSP 7601

	value: 8.78		
7	Match to: LOGL6_ORYSJ Score: 47 Expect: 0.067 Probable cytokinin riboside 5'-monophosphate phosphoribohydrolase LOGL6 OS=Oryza sativa subsp. japonica GN=LOGL6 PE=2 SV=1 Nominal mass (M_r): 27704; Calculated pI value: 5.92		
8	Match to: gi|57283874 Score: 126 Expect: 1.7e-07 ribulose-1,5-bisphosphate carboxylase/oxygenase large subunit [Oryza sativa] Nominal mass (M_r): 53331; Calculated pI value: 6.23		
9	Match to: gi|290585768 Score: 111 Expect: 1.1e-06 ribulose-1,5-bisphosphate carboxylase/oxygenase large subunit [Oryza sativa] Nominal mass (M_r): 26496; Calculated pI value: 7.00		
10	Match to: P2C70_ORYSJ Score: 26 Expect: 8.7 Probable protein phosphatase 2C 70 OS=Oryza sativa subsp. japonica GN=Os09g0558000 PE=2 SV=2 Nominal mass (M_r): 40108; Calculated pI value: 5.03		
11	Match to: gi|115488238 Score: 117 Expect: 2.7e-07 Os12g0291400 [Oryza sativa Japonica Group] Nominal mass (M_r): 19714; Calculated pI value: 8.87		

References

References

Agarwal, G.K., Rakwal, R., Yonekura, M., Kubo, A. and Saji, H., 2002, Proteome analysis of differentially displayed proteins as a tool for investigating ozone stress in rice (Oryza sativa L.) seedlings. Proteomics 2, 947-959.

Ahsan, N., Renaut, J. and Komatsu, S., 2009, Recent developments in the application of proteomics to the analysis of plant responses to heavy metals. Proteomics 9, 2602-21.

Albertsson, P., 2001, A quantitative model of the domain structure of the photosynthetic membrane. Trends Plant Sci 6, 349-58.

Ali, G.M. and Komatsu, S., 2006, Proteomic analysis of rice leaf sheath during drought stress. J Proteome Res 5, 396-403.

Allen, J.P., Feher, G., Yeates, T.O., Komiya, H. and Rees, D.C., 1987, Structure of the reaction center from Rhodobacter sphaeroides R-26: the protein subunits. Proc Natl Acad Sci U S A 84, 6162-6.

Allen, J.P., Feher, G., Yeates, T.O., Komiya, H. and Rees, D.C., 1988, Structure of the reaction center from Rhodobacter sphaeroides R-26: protein-cofactor (quinones and Fe2+) interactions. Proc Natl Acad Sci U S A 85, 8487-91.

Altschul, S.F., Gish, W., Miller, W., Myers, E.W. and Lipman, D.J., 1990, Basic local alignment search tool. J Mol Biol 215, 403-10.

Amunts, A., Drory, O. and Nelson, N., 2007, The structure of a plant photosystem I supercomplex at 3.4 Å resolution. Nature 447, 58-63.

Amunts, A., Toporik, H., Borovikova, A. and Nelson, N., 2010, Structure determination and improved model of plant photosystem I. J Biol Chem 285, 3478-3486.

Antal, T. and Rubin, A., 2008, In vivo analysis of chlorophyll a fluorescence induction. Photosynth Res 96, 217-26.

Antal, T.K., Volgusheva, A.A., Kukarskih, G.P., Bulychev, A.A., Krendeleva, T.E. and Rubin, A.B., 2006, Effects of sulfur limitation on photosystem II functioning in Chlamydomonas reinhardtii as probed by chlorophyll a fluorescence. Physiol Plantarum 128, 360-367.

Armstrong, B., 2002, Review: iron treatment does not improve psychomotor development and cognitive function at 30 days in children with iron deficiency anaemia. Evid Based Ment Health 5, 17.

Arnon, D.I., 1949, Copper Enzymes in Isolated Chloroplasts. Polyphenoloxidase in Beta Vulgaris. Plant Physiol 24, 1-15.

Barbato, R., Race, H.L., Friso, G. and Barber, J., 1991, Chlorophyll levels in the pigment-binding proteins of photosystem II. A study based on the chlorophyll to cytochrome ratio in different photosystem II preparations. FEBS Lett 286, 86-90.

Barber, J., 2001, The structure of photosystem I. Nat Struct Biol 8, 577-9.

Barber, J., Morris, E. and Buchel, C., 2000, Revealing the structure of the photosystem II chlorophyll binding proteins, CP43 and CP47. Biochim Biophys Acta 1459, 239-47.

Bassi, R., Hoyer-Hansen, G., Barbato, R., Giacometti, G.M. and Simpson, D.J., 1987, Chlorophyll-proteins of the photosystem II antenna system. J Biol Chem 262, 13333-41.

Bassi, R., Machold, O. and Simpson, D., 1985, Chlorophyll-proteins of two photosystem I preparations from maize. Carlsberg Res Commun 50, 145-162.

Bassi, R. and Simpson, D., 1987, Chlorophyll-protein complexes of barley photosystem I. Eur J Biochem 163, 221-230.

Bassi, R., Soen, S.Y., Frank, G., Zuber, H. and Rochaix, J.D., 1992, Characterization of chlorophyll a/b proteins of photosystem I from Chlamydomonas reinhardtii. J Biol Chem 267, 25714-21.

Batsmanova, L.M., 2008, Superoxide dismutase and catalase activity in the winter wheat sprout leaves under the effect of exogenous hydrogen peroxide. Ukr Biokhim Zh 80, 101-5.

Baum, J.A. and Scandalios, J.G., 1979, Developmental expression and intracellular localization of superoxide dismutase in maize. Differentiation 13, 133–140.

Beard, J., 1995, One person's view of iron deficiency, development, and cognitive function. Am J Clin Nutr 62, 709-10.

Beauchamp, C. and Fridovich, I., 1971, Superoxide dismutase: Improved assays and an assay applicable to acrylamide gels. Anal Biochem 44, 276-287.

Belkhodja, R., Morales, F., Quílez, R., López-Millán, A.F., Abadía, A. and Abadía, J., 1998, Iron deficiency causes changes in chlorophyll fluorescence due to the reduction in the dark of the Photosystem II acceptor side. Photosynth Res 56, 265-276.

Benshem, A., Frolow, F. and Nelson, N., 2004, Evolution of photosystem I – from symmetry through pseudosymmetry to asymmetry. FEBS Lett 564, 274-280.

Bibby, T.S., Nield, J. and Barber, J., 2001, Iron deficiency induces the formation of an antenna ring around trimeric photosystem I in cyanobacteria. Nature 412, 743-5.

Boekema, E.J., Dekker, J.P., van Heel, M.G., Roigner, M., Saenger, W., Witt, I. and Witt, H.T., 1987, Evidence for a trimeric organization of the photosystem I complex from the thermophilic cyanobacterium Synechococcus sp. FEBS Lett 217, 283–286.

Boekema, E.J., Hifney, A., Yakushevska, A.E., Piotrowski, M., Keegstra, W., Berry, S., Michel, K.P., Pistorius, E.K. and Kruip, J., 2001a, A giant chlorophyll-protein complex induced by iron deficiency in cyanobacteria. Nature 412, 745-8.

Boekema, E.J., Jensen, P.E., Schlodder, E., van Breemen, J.F., van Roon, H., Scheller, H.V. and Dekker, J.P., 2001b, Green plant photosystem I binds light-harvesting complex I on one side of the complex. Biochemistry 40, 1029-36.

Boekema, E.J., Van Roon, H., Van Breemen, J.F. and Dekker, J.P., 1999, Supramolecular organization of photosystem II and its light-harvesting antenna in partially solubilized photosystem II membranes. Eur J Biochem 266, 444-52.

Briat, J.F., Curie, C. and Gaymard, F., 2007, Iron utilization and metabolism in plants. Curr Opin Plant Biol 10, 276-82.

Broser, M., Gabdulkhakov, A., Kern, J., Guskov, A., Mueh, F., Saenger, W. and Zouni, A., 2010, Crystal structure of monomeric photosystem II from Thermosynechococcus elongatus at 3.6 A resolution. J Biol Chem, 26255-62.

Bukharov, A.A., Kolosov, V.L. and Zolotarev, A.S., 1990, Rye photosystem II. Nucleotide sequence of the psbC gene coding 43- kDa chlorophyll(a)-binding proteins. Bioorg Khim 16, 1210-7.

Bullerjahn, G.S. and Sherman, L.A., 1986, Immunological characterization of photosystem II chlorophyll-binding proteins from the cyanobacterium, Aphanocapsa 6714. J Bioenerg Biomembr 18, 285-93.

Camara-Artigas, A., Magee, C., Goetsch, A. and Allen, J.P., 2002, The structure of the heterodimer reaction center from Rhodobacter sphaeroides at 2.55 a resolution. Photosynth Res 74, 87-93.

Carter, R.C., Jacobson, J.L., Burden, M.J., Armony-Sivan, R., Dodge, N.C., Angelilli, M.L., Lozoff, B. and Jacobson, S.W., 2010, Iron deficiency anemia and cognitive function in infancy. Pediatrics 126, e427-34.

Chaney, R.L., Chen, Y., Green, C.E., Holden, M.J., Bell, P.F., Luster, D.G. and (1992), A.J., 1992, Root hairs on chlorotic tomatoes are an effect of chlorosis rather than part of the adaptative Fe-stress response. J Plant Nutr 15, 1857-1875.

Chauhan, D., Folea, I.M., Jolley, C.C., Kouril, R., Lubner, C.E., Lin, S., Kolber, D., Wolfe-Simon, F., Golbeck, J.H., Boekema, E.J. and Fromme, P., 2011, A novel photosynthetic strategy for adaptation to low-iron aquatic environments. Biochemistry 50, 686-92.

Chen, C.-N. and Pan, S.-M., 1996, Assay of superoxide dismutase activity by combining electrophoresis and densitometry. Bot. Bull. Acad. Sin. 37, 107-111.

Cheng, Y.C. and Fleming, G.R., 2009, Dynamics of light harvesting in photosynthesis. Annu Rev Phys Chem 60, 241-62.

Chi, G., Chen, X., Shi, Y. and Liu, X., 2009, Spectral response of rice (Oryza sativa L.) leaves to Fe^{2+} stress. Sci China C Life Sci 52, 747-753.

Chitnis, P.R., 2001, Photosystem I: Function and Physiology. Annu Rev Plant Physiol Plant Mol Biol 52, 593-626.

Chitnis, P.R., Xu, Q., Chitnis, V.P. and Nechushtai, R., 1995, Function and organization of Photosystem I polypeptides. Photosynth Res 44, 23-40.

Chitnis, V.P., Jung, Y.S., Albeet, L., Golbeck, J.H. and Chitnis, P.R., 1996, Mutational analysis of photosystem I polypeptides: Role of PsaD and the LYSYL 106 residue in the reductase activity of photosystem I. J Biol Chem 271, 11772-11780.

Cho, H.M., Mancino, L.J. and Blankenship, R.E., 1984, Light saturation curves and quantum yields in reaction centers from photosynthetic bacteria. Biophys J 45, 455-461.

Clark, S.E. and Lamppa, G.K., 1992, Processing of the Precursors for the Light-Harvesting Chlorophyll-Binding Proteins of Photosystem II and Photosystem I during Import and in an Organelle-Free Assay. Plant Physiol 98, 595-601.

Coale, K.H., Fitzwater, S.E., Gordon, R.M., Johnson, K.S. and Barber, R.T., 1996, Control of community growth and export production by upwelled iron in the equatorial Pacific Ocean. Nature 379, 621-624.

Curie, C. and Briat, J.F., 2003, Iron transport and signaling in plants. Annu Rev Plant Biol 54, 183-206.

Dainese, P. and Bassi, R., 1991, Subunit stoichiometry of the chloroplast photosystem II antenna system and aggregation state of the component chlorophyll a/b binding proteins. J Biol Chem 266, 8136-42.

Datta, K., Baisakh, N., Oliva, N., Torrizo, L., Abrigo, E., Tan, J., Rai, M., Rehana, S., Al-Babili, S., Beyer, P., Potrykus, I. and Datta, S.K., 2003, Bioengineered 'golden' indica rice cultivars with beta-carotene metabolism in the endosperm with hygromycin and mannose selection systems. Plant Biotechnol J 1, 81-90.

Deisenhofer, J., Miki, O.E., K. , Huber, R. and Michel, H., 1985, Structure of the protein subunits in the photosynthetic reaction centre of Rhodopseudomonas viridis at 3Å resolution. Nature 318, 618 - 624.

Deshpande, N., Addess, K.J., Bluhm, W.F., Merino-Ott, J.C., Townsend-Merino, W., Zhang, Q., Knezevich, C., Xie, L., Chen, L., Feng, Z., Green, R.K., Flippen-Anderson, J.L., Westbrook, J., Berman, H.M. and Bourne, P.E., 2005, The RCSB Protein Data Bank: a redesigned query system and relational database based on the mmCIF schema. Nucleic Acids Res 33, D233-7.

Desquilbet, T.E., Duval, J.C., Robert, B., Houmard, J. and Thomas, J.C., 2003, In the unicellular red alga Rhodella violacea iron deficiency induces an accumulation of uncoupled LHC. Plant Cell Physiol 44, 1141-51.

Doan, J.M., Schoefs, B., Ruban, A.V. and Etienne, A.L., 2003, Changes in the LHCI aggregation state during iron repletion in the unicellular red alga Rhodella violacea. FEBS Lett 533, 59-62.

Dolcini, B. and Carobi, C., 1971, Energy expenditure (cal-kg-24 H) of the albino rat as a function of the days of survival in fasting and of the behavior of weight loss. Boll Soc Ital Biol Sper 47, 263-7.

Drazkiewicz, M., Skorzynska-Polit, E. and Krupa, Z., 2007, The redox state and activity of superoxide dismutase classes in Arabidopsis thaliana under cadmium or copper stress. Chemosphere 67, 188-93.

Dufau, M.L., Ryan, D.W., Baukal, A.J. and Catt, K.J., 1975, Gonadotropin receptors. Solubilization and purification by affinity chromatography. J Biol Chem 250, 4822-4.

Dunford, H.B., 1987, Free radicals in iron-containing systems. Free Radic Biol Med 3, 405-21.

Eswar, N., Webb, B., Marti-Renom, M.A., Madhusudhan, M.S., Eramian, D., Shen, M.Y., Pieper, U. and Sali, A., 2007, Comparative protein structure modeling using MODELLER. Curr Protoc Protein Sci Chapter 2, Unit 2 9.

Farah, J., Rappaport, F., Choquet, Y., Joliot, P. and Rochaix, J.D., 1995, Isolation of a psaF-deficient mutant of Chlamydomonas reinhardtii: efficient interaction of plastocyanin with the photosystem I reaction center is mediated by the PsaF subunit. EMBO J 14, 4976-84.

Fernandez, V. and Ebert, G., 2003, Regreening of Fe-deficient plants: a review on the physiological background and the chemistry of the applied solution. Curr Top Plant Biol 4, 79-92.

Fischer, N., Sétif, P. and Rochaix, J.D., 1997, Targeted mutations in the psaC gene of Chlamydomonas reinhardtii: Preferential reduction of F(B) at low temperature is not accompanied by altered electron flow from photosystem I to ferredoxin. Biochemistry 36, 93-102.

Franck, F., Juneau, P. and Popovic, R., 2002, Resolution of the Photosystem I and Photosystem II contributions to chlorophyll fluorescence of intact leaves at room temperature. Biochim Biophys Acta 1556, 239-46.

Fromme, P., Jordan, P. and Krauss, N., 2001, Structure of photosystem I. Biochim Biophys Acta 1507, 5-31.

Fyfe, P.K., Jones, M.R. and Heathcote, P., 2002, Insights into the evolution of the antenna domains of Type-I and Type-II photosynthetic reaction centres through homology modelling. FEBS Lett 530, 117-123.

Gasteiger, E., Gattiker, A., Hoogland, C., Ivanyi, I., Appel, R.D. and Bairoch, A., 2003, ExPASy: The proteomics server for in-depth protein knowledge and analysis. Nucleic Acids Res 31, 3784-8.

Geider, R.J., 1999, Biological oceanography - Complex lessons of iron uptake. Nature 400, 815-816.

Geyer, H., Wuhrer, M., Resemann, A. and Geyer, R., 2005, Identification and characterization of keyhole limpet hemocyanin N-glycans mediating cross-reactivity with Schistosoma mansoni. J Biol Chem 280, 40731-48.

Gibasiewicz, K., Ramesh, V.M., Lin, S., Woodbury, N.W. and Webber, A.N., 2002, Excitation dynamics in eukaryotic PS I from Chlamydomonas reinhardtii CC 2696 at 10 K. Direct detection of the reaction center exciton states. J Phys Chem B 106, 6322-6330.

Gibasiewicz, K., Ramesh, V.M., Melkozernov, A.N., Lin, S., Woodbury, N.W., Blankenship, R.E. and Webber, A.N., 2001, Excitation dynamics in the core antenna of PS I from Chlamydomonas reinhardtii CC 2696 at room temperature. J Phys Chem B 105, 11498-11506.

Gibasiewicz, K., Szrajner, A., Ihalainen, J.A., Germano, M., Dekker, J.P. and van Grondelle, R., 2005, Characterization of low-energy chlorophylls in the PSI-LHCI supercomplex from Chlamydomonas reinhardtii. A site-selective fluorescence study. J Phys Chem B 109, 21180-6.

Gnanamanickam, S.S. 2009 Rice and Its Importance to Human Life. In: Biological Control of Rice Diseases, Vol. 8, Progress in Biological Control. Springer Netherlands, p. 1-11.

Gobets, B. and Van Grondelle, R., 2001, Energy transfer and trapping in photosystem I. Biochim Biophys Acta 1507, 80-99.

Gohre, V., Ossenbuhl, F., Crevecoeur, M., Eichacker, L.A. and Rochaix, J.D., 2006, One of two Alb3 proteins is essential for the assembly of the photosystems and for cell survival in Chlamydomonas. Plant Cell 18, 1454-1466.

Golbeck, J.H., 1999, A comparative analysis of the spin state distribution of in vitro and in vivo mutants of PsaC. A biochemical argument for the sequence of electron transfer in Photosystem I as $F(X) \rightarrow F(A) \rightarrow F(B) \rightarrow$ ferredoxin/flavodoxin. Photosynth Res 61, 107-144.

Grossman, A.R., 2000, Chlamydomonas reinhardtii and photosynthesis: genetics to genomics. Curr Opin Plant Biol 3, 132-7.

Grotz, N. and Guerinot, M.L., 2006, Molecular aspects of Cu, Fe and Zn homeostasis in plants. Biochim Biophys Acta 1763, 595-608.

Guerinot, M.L., 2001, Improving rice yields--ironing out the details. Nat Biotechnol 19, 417-8.

Guerinot, M.L. and Yi, Y., 1994, Iron: nutritious, noxious, and not readily available. Plant Physiol 104, 815-820.

Guikema, J.A. and Sherman, L.A., 1984, Influence of Iron Deprivation on the Membrane Composition of Anacystis nidulans. Plant Physiol 74, 90-5.

Hankamer, B., Morris, E., Nield, J., Gerle, C. and Barber, J., 2001, Three-dimensional structure of the photosystem II core dimer of higher plants determined by electron microscopy. J Struct Biol 135, 262-9.

Harlaow, E. and Lane, D. 1988 Antibodies: A laboratory manual, cold spring Harbor Laboratory. In, Cold spring Harbor, N.Y.

Harris, E.H., 2001, Chlamydomonas as a Model Organism. Annu Rev Plant Physiol Plant Mol Biol 52, 363-406.

Haworth, P., Watsona, J.L. and Arntzen, C.J., 1983, The detection, isolation and characterization of a light-harvesting complex which is specifically associated with Photosystem I Biochim Biophys Acta 724, 151-158

Heathcote, P., Jones, M.R. and Fyfe, P.K., 2003, Type I photosynthetic reaction centres: structure and function. Philos Trans R Soc Lond B Biol Sci 358, 231-243.

Herrin, D.L., Plumley, F.G., Ikeuchi, M., Michaels, A.S. and Schmidt, G.W., 1987, Chlorophyll antenna proteins of photosystem I: topology, synthesis, and regulation of the 20-kDa subunit of Chlamydomonas light-harvesting complex of photosystem I. Arch Biochem Biophys 254, 397-408.

Hippler, M., Drepper, F., Farah, J. and Rochaix, J.D., 1997, Fast electron transfer from cytochrome c6 and plastocyanin to photosystem I of Chlamydomonas reinhardtii requires PsaF. Biochemistry 36, 6343-9.

Hippler, M., Klein, J., Fink, A., Allinger, T. and Hoerth, P., 2001, Towards functional proteomics of membrane protein complexes: analysis of thylakoid membranes from Chlamydomonas reinhardtii. Plant J 28, 595-606.

Hirano, A., Sugawara, M., Uchino, S. and Nakajima-Iijima, S., 1999, Comparison of total ion fluxes through a single recombinant epsilon/zeta 1 NMDA receptor among different subunit compositions. Biophys J 76, A335-A335.

Hirano, A., Wakabayashi, M., Sugawara, M., Uchino, S. and Nakajima-Iijima, S., 2000, Evaluation and comparison of ion permeation and agonist selectivities for N-methyl-D-aspartate receptor channels with different subunit compositions in bilayer lipid membranes based on integrated single-channel currents. Anal Biochem 283, 258-265.

Hoagland, D.R. and Arnon, D.I., 1938, The water-culture method for growing plants without soil. 347, 35–37. Calif Agric Ext Publ 347, 35-37.

Hong, S.K., Pawlikowski, S.A., Vander Meulen, K.A. and Yocum, C.F., 2001, The oxidation state of the photosystem II manganese cluster influences the structure of manganese stabilizing protein. Biochim Biophys Acta 1504, 262-74.

Hoober, J.K. 1989 The Chlamydomonas Sourcebook. A Comprehensive Guide to Biology and Laboratory Use. In: E.H. Harris (Ed.), Vol. 246. Academic Press, San Diego, CA, p. 1503-4.

Hopp, T.P. and Woods, K.R., 1983, A computer program for predicting protein antigenic determinants. Mol Immunol 20, 483-489.

Hothem, S.D., Marley, K.A. and Larson, R.A., 2003, Photochemistry in Hoagland's nutrient solution. J Plant Nutr 26, 845-854.

Hui, Y., Jie, W. and Carpentier, R., 2000, Degradation of the photosystem I complex during photoinhibition. Photochem Photobiol 72, 508-12.

Humbeck, K. and Krupinska, K., 2003, The abundance of minor chlorophyll a/b-binding proteins CP29 and LHCI of barley (Hordeum vulgare L.) during leaf senescence is controlled by light. J Exp Bot 54, 375-83.

Huner, N.P.A., Öquist, G. and Sarhan, F., 1998, Energy balance and acclimation to light and cold. Trends Plant Sci 3, 224-230.

Hwang-Schweitzer, R.H., Knox, R.S., Gibbs, P.B. and Biggins, J., 1992, Fluorescence studies of photoregulation in the chrysophyte Ochromonas danica. J Luminescence 51, 99-109.

Ihalainen, J.A., Klimmek, F., Ganeteg, U., Van Stokkum, I.H.M., Van Grondelle, R., Jansson, S. and Dekker, J.P., 2005, Excitation energy trapping in photosystem I complexes depleted in Lhca1 and Lhca4. FEBS Lett 579, 4787-4791.

Ikeda, Y., Komura, M., Watanabe, M., Minami, C., Koike, H., Itoh, S., Kashino, Y. and Satoh, K., 2008, Photosystem I complexes associated with fucoxanthin-chlorophyll-binding proteins from a marine centric diatom, Chaetoceros gracilis. Biochim Biophys Acta 1777, 351-61.

Itai, R., Suzuki, K., Yamaguchi, H., Nakanishi, H., Nishizawa, N.K., Yoshimura, E. and Mori, S., 2000, Induced activity of adenine phosphoribosyltransferase (APRT) in iron-deficiency barley roots: a possible role for phytosiderophore production. J Exp Bot 51, 1179-88.

Ivanov, A.G., Park, Y.I., Miskiewicz, E., Raven, J.A., Huner, N.P. and Oquist, G., 2000, Iron stress restricts photosynthetic intersystem electron transport in Synechococcus sp. PCC 7942. FEBS Lett 485, 173-7.

Jahns, P. and Junge, W., 1990, Dicyclohexylcarbodiimide-binding proteins related to the short circuit of the proton-pumping activity of photosystem II. Identified as light-harvesting chlorophyll-a/b-binding proteins. Eur J Biochem 193, 731-6.

Jansson, S., Andersen, B. and Scheller, H.V., 1996, Nearest-neighbor analysis of higher-plant photosystem I holocomplex. Plant Physiol 112, 409-20.

Jeanjean, R., Latifi, A., Matthijs, H.C.P. and Havaux, M., 2008, The PsaE subunit of photosystem I prevents light-induced formation of reduced oxygen species in the cyanobacterium Synechocystis sp. PCC 6803. Biochim Biophys Acta 1777, 308-316.

Jensen, P.E., Bassi, R., Boekema, E.J., Dekker, J.P., Jansson, S., Leister, D., Robinson, C. and Scheller, H.V., 2007, Structure, function and regulation of plant photosystem I. Biochim Biophys Acta 1767, 335-52.

Jolley, C.C., Wells, S.A., Hespenheide, B.M., Thorpe, M.F. and Fromme, P., 2006, Docking of photosystem I subunit C using a constrained geometric simulation. J Am Chem Soc 128, 8803-8812.

Jordan, P., Fromme, P., Witt, H.T., Klukas, O., Saenger, W. and Krauss, N., 2001, Three-dimensional structure of cyanobacterial photosystem I at 2.5 A resolution. Nature 411, 909-17.

Kamiya, N. and Shen, J.R., 2003, Crystal structure of oxygen-evolving photosystem II from Thermosynechococcus vulcanus at 3.7-A resolution. Proc Natl Acad Sci U S A 100, 98-103.

Kargul, J., Nield, J. and Barber, J., 2003, Three-dimensional reconstruction of a light-harvesting complex I-photosystem I (LHCI-PSI) supercomplex from the green alga Chlamydomonas reinhardtii. Insights into light harvesting for PSI. J Biol Chem 278, 16135-41.

Karlsen, A., Lernmark, A., Kofod, H. and Dyrberg, T., 1990, A novel affinity purification method to isolate peptide specific antibodies. J Immunol Methods 128, 151-7.

Kilian, R., Bassi, R. and Schafer, C., 1998, Identification and characterization of photosystem II chlorophyll a/b binding proteins in Marchantia polymorpha L. Planta 204, 260-7.

Knoetzel, J., Bossmann, B. and Grimme, L.H., 1998, Chlorina and viridis mutants of barley (Hordeum vulgare L.) allow assignment of long-wavelength chlorophyll forms to individual Lhca proteins of photosystem I in vivo. FEBS Lett 436, 339-42.

Knoetzel, J., Svendsen, I. and Simpson, D.J., 1992, Identification of the photosystem I antenna polypeptides in barley. Isolation of three pigment-binding antenna complexes. Eur J Biochem 206, 209-15.

Kobayashi, T., Itai, R.N., Ogo, Y., Kakei, Y., Nakanishi, H., Takahashi, M. and Nishizawa, N.K., 2009, The rice transcription factor IDEF1 is essential for the early response to iron deficiency, and induces vegetative expression of late embryogenesis abundant genes. Plant J 60, 948-61.

Kobayashi, T., Nakanishi, H. and Nishizawa, N.K., 2010, Recent insights into iron homeostasis and their application in graminaceous crops. Proc Jpn Acad Ser B Phys Biol Sci. 86, 900-913.

Kolar, C., Adam, E., Schafer, E. and Nagy, F., 1995, Expression of tobacco genes for light-harvesting chlorophyll a/b binding proteins of photosystem II is controlled by two circadian oscillators in a developmentally regulated fashion. Proc Natl Acad Sci U S A 92, 2174-8.

Kolaskar, A.S. and Tongaonkar, P.C., 1990, A semi-empirical method for prediction of antigenic determinants on protein antigens. FEBS Lett 276, 172-174.

Kostek, S.A., Grob, P., De Carlo, S., Lipscomb, J.S., Garczarek, F. and Nogales, E., 2006, Molecular architecture and conformational flexibility of human RNA polymerase II. Structure 14, 1691-700.

Kouril, R., Zygadlo, A., Arteni, A.A., de Wit, C.D., Dekker, J.P., Jensen, P.E., Scheller, H.V. and Boekema, E.J., 2005, Structural characterization of a complex of

photosystem I and light-harvesting complex II of Arabidopsis thaliana. Biochemistry 44, 10935-40.

Lam, E., Ortiz, W. and Malkin, R., 1984, Chlorophyll a/b proteins of Photosystem I. FEBS Lett 168, 10-14.

Larbi, A., Abadia, A., Morales, F. and Abadia, J., 2004, Fe Resupply to Fe-deficient Sugar Beet Plants Leads to Rapid Changes in the Violaxanthin Cycle and other Photosynthetic Characteristics without Significant de novo Chlorophyll Synthesis. Photosynth Res 79, 59-69.

Laskowski, R.A., Chistyakov, V.V. and Thornton, J.M., 2005, PDBsum more: new summaries and analyses of the known 3D structures of proteins and nucleic acids. Nucleic Acids Res 33, D266-8.

Laskowski, R.A., Hutchinson, E.G., Michie, A.D., Wallace, A.C., Jones, M.L. and Thornton, J.M., 1997, PDBsum: a Web-based database of summaries and analyses of all PDB structures. Trends Biochem Sci 22, 488-90.

Laskowski, R.A., MacArthur, M.W., Moss, D.S. and Thornton, J.M., 1993, PROCHECK: a program to check the stereochemical quality of protein structures. J Appl Cryst 26, 283–291.

Law, R.D. and Crafts-Brandner, S.J., 2001, High temperature stress increases the expression of wheat leaf ribulose-1,5-bisphosphate carboxylase/oxygenase activase protein. Arch Biochem Biophys 386, 261-7.

Lazar, D., 2003, Chlorophyll a fluorescence rise induced by high light illumination of dark-adapted plant tissue studied by means of a model of photosystem II and considering photosystem II heterogeneity. J Theor Biol 220, 469-503.

Lelong, C., Boekema, E.J., Kruip, J., Bottin, H., Rögner, M. and Sétif, P., 1996, Characterization of a redox active cross-linked complex between cyanobacterial photosystem I and soluble ferredoxin. EMBO Journal 15, 2160-2168.

Li, N., Zhao, J.D., Warren, P.V., Warden, J.T., Bryant, D.A. and Golbeck, J.H., 1991, PsaD is required for the stable binding of PsaC to the photosystem I core protein of Synechococcus sp. PCC 6301. Biochemistry 30, 7863-72.

Li, W., Qi, L., Lin, X., Chen, H., Ma, Z., Wu, K. and Huang, S., 2009, The expression of manganese superoxide dismutase gene from Nelumbo nucifera responds strongly to chilling and oxidative stresses. J Integr Plant Biol 51, 279-86.

Liang, X., Qiao, D., Huang, M., Yi, X., Bai, L., Xu, H., Wei, L., Zeng, J. and Cao, Y., 2008, Identification of a gene encoding the light-harvesting chlorophyll a/b proteins of photosystem I in green alga Dunaliella salina. DNA Seq 19, 137-45.

Liddell, P.A., Gervaldo, M., Bridgewater, J.W., Keirstead, A.E., Lin, S., Moore, T.A., Moore, A.L. and Gust, D., 2008, Porphyrin-based hole conducting electropolymer. Chem Mater 20, 135-142.

Link, G., Berthold, T., Bechtold, M., Weidner, J.U., Ohmes, E., Tang, J., Poluektov, O., Utschig, L., Schlesselman, S.L., Thurnauer, M.C. and Kothe, G., 2001, Structure of the P700(+)A1(-) radical pair intermediate in photosystem I by high time resolution multifrequency electron paramagnetic resonance: analysis of quantum beat oscillations. J Am Chem Soc 123, 4211-22.

Logan, S., Martins, S. and Gilbert, R., 2001, Iron therapy for improving psychomotor development and cognitive function in children under the age of three with iron deficiency anaemia. Cochrane Database Syst Rev, CD001444.

Loll, B., Kern, J., Saenger, W., Zouni, A. and Biesiadka, J., 2005, Towards complete cofactor arrangement in the 3.0 A resolution structure of photosystem II. Nature 438, 1040-4.

Long, J.C., Sommer, F., Allen, M.D., Lu, S.F. and Merchant, S.S., 2008, FER1 and FER2 encoding two ferritin complexes in Chlamydomonas reinhardtii chloroplasts are regulated by iron. Genetics 179, 137-47.

Lucca, P., Hurrell, R. and Potrykus, I., 2002, Fighting iron deficiency anemia with iron-rich rice. J Am Coll Nutr 21, 184S-190S.

Lunde, C., Jensen, P.E., Haldrup, A., Knoetzel, J. and Scheller, H.V., 2000, The PSI-H subunit of photosystem I is essential for state transitions in plant photosynthesis. Nature 408, 613-615.

Lüneberg, J., Fromme, P., Jekow, P. and Schlodder, E., 1994, Spectroscopic characterization of PSI core complexes from thermophilic Synechococcus sp: Identical reoxidation kinetics of A−1 before and after removal of the iron-sulfur-clusters FA and FB. FEBS Lett 338, 197-202.

Lynnes, J.A., Derzaph, T.L.M. and Weger, H.G., 1998, Iron limitation results in induction of ferricyanide reductase and ferric chelate reductase activities in Chlamydomonas reinhardtii. Planta 204, 360-365.

Marschner, H. 1995 Mineral nutrition of higher plants. In. Academic, London.

Martin, J.H., Coale, K.H., Johnson, K.S., Fitzwater, S.E., Gordon, R.M., Tanner, S.J. and Hunter, C.N., 1994, Testing the iron hypothesis in ecosystems of the equatorial Pacific Ocean. Nature 371, 123-129.

May, R.J., Beenhouwer, D.O. and Scharff, M.D., 2003, Antibodies to keyhole limpet hemocyanin cross-react with an epitope on the polysaccharide capsule of Cryptococcus neoformans and other carbohydrates: implications for vaccine development. J Immunol 171, 4905-12.

McCann, J.C. and Ames, B.N., 2007, An overview of evidence for a causal relation between iron deficiency during development and deficits in cognitive or behavioral function. Am J Clin Nutr 85, 931-45.

Merchant, S.S. and et al., 2007, The Chlamydomonas genome reveals the evolution of key animal and plant functions. Science 318, 245-50.

Mezo, G., Mihala, N., Andreu, D. and Hudecz, F., 2000, Conjugation of Epitope Peptides with SH Group to Branched Chain Polymeric Polypeptides via Cys(Npys). Bioconjugate Chem. 11, 484-491.

Mori, S., 1999, Iron acquisition by plants. Curr Opin Plant Biol 2, 250-3.

Mori, S., Nishizawa, N.K., Hayashi, H., Chino, M., Yoshimura, E. and Ishihara, J., 1991, Why are young rice plants highly susceptible to iron deficiency? . Plant Soil 130, 143–156.

Morishige, D.T., Anandan, S., Dreyfuss, B.W., Williams, R.S., Ellis, R.J. and Thornber, J.P., 1993, A pea cDNA clone (Ihca3) encoding the 24-kilodalton light-harvesting protein of photosystem I. Plant Physiol 103, 1461-2.

Morosinotto, T., Breton, J., Bassi, R. and Croce, R., 2003, The nature of a chlorophyll ligand in Lhca proteins determines the far red fluorescence emission typical of photosystem I. J Biol Chem 278, 49223-9.

Moseley, J.L., Allinger, T., Herzog, S., Hoerth, P., Wehinger, E., Merchant, S. and Hippler, M., 2002, Adaptation to Fe-deficiency requires remodeling of the photosynthetic apparatus. EMBO J 21, 6709-20.

Mozzo, M., Mantelli, M., Passarini, F., Caffarri, S., Croce, R. and Bassi, R., 2010, Functional analysis of Photosystem I light-harvesting complexes (Lhca) gene products of Chlamydomonas reinhardtii. Biochim Biophys Acta 1797, 212-221.

Muh, F., Renger, T. and Zouni, A., 2008, Crystal structure of cyanobacterial photosystem II at 3.0 A resolution: a closer look at the antenna system and the small membrane-intrinsic subunits. Plant Physiol Biochem 46, 238-64.

Mullet, J.E., Burke, J.J. and Arntzen, C.J., 1980a, Chlorophyll proteins of photosystem I. Plant Physiol 65, 814-22.

Mullet, J.E., Burke, J.J. and Arntzen, C.J., 1980b, A developmental study of photosystem I peripheral chlorophyll proteins. Plant Physiol 65, 823-7.

Naumann, B., Busch, A., Allmer, J., Ostendorf, E., Zeller, M., Kirchhoff, H. and Hippler, M., 2007, Comparative quantitative proteomics to investigate the remodeling of bioenergetic pathways under iron deficiency in Chlamydomonas reinhardtii. Proteomics 7, 3964-79.

Naumann, B., Stauber, E.J., Busch, A., Sommer, F. and Hippler, M., 2005, N-terminal processing of Lhca3 Is a key step in remodeling of the photosystem I-light-harvesting complex under iron deficiency in Chlamydomonas reinhardtii. J Biol Chem 280, 20431-41.

Nelson, N. and Ben-Shem, A., 2004, The complex architecture of oxygenic photosynthesis. Nat Rev Mol Cell Biol 5, 971-82.

Nelson, N. and Yocum, C.F., 2006, Structure and function of photosystems I and II. Annu Rev Plant Biol 57, 521-65.

Neuhoff, V., Arold, N., Taube, D. and Ehrhardt, W., 1988, Improved staining of proteins in polyacrylamide gels including isoelectric focusing gels with clear background at nanogram sensitivity using Coomassie Brilliant Blue G-250 and R-250. Electrophoresis 9, 255-62.

Neumann, E.M., 1988, Primary structure of barley genes encoding quinone and chlorophyll a binding proteins of photosystem II. Carlsberg Res Commun 53, 259-75.

Nwugo, C.C. and Huerta, A.J., 2011, The effect of silicon on the leaf proteome of rice (Oryza sativa L.) plants under cadmium-stress. J Proteome Res 10, 518-28.

Ogo, Y., Itai, R.N., Nakanishi, H., Kobayashi, T., Takahashi, M., Mori, S. and Nishizawa, N.K., 2007, The rice bHLH protein OsIRO2 is an essential regulator of the genes involved in Fe uptake under Fe-deficient conditions. Plant J 51, 366-77.

Oh-oka, H., Takahashi, Y., Kuriyama, K., Saeki, K. and Matsubara, H., 1988, The protein responsible for center A/B in spinach photosystem I: isolation with iron-sulfur cluster(s) and complete sequence analysis. J Biochem 103, 962-968.

Ozawa, S., Onishi, T. and Takahashi, Y., 2010, Identification and characterization of an assembly intermediate subcomplex of photosystem I in the green alga Chlamydomonas reinhardtii. J Biol Chem 285, 20072-9.

Papageorgiou, G.C., Tsimilli-Michael, M. and Stamatakis, K., 2007, The fast and slow kinetics of chlorophyll a fluorescence induction in plants, algae and cyanobacteria: a viewpoint. Photosynth Res 94, 275-90.

Parker, R., Flowers, T.J., Moore, A.L. and Harpham, N.V., 2006, An accurate and reproducible method for proteome profiling of the effects of salt stress in the rice leaf lamina. J Exp Bot 57, 1109-18.

Philpott, C.C., 2006, Iron uptake in fungi: a system for every source. Biochim Biophys Acta 1763, 636-45.

Pollitt, E., 1993, Iron deficiency and cognitive function. Annu Rev Nutr 13, 521-37.

Price, C.A., 1968, Iron compounds and plant nutrition. Annu Rev Plant Physiol 19, 239-248.

Qin, X., Wang, K., Chen, X., Qu, Y., Li, L. and Kuang, T., 2006, Rapid purification of photosystem I chlorophyll-binding proteins by differential centrifugation and vertical rotor. Photosynth Res 90, 195-204.

Rakwal, R. and Agrawal, G.K., 2003, Rice proteomics: current status and future perspectives. Electrophoresis 24, 3378-89.

Rigoni, F., Barbato, R., Friso, G. and Giacometti, G.M., 1992, Evidence for direct interaction between the chlorophyll-proteins CP29 and CP47 in photosystem II. Biochem Biophys Res Commun 184, 1094-100.

Rikin, A. and Schwartzbach, S.D., 1988, Extremely large and slowly processed precursors to the Euglena light-harvesting chlorophyll a/b binding proteins of photosystem II. Proc Natl Acad Sci U S A 85, 5117-21.

Rochaix, J.D., 2002, Chlamydomonas, a model system for studying the assembly and dynamics of photosynthetic complexes. FEBS Lett 529, 34-8.

Ruban, A.V., Pesaresi, P., Wacker, U., Irrgang, K.D., Bassi, R. and Horton, P., 1998, The relationship between the binding of dicyclohexylcarbodiimide and

quenching of chlorophyll fluorescence in the light-harvesting proteins of photosystem II. Biochemistry 37, 11586-91.

Ruban, A.V., Young, A.J. and Horton, P., 1996, Dynamic properties of the minor chlorophyll a/b binding proteins of photosystem II, an in vitro model for photoprotective energy dissipation in the photosynthetic membrane of green plants. Biochemistry 35, 674-8.

Saenger, W., Jordan, P. and Krauss, N., 2002, The assembly of protein subunits and cofactors in photosystem I. Curr Opin Struct Biol 12, 244-54.

Salekdeh, G.H., Siopongco, J., Wade, L.J., Ghareyazie, B. and Bennett, J., 2002, Proteomic analysis of rice leaves during drought stress and recovery. Proteomics 2, 1131-1145.

Sali, A., Potterton, L., Yuan, F., van Vlijmen, H. and Karplus, M., 1995, Evaluation of comparative protein modeling by MODELLER. Proteins 23, 318-26.

Sandmann, G. and Malkin, R., 1983, Iron-sulfur centers and activities of the photosynthetic electron transport chain in iron-deficient cultures of the blue-green alga aphanocapsa. Plant Physiol 73, 724-8.

Satoh, S., Ikeuchi, M., Mimuro, M. and Tanaka, A., 2001a, Chlorophyll b expressed in Cyanobacteria functions as a light-harvesting antenna in photosystem I through flexibility of the proteins. J Biol Chem 276, 4293-7.

Satoh, S., Ikeuchi, M., Mimuro, M. and Tanaka, A., 2001b, Chlorophyll b expressed in cyanobacteria functions as a light harvesting antenna in photosystem I through flexibility of the proteins. J Biol Chem 276, 4293-4297.

Schagger, H., 2006, Tricine-SDS-PAGE. Nat Protoc 1, 16-22.

Scheller, H.V., Jensen, P.E., Haldrup, A., Lunde, C. and Knoetzel, J., 2001, Role of subunits in eukaryotic Photosystem I. Biochim Biophys Acta 1507, 41-60.

Scheller, H.V. and Haldrup, A., 2005, Photoinhibition of photosystem I. Planta 221, 5-8.

Schluchter, W.M., Shen, G., Zhao, J. and Bryant, D.A., 1996, Characterization of psaI and psaL mutants of Synechococcus sp. strain PCC 7002: a new model for state transitions in cyanobacteria. Photochem Photobiol 64, 53-66.

Schmidt, W., Tittel, J. and Schikora, A., 2000, Role of hormones in the induction of iron deficiency responses in Arabidopsis roots. Plant Physiol 122, 1109-18.

Sétif, P., Fischer, N., Lagoutte, B., Bottin, H. and Rochaix, J.D., 2002, The ferredoxin docking site of photosystem I. Biochim Biophys Acta 1555, 204-209.

Shine, M.B., Guruprasad, K.N. and Anand, A., 2011, Enhancement of germination, growth, and photosynthesis in soybean by pre-treatment of seeds with magnetic field. Bioelectromagnetics 4, 4-11.

Singh, A.K., McIntyre, L.M. and Sherman, L.A., 2003, Microarray analysis of the genome-wide response to iron deficiency and iron reconstitution in the cyanobacterium Synechocystis sp. PCC 6803. Plant Physiol 132, 1825-39.

Smith, P.K., Krohn, R.I., Hermanson, G.T., Mallia, A.K., Gartner, F.H., Provenzano, M.D., Fujimoto, E.K., Goeke, N.M., Olson, B.J. and Klenk, D.C., 1985, Measurement of protein using bicinchoninic acid. Anal Biochem 150, 76-85.

Sperotto, R.A., Ricachenevsky, F.K. and Fett, J.P., 2007, Iron deficiency in rice shoots: identification of novel induced genes using RDA and possible relation to leaf senescence. Plant Cell Rep 26, 1399-411.

Spiller, S. and Terry, N., 1980, Limiting Factors in Photosynthesis: II. Iron stress diminishes photochemical capacity by reducing the number of photosynthetic units. Plant Physiol 65, 121-5.

Spiller, S.C., Kaufman, L.S., Thompson, W.F. and Briggs, W.R., 1987, Specific mRNA and rRNA Levels in Greening Pea Leaves during Recovery from Iron Stress. Plant Physiol 84, 409-14.

Stauber, E.J., Fink, A., Markert, C., Kruse, O., Johanningmeier, U. and Hippler, M., 2003, Proteomics of Chlamydomonas reinhardtii light-harvesting proteins. Eukaryot Cell 2, 978-94.

Storf, S., Stauber, E.J., Hippler, M. and Schmid, V.H., 2004, Proteomic analysis of the photosystem I light-harvesting antenna in tomato (Lycopersicon esculentum). Biochemistry 43, 9214-24.

Strasser, B.J. and Strasser, R.J. 1995 Measuring fast fluorescence transients to address environmental questions: the JIP-test. In: P. Mathis (Ed.) Photosynthesis: from light to biosphere. Kluwer Academic Publishers, Dordrecht, p. 977–9.

Strasser, R.J., Srivastava, A. and Govindjee. 1995, Polyphasic chlorophyll a fluorescence transients in plants and cyanobacteria. Photochem Photobiol 61, 32-42.

Strasser, R.J., Srivastava, A. and Tsimilli-Michael, M. 2000. The fluorescence transient as a tool to characterize and screen photosynthetic samples. Taylor and Francis, London.

Strasser, R.J., Srivastava, A. and Tsimilli-Michael, M. 2004 Analysis of thefluorescence transient. In: G. Papageogiou G (Ed.) Chlorophyll a fluorescence: a signature of photosynthesis. Advances in photosynthesis and respiration, Vol. 19. Springer, Dordrecht.

Straus, N.A. 1994 Iron deprivation: physiology and gene regulation. In: D.A. Bryant (Ed.) The Molecular Biology of Cyanobacteria. Kluwer Academic, Dordrecht, The Netherlands, p. 731-750.

Strzepek, R.F. and Harrison, P.J., 2004, Photosynthetic architecture differs in coastal and oceanic diatoms. Nature 431, 689-92.

Subramanyam, R., Fromme, P. and Webber, A. 2010a Purification and characterization of photosystem I-light harvesting complex I supercomplexes from chlamydomonas reinhardtii. In: S.N. Bagachi, Mohanty, P., Kleiner, D) (Ed.)

Protocols on algal research and cyanobacterial research. Narosa Publishers Pvt. Ltd, New Delhi, India, p. 138.

Subramanyam, R., Jolley, C., Brune, D.C., Fromme, P. and Webber, A.N., 2006, Characterization of a novel Photosystem I-LHCI supercomplex isolated from Chlamydomonas reinhardtii under anaerobic (State II) conditions. FEBS Lett 580, 233-8.

Subramanyam, R., Jolley, C., Thangaraj, B., Nellaepalli, S., Webber, A.N. and Fromme, P., 2010b, Structural and functional changes of PSI-LHCI supercomplexes of Chlamydomonas reinhardtii cells grown under high salt conditions. Planta, 913-922.

Subramanyam, R., Sicora, C., Varkonyi, Z., Mustardy, L. and Mohanty, P., 2005, Protective effect of supplemental low intensity white light on ultraviolet-B exposure-induced impairment in cyanobacterium Spirulina platensis: formation of air vacuoles as a possible protective measure. Photosynth Res 85, 181-9.

Takahashi, M., Nakanishi, H., Kawasaki, S., Nishizawa, N.K. and Mori, S., 2001, Enhanced tolerance of rice to low iron availability in alkaline soils using barley nicotianamine aminotransferase genes. Nat Biotechnol 19, 466-9.

Takahashi, Y., Yasui, T.A., Stauber, E.J. and Hippler, M., 2004, Comparison of the subunit compositions of the PSI-LHCI supercomplex and the LHCI in the green alga Chlamydomonas reinhardtii. Biochemistry 43, 7816-23.

Taylor, S. and Terry, N., 1986, Variation in photosynthetic electron transport capacity in vivo and its effects on the light modulation of ribulose bisphosphate carboxylase. Photosynth Res 8, 249-256.

Teramoto, H., Nakamori, A., Minagawa, J. and Ono, T.A., 2002, Light-intensity-dependent expression of Lhc gene family encoding light-harvesting chlorophyll-a/b proteins of photosystem II in Chlamydomonas reinhardtii. Plant Physiol 130, 325-33.

Teramoto, H., Ono, T. and Minagawa, J., 2001, Identification of Lhcb gene family encoding the light-harvesting chlorophyll-a/b proteins of photosystem II in Chlamydomonas reinhardtii. Plant Cell Physiol 42, 849-56.

Terry, N., 1980, Limiting Factors in Photosynthesis: I. Use of iron stress to control photochemical capacity in vivo. Plant Physiology 65, 114-120.

Thangaraj, B., Jolley, C.C., Sarrou, I., Bultema, J.B., Greyslak, J., Whitelegge, J.P., Lin, S., Kouril, R., Subramanyam, R., Boekema, E.J. and Fromme, P., 2011, Efficient light harvesting in a dark, hot, acidic environment: the structure and function of PSI-LHCI from Galdieria sulphuraria. Biophys J 100, 135-43.

Thompson, J.D., Higgins, D.G. and Gibson, T.J., 1994, CLUSTAL W: improving the sensitivity of progressive multiple sequence alignment through sequence weighting, position-specific gap penalties and weight matrix choice. Nucleic Acids Res 22, 4673-80.

Tjus, S., Roobol-Boza, M., Pålsson, L. and Andersson, B., 1995, Rapid isolation of photosystem I chlorophyll-binding proteins by anion exchange perfusion chromatography. Photosynth Res 45, 41-49.

Torda, A.E., Procter, J.B. and Huber, T., 2004, Wurst: a protein threading server with a structural scoring function, sequence profiles and optimized substitution matrices. Nucleic Acids Res 32, W532-5.

Towbin, H., Stahelin, T. and Gordon, J., 1979, Electrophoresis transfer of proteins from polyacrylamide gels to nitrocellulose sheets: Procedure and some application. Proc Natl Acad Sci USA 76, 43450-43454.

Tremolieres, A., Dainese, P. and Bassi, R., 1994, Heterogenous lipid distribution among chlorophyll-binding proteins of photosystem II in maize mesophyll chloroplasts. Eur J Biochem 221, 721-30.

Tsuda, A., Takeda, S., Saito, H., Nishioka, J., Nojiri, Y., Kudo, I., Kiyosawa, H., Shiomoto, A., Imai, K., Ono, T., Shimamoto, A., Tsumune, D., Yoshimura, T., Aono, T., Hinuma, A., Kinugasa, M., Suzuki, K., Sohrin, Y., Noiri, Y., Tani, H.,

Deguchi, Y., Tsurushima, N., Ogawa, H., Fukami, K., Kuma, K. and Saino, T., 2003, A mesoscale iron enrichment in the western subarctic Pacific induces a large centric diatom bloom. Science 300, 958-61.

Tsuruta, L.R., Hayashi, M.A., Konno, K., Tambourgi, D.V., Assakura, M.T., Camargo, A.C. and Sant'Anna, O.A., 2006, A natural carrier effect and the generation of specific antibodies to biologically active peptides. Anal Biochem 353, 174-80.

Umena, Y., Kawakami, K., Shen, J.R. and Kamiya, N., 2011, Crystal structure of oxygen-evolving photosystem II at a resolution of 1.9 A. Nature.

Vanselow, C., Weber, A.P., Krause, K. and Fromme, P., 2009, Genetic analysis of the Photosystem I subunits from the red alga, Galdieria sulphuraria. Biochim Biophys Acta 1787, 46-59.

Varsano, T., Wolf, S.G. and Pick, U., 2006, A chlorophyll a/b-binding protein homolog that is induced by iron deficiency is associated with enlarged photosystem I units in the eucaryotic alga Dunaliella salina. J Biol Chem 281, 10305-15.

Vasil'ev, S., Orth, P., Zouni, A., Owens, T.G. and Bruce, D., 2001, Excited-state dynamics in photosystem II: insights from the x-ray crystal structure. Proc Natl Acad Sci U S A 98, 8602-7.

Vassiliev, I.R., Antonkine, M.L. and Golbeck, J.H., 2001, Iron-sulfur clusters in type I reaction centers. Biochim Biophys Acta 1507, 139-160.

Vassiliev, I.R., Kolber, Z., Wyman, K.D., Mauzerall, D., Shukla, V.K. and Falkowski, P.G., 1995, Effects of Iron Limitation on Photosystem II Composition and Light Utilization in Dunaliella tertiolecta. Plant Physiol 109, 963-972.

Vavilin, D., Yao, D. and Vermaas, W., 2007, Small Cab-like proteins retard degradation of photosystem II-associated chlorophyll in Synechocystis sp. PCC 6803: kinetic analysis of pigment labeling with 15N and 13C. J Biol Chem 282, 37660-8.

Veith, T. and Buchel, C., 2007, The monomeric photosystem I-complex of the diatom Phaeodactylum tricornutum binds specific fucoxanthin chlorophyll proteins (FCPs) as light-harvesting complexes. Biochim Biophys Acta 1767, 1428-35.

Walker, A.R., 1996, Iron deficiency, development, and cognitive function. Am J Clin Nutr 64, 120-1.

Walker, E.L. and Connolly, E.L., 2008, Time to pump iron: iron-deficiencysignaling mechanisms of higher plants. Curr Opin Plant Biol 11, 530–535.

Wei, L., Cao, Y., Liang, X., Liu, Y., Deng, T., Bai, L. and Qiao, D., 2006, Identification of two genes encoding the major light-harvesting chlorophyll a/b proteins of photosystem II in green alga Dunaliella salina. DNA Seq 17, 370-7.

Winder, T.L. and Nishio, J.N., 1995, Early iron deficiency stress response in leaves of sugar beet. Plant Physiol 108, 1487-94.

Wollman, F.A. and Bennoun, P., 1982, A new chlorophyllprotein complex related to photosystem I in Chlamydomonas reinhardtii. Biochim Biophys Acta 680, 352-360.

Yadavalli, V., Nellaepalli, S. and Subramanyam, R., 2011, Proteomic analysis of thylakoid membranes. Methods Mol Biol 684, 159-70.

Yadavalli, V., Malleda, C. and Subramanyam, R. (2011). 3D model of PSI-LHCIsupercomplexes from *Chlamydomonas reinhardtii.* Proceedings of 15th International Congress on Photosynthesis.

Yan, S.P., Zhang, Q.Y., Tang, Z.C., Su, W.A. and Sun, W.N., 2006, Comparative proteomic analysis provides new insights into chilling stress responses in rice. Mol Cell Proteomics 5, 484-496.

Yu, J., Smart, L.B., Jung, Y.-S., Golbeck, J. and McIntosh, L., 1995, Absence of PsaC subunit allows assembly of Photosystem I core but prevents the binding of PsaD and PsaE in Synechocystis sp. PCC6803. Plant Mol Biol 29, 331-342.

Zhao, J., Snyder, W.B., Muhlenhoff, U., Rhiel, E., Warren, P.V., Golbeck, J.H. and Bryant, D.A., 1993, Cloning and characterization of the psaE gene of the cyanobacterium Synechococcus sp. PCC 7002: Characterization of a spaE mutant and overproduction of the protein in Escherichia coli. Mol Microbiol 9, 183-194.

Zheng, L., Ying, Y., Wang, L., Wang, F., Whelan, J. and Shou, H., 2010, Identification of a novel iron regulated basic helix-loop-helix protein involved in Fe homeostasis in Oryza sativa. BMC Plant Biol 10, 166.

Zouni, A., Witt, H.T., Kern, J., Fromme, P., Krauss, N., Saenger, W. and Orth, P., 2001, Crystal structure of photosystem II from Synechococcus elongatus at 3.8 A resolution. Nature 409, 739-43.

Publications

Publications

1. **Yadavalli, V.,** Nellaepalli, S. and Subramanyam, R. (2011). Proteomic analysis of thylakoid membranes. **Methods Mol Biol** *684*, 159-170.

2. **Yadavalli, V.,** Malleda, C. and Subramanyam, R. (2011). 3D model of PSI-LHCIsupercomplexes from *Chlamydomonas reinhardtii.* **Proceedings of 15th International Congress on Photosynthesis**.

3. **Yadavalli, V.,** Jolley, C., Malleda, C., Thangaraj, B., Fromme, P. and Subramanyam, R. (2011). Protein and functional characterization of photosystems under iron deficiency from *Chlamydomonas reinhardtii.* **Plos One (Submitted).**

4. **Yadavalli, V.,** Malleda, C. and Subramanyam, R. (2011). Structural elucidation of PSI-LHCI supercomplexes by 3D modeling of *Chlamydomonas reinhardtii.* **Biochim Biophys Acta (Submitted)**

5. **Yadavalli, V.,** Tirupati, M. and Subramanyam, R. (2011). Devlopment of peptide tag antibodies against LHCI subunits of *Chlamydomonas reinhardtii.* **J. Photochem. Photobiol. B (Submitted)**

6. **Yadavalli, V.** and Subramanyam, R. (2011). Characterization of PSI and LHCI isoforms of *Oryza sativa* by 2D approach. **Photosynth Res (Submitted)**

Conferences attended

1. Presented poster at 76th meeting of 'Society of Biological chemists of India' during 25th-27th November, 2007 organized by Department of Biochemistry, Sri Venkateswara University, Tirupati.

2. Presented poster at International symposium on 'Light & Life' during August 29-31st, 2007 organized by Department of Plant Sciences, University of Hyderabad and Indian Photobiology society

Chapter 14

Proteomic Analysis of Thylakoid Membranes

**Venkateswarlu Yadavalli, Sreedhar Nellaepalli,
and Rajagopal Subramanyam**

Abstract

Chlamydomonas is a model organism to study photosynthesis. Thylakoid membranes comprise several proteins belonging to photosystems I and II. In this chapter, we show the accurate proteomic measurements in thylakoid membranes. The chlorophyll-containing membrane protein complexes were precipitated using chloroform/methanol solution. These complexes were separated using two-dimensional gel electrophoresis, and the resolved spots were exercised from the gel matrix and digested with trypsin. These peptide fragments were separated by MALDI-TOF, and the isotopic masses were blasted to a MASCOT server to obtain the protein sequence. Matrix-assisted laser desorption/ionization-time of flight mass spectrometry (MALDI-TOF). The method discussed here would be a useful method for the separation and identification of thylakoid membrane proteins.

Key words: 2D electrophoresis, *Chlamydomonas*, IEF, MALDI-TOF, Peptide fragments, Photosystems, SDS-PAGE, Thylakoid proteins, Trypsin digestion

1. Introduction

The primary reactions of oxygenic photosynthesis occur at the thylakoid membrane and are catalyzed by several multi-molecular complexes including photosystem II (PSII), photosystem I (PSI), their associated light-harvesting complexes, the cytochrome b_6f complex, and the ATP synthase. Each of these complexes consists of multiple subunits, pigments, and redox cofactors (1). *Chlamydomonas reinhardtii* is a valuable model system for determining the structure and function of polypeptides of the photosynthetic apparatus and the dynamic aspects of photosynthesis (2).

We present here an easy analytical method for the separation and identification of thylakoid proteins by proteomics tools. The three major steps in proteome analysis are (1) the separation of complex protein mixtures, (2) the characterization of the separated

172

3D model of PSI-LHCI supercomplexes from *Chlamydomonas reinhardtii*

Venkateswarlu Yadavalli[a], Chandramouli Malleda[a] and Rajagopal Subramanyam[a,b*]

[a]Department of Biochemistry, [b]Department of Plant Sciences, School of Life Sciences,
University of Hyderabad, Hyderabad (A.P), India 500046,
*Corresponding author. Tel. No. +91-40-2313 4572; Fax No. +91-40-2301 0120; E-mail: srgsl@uohyd.ernet.in

Abstract: The function of Photosystem I (PSI) is catalyzing one of the initial steps in driving oxygenic photosynthesis in cyanobacteria, algae and higher plants. The recent crystallographic model at 3.3 Å resolution represents the most complete plant PSI structure. The *Chlamydomonas reinhardtii* PSI-LHCI supercomplex structure is not known since it contains a unique structure having additional subunits of light harvesting complex I (LHCI). We have modeled PSI core and LHCI in order to elucidate the structure of PSI-LHCI supercomplexes of *C. reinhardtii*. Most of the core subunits are homologous to the higher plants except PsaO and now it has been modeled based on threading. All core subunits were located similarly like pea structure however, PsaO, a new subunit is closely located to the PsaH, PsaI and PsaL subunits. The location of PsaO subunit at this position may suggest that it may be involved in state transition mechanism in *C. reinhardtii*. From our model, it indicates that there are non-covalent strong inter protein-protein relationship, especially from PSI core to LHCI. Our 3D model may give the structural information for better understanding of PSI-LHCI arrangement and its physiological role in *C. reinhardtii* as well as other algae, where it serves many biotechnological applications.

Keywords: *C. reinhardtii*; 3D Model; PS I-LHCI supercomplex

Introduction

Photosynthesis occurs on thylakoid membranes catabolised by several multimeric membrane supercomplexes that include PSI, PSII, their associated light harvesting complexes, Cyt b₆f complex and ATP synthase (Jensen *et al.*, 2007; Scheller *et al.*, 2001). PSI catalyzes the light-driven electron transfer from the soluble electron carrier plastocyanin, located at the lumenal side (inside) of the thylakoid membrane, to ferredoxin, at the stromal side (outside) of the natural photosynthetic membrane. The structure of PSI supercomplex comprises of core subunits and light harvesting complexes, chlorophylls, phylloquinones and Fe₄S₄ clusters (Amunts *et al.*, 2007; Amunts *et al.*, 2010; Ben-Shem *et al.*, 2003; Jensen *et al.*, 2007). Also, the structure of PSI is highly conserved between cyanobacteria and higher plants which acts as a light driven plastocyanin-ferridoxin-oxidoreductase contained several nucleate and chloroplast encoded subunits (Fyfe *et al.*, 2002; Jordan *et al.*, 2001; Rochaix, 2002; Subramanyam *et al.*, 2006). However, the structure of PSI-LHCI supercomplexes of *C. reinhardtii* is unique as LHCI composition is different and so far there is no structure available to understand the function of PSI-LHCI integrity. By various biochemical and electron

microscopy studies, it was revealed that there could be even more than 10 LHCI polypeptides (Hippler *et al.*, 1998; Mozzo *et al.*, 2010). Thus, in the present study, we build a model with 14 PSI core subunits and 9 LHCI subunits based on the crystallographic model of plant PS I at 3.3 Å (Amunts *et al.*, 2010) which contains 13 PSI core subunits and four Lhca polypeptides.

Materials and Methods

Protein sequences of *C. reinhardtii* PSI-LHCI was collected from expasy database. Target sequences were used for getting the template that has detectable similarity to the target sequence by using BLAST. All the sequences were taken as a single FASTA format file where in each chain has been separated and scanned against a library of sequences extracted from known protein structures in the Protein Data Bank to find the templates. All the chains of both target and templates with their highest percentage of identity were individually aligned in CLUSTALW. The alignment of output file was set to PIR format of target and template sequence. Further, target sequences were aligned with template (2WSC) sequence (Amunts *et al.*, 2010). The output alignment of multiple sequences was exported to .ali and .pap of